ON THE STRUCTURE OF THE ACETYLCHOLINE RECEPTOR FROM *TORPEDO CALIFORNICA* ELECTROPLAQUES

Thesis by

Michael William Klymkowsky

In Partial Fulfillment of the Requirements

for the Degree of

Doctor of Philosophy

California Institute of Technology

Pasadena, California

1980

(submitted 14 December, 1979)

To my parents,

my sisters Susan and Marian,

& Stacey

And Polo said: "The inferno of the living is not something that will be, if there is one, it is what is already here, the inferno where we live everyday, that we form by being together. There are two ways to escape suffering it. The first is easy for many: accept the inferno and become such a part of it that you can no longer see it. The second is risky and demands constant vigilance and apprehension: seek and learn to recognize who and what, in the midst of the inferno, are not inferno, then make them endure, give them space."

from: Invisible Cities

by Italo Calvino

ACKNOWLEDGEMENTS

There are so many people to thank, and while I'll try to remember them all here, some will be temporarily forgotten, except that their imprint remains.

Geraldine Cranmer and the entire staff of the Biology Division at CalTech for their concern and cheerful help with my short and long distance requests.

Pat Koen for teaching me how to use an electron microscope, a mixed blessing, and for good talks.

John Glennon and Louise Guy for being amused by my hysterics, late night space battles and general friendship.

Mike Ross and my fellow graduate students for providing a stimulating environment.

Robert Stroud for his support during the difficult moments, even though provoked by my immaturity.

David McKay for helping me get set up on the right track.

Zach Hall, Joshua Sanes, Neil Nathanson, Gary Reiness, Jeffery Miller and Laura Silberstein for their encouragement, good humor, beer and openness.

The UCSF Neurobiology group for being inspiring.

Vic Foe for being into gold and good humor.

Elwood Linney for the advice years bring.

Richard Parker, Susan Conrad, Myra Tuckerman and Cathy van Ingen for making CalTech more fun in a variety of ways.

Robert, Mary Jane and Elisa Neimack for allowing me to share their home for a while.

Ric Bornstein for patience, waiting for the revolution and seemingly endless revisions.

CalTech for providing an excellent woodshop.

For my old friends Stanton Mallis and Eileen McNamara for their unrestricted love.

And Stacey Sperling for being just crazy enough.

Reprints included in Chapters Two & Three are used with the permission of the publishers, Academic Press, Inc. Excerpts from Italo Calvino's Invisible Cities are used with the permission of the publishers, Harcourt Brace Jovanovich, Inc.

ABSTRACT:

Membranes highly enriched in nicotinic acetylcholine receptor from the electroplaque organ of Torpedo californica were studied using x-ray diffraction, electron microscopy, Fourier image analysis and biochemical techniques. High angle diffraction indicated that the receptor molecule contains 8 nm long alpha-helical stretches that run perpendicular to the membrane plane. The lipids are mostly fluid even at 2°C. Low angle diffraction analysis of oriented membranes under conditions where the continuous diffraction is recorded resulted in electron density profiles of the receptor-rich membranes in which the protein component has an overall length of 11 nm and is asymmetrically distributed with respect to the membrane bilayer, extending by 5.5 ± 0.5 nm on the extracellular side and 1.0 ± 0.5 nm on the other. Greater detail of the individual receptor molecule's structure normal to the membrane bilayer was attained by direct electron microscopic imaging which revealed the flaired, rivet-like shape of the extracellular part of the molecule and the extent to which the molecule extends beyond the intracellular surface (less than 1.0 nm).

The receptor molecules were directly identified in negative-stain electron microscopy for the first time by immunological techniques using anti-receptor antibodies and recognized either by direct imaging, via ferritin-conjugated second antibody, or colloidal-gold labeled primary antibody (the first time the colloidal gold technique had been used in negative-stain microscopy).

Small areas of receptor molecules form ordered lattices and this

ordering is increased if the receptor membranes are prepared in native dimeric form, and stripped of peripheral proteins by alkali-treatment. The ordered areas have been Fourier image processed and result in a low resolution (3.8 nm) model of the surface projection in negative-stain of the receptor. A single monomeric unit packs in an a=8.8, b=8.8 nm, γ= 118° unit cell. The molecule's circular shape results in roughly centrosymmetric phases in the reflections observed, and yet the image reconstructions consistently reveal a common asymmetric structure. Combination of electron microscopic and x-ray diffraction data allows an estimate of the molecular weight of the membrane-bound monomer of 280000 and a radius of gyration of 4.2 nm. Image analysis tentatively indicates that the dimeric molecule does not contain a two-fold symmetry axis.

The conventionally prepared membrane-bound receptor molecule is resistant to trypsin degradation, but removal of peripheral protein by alkali-treatment or solubilization of the membrane by detergents renders the molecule much more susceptible. All four subunits of the receptor can then be degraded and yet the receptor still binds both d-tubocurarine and α-bungarotoxin, and remains an approximately 9S structure in detergent. Proteolysis of the receptor results in a radical change in overall membrane morphology most probably the result of receptor aggregation in the plane of the membrane. Ethanol concentrations above 10% radically effect membrane morphology and may be useful in producing receptor membranes depleted in lipids.

The presence of an endogenous protease activity in highly purified membrane fractions and the formation of receptor membrane sheets by

osmotic shock onto clean water surfaces are described. Such sheets may hold a possibility for two-dimensional crystallization of the membrane-bound receptor.

TABLE OF CONTENTS

TITLE PAGE i

DEDICATION ii

ACKNOWLEDGEMENTS iii

ABSTRACT v

TABLE OF CONTENTS viii

CHAPTER ONE - INTRODUCTION 1

CHAPTER TWO - PRELIMINARY STUDIES 6

Introduction 7

REPRINT - "Structural Studies of a Membrane-Bound Acetylcholine Receptor from Torpedo californica"

Abstract 9
Introduction 9
Materials & Methods 10
Results 15
Discussion 28
Conclusion 31
Acknowledgements & References 32

CHAPTER THREE - IMMUNOSPECIFIC IDENTIFICATION & RECEPTOR STRUCTURE 34

Introduction 35

REPRINT - "Immunospecific Identification and Three-Dimensional Structure of a Membrane-Bound Acetylcholine Receptor from Torpedo californica"

Abstract 37
Introduction 37
Materials & Methods 39
Results 40
Discussion 47
Acknowledgements & References 50

CHAPTER FOUR - PROTEASES AS PROBES OF RECEPTOR & MEMBRANE STRUCTURE 53

Introduction 54

PART I - PREPRINT - "Protease Effects on the Structure of Acetylcholine Receptor Membranes from Torpedo californica"

Title page 56
Abstract 57
Introduction 58
Materials & Methods 60
Results 66
Discussion 72
Acknowledgements & References 76
Figure Legends 81
Figures 86

PART II - Detergent Effects on Trypsin Digestion of the Torpedo Acetylcholine Receptor" 98

References 100
Figure Legends 101
Figures 103

CHAPTER FIVE - LOW RESOLUTION STRUCTURE 106

Introduction 107

PREPRINT - "On the Low Resolution Structure of the Acetylcholine Receptor of Torpedo Electroplaques"

Title Page 108
Abstract 109
Introduction 111
Materials & Methods 112
Results 115
Discussion 121
Table 127
References 128
Figure Legends 130
Figures 133

APPENDICES 146

Appendix I

Ethanol Effects on Receptor Membrane Morphology & Membrane Delipidation 147

Figure Legends & Figures 150

Appendix II

Endogenous Proteases & Receptor Membrane Morphology 156

Figure Legends & Figures 158

Appendix III

Receptor Membrane Sheets Formed Under Negative-Stain Conditions 165

Figure Legends & Figures 167

Appendix IV

Receptor Membrane Sheets Formed on Ultraclean Water Surfaces 171

Figure Legends & Figures 174

CHAPTER ONE

INTRODUCTION

Born as we are out of chaos,
Why can we never establish contact with it?
No sooner do we look at it than order,
pattern, shape is born under our eyes.

W. Gombrowicz

It is the cell surface through which all information passes into and out of the cell, and which holds the organism together, yet the overall structure of the plasma membrane and the integral proteins which form its functional parts are understood in only the most general terms. The most powerful method for determining molecular structure is x-ray crystallography. While the success of crystallographic analysis has been well demonstrated it does suffer from one great limitation: the preparation of a tractable crystal. The task of obtaining useable crystals of membrane proteins faces two distinct hurdles. The first is the general difficulty in purifying an integral membrane protein, and the difficulty in determining whether or not a non-enzymatic protein, such as a channel, signal modulator or structural anchor protein, in short some of the most interesting membrane proteins, is in its native conformation outside of a membrane or membrane-like environment.

of course, the second problem is that the purified protein must be crystallized. A priori there are good reasons to believe that the crystallization of membrane proteins will be innately difficult. The problem lies in the large hydrophilic and hydrophobic surfaces which occur on integral membrane proteins; a water soluble protein will have a predominantly hydrophilic surface. This double nature means that as the polarity of the solvent is reduced the relatively bland hydrophobic portions of the molecules will tend to aggregate out of solution into large sheets resembling their initial membrane environment, or into protein micelles, like a detergent. Moving in the other direction

towards a more polar solvent would then seem to be the most hopeful direction to take, but it may well cause the denaturation of the protein. And as mentioned above such denaturation may be quite difficult to discern.

Without tractable three-dimensional cyrstals the utilization of naturally occurring crystalline membrane proteins or artifically formed crystalline sheets can still provide significant detail of overall molecular structure, although true atomic detail is quite a distant goal. Such low resolution structures are important because together with biochemical information they provide an anchor in reality with respect to which new data can be integrated and interpreted. It should be pointed out the high resolution structural information alone often does not determine how a molecule functions, as is well illustrated by the case of the serine protease trypsin.

The major problem inherent in structural studies limited by the availability of crystals is that one must possess the rare talent of developing an interest in those systems that can be fruitfully studied by x-ray crystallography. Sometimes, however, nature is kind and provides a system which is both tractable and representative of a wider class of membrane proteins. We must only be somewhat opportunistic in our choice of methods in order to successfully study it.

This thesis deals with one such happy instance, and demonstrates how the combination of x-ray diffraction analysis, direct electron microscopy and image reconstruction techniques can be used together

to provide a low resolution structure of a membrane protein.

The electric organ of the torpedinid fishes, the electroplaques, is our boon and a remarkably accessible model system for studying neuromuscular type junctions. The electric cells, electrocytes, are large (1 to 4 millimeter diameter) and extremely thin (50 micrometers) cells stacked into columns similar to a voltaic pile. Each electrocyte is divided by a girdling collagen sheet, which wraps the entire column of stacked electrocytes, into a densely innervated ventral surface and a intricately invaginated dorsal surface. The innervating neurons release the neurotransmitter acetylcholine and the electrocytes sense this transmitter through a membrane-bound receptor in their ventral membrane. Upon binding acetylcholine the receptor responds by increasing the cation flux, depolarizing the electrocyte. This acetylcholine receptor has been the subject of intensive biochemical and pharmacological characterization (for the latest and most comprehensive review see (3)).

The electroplaques organ is a simple tissue dominated by the electrocytes, both with respect to cell type and membrane surface area. Homogenization of the tissue and isopycnic centrifugation results in the isolation of vesicles derived from the post-synaptic membrane in relatively pure form (1,2). These vesicles are densely packed with the nicotinic acetylcholine receptor of the electrocytes and represent a unique opportunity for the study of a neurotransmitter receptor in its native membrane. It is the structure of this acetylcholine receptor and the membrane in which it exists that is the subject of this thesis.

REFERENCES:

1. Cohen, J.B., Weber, M., Huchet, M. & Changeux, J.-P. (1972). FEBS Lett. 26, 43-47.

2. Duguid, J.R. & Raftery, M.A. (1973). Biochem. 12, 3593-3597.

3. Fambrough, D.M. (1979). Physiol. Rev. 59, 165-227.

CHAPTER TWO

PRELIMINARY STUDIES

Then Marco Polo spoke:

> "Your chessboard, sire, is inlaid with two woods: ebony and maple. The square on which your enlightened gaze is fixed was cut from the ring of a tree that grew in a year of drought: you see how its fibers are arranged? Here a barely hinted knot can be made out, a bud tried to burgeon on a premature spring day, but the night's frost forced it to desist."

Until then the Great Khan had not realized that the foreigner knew how to express himself fluently in his language, but it was not his fluency that amazed him.

> "Here is a thicker pore: perhaps it was a larva's nest: not a woodworm, because, once born, it would have begun to dig, but a caterpillar that gnawed the leaves, and was the cause of the tree's being chosen for chopping down... This edge was scored by the wood carver with his gouge so that it would adhere to the next square, more protruding...."

The quantity of things that could be read in a little piece of smooth and empty wood overwhelmed Kublai; Polo was already talking about ebony forests, about rafts laden with logs that come down the rivers, of docks, of women at the windows....

from: Invisible Cities
by Italo Calvino

INTRODUCTION:

Large and small angle x-ray diffraction of the acetylcholine receptor-rich membrane fragments were begun by Michael J. Ross and R.M. Stroud in collaboration with M.A. Raftery (1, 2). In the spring of 1975, I joined Dr. Stroud's research group and together with Mike Ross began electron microscopic analysis of the membrane-bound receptor. Mike Ross discovered the first large crystalline membrane sheet in these receptor-rich fractions and subsequent analysis revealed that while rare, they did occur often enough to suggest that they were the remnants of a normally occurring receptor structure. The frequent observation of small ordered regions in the membrane vesicles identified with the receptor lead to identifying the large crystalline sheets with receptor. Later work (see Chapter Five & Appendix III) indicates that these sheets are not in fact made up of the receptor.

A great deal of effort was made to determine conditions, such as temperature, pH, ionic strength and composition, and effects of agonist and antagonists, which either would enhance the survival or the formation of two-dimensional crystalline regions of acetylcholine receptor. None of these manipulations resulted in a noticeable increase in ordering. The critical factor in receptor membrane ordering appears to be the presence of residual peripheral proteins (see Chapter Five), proteins which were still present in the membranes used at this stage.

The following paper describes the x-ray diffraction and electron microscopic analysis which served as the starting point for my subsequent studies of receptor structure.

REFERENCES:

1. Raftery, M.A., Bode, J., Vandlen, R., Michaelson, D., Deutsch, J., Moody, T., Ross, M., and Stroud, R.M. (1974) FEBS Meeting (Proc.), 9th, 24, 9-23.

2. Raftery, M.A., Bode, J., Vandlen, R., Michaelson, D., Deutsch, J., Moody, T., Ross, M.J., and Stroud, R.M. (1975) in Protein-Ligand Interaction (H. Sund & G. Blaner, eds.) pp. 328-352, Walter de Gruyter & Co., Berlin.

J. Mol. Biol. (1977) **116**, 635–659

Structural Studies of a Membrane-bound Acetylcholine Receptor from *Torpedo californica*

MICHAEL J. ROSS†, MICHAEL W. KLYMKOWSKY‡
DAVID A. AGARD‡ AND ROBERT M. STROUD‡

Norman W. Church Laboratory of Chemical Biology
California Institute of Technology, Pasadena, Calif. 91125, U.S.A.

(*Received 29 June 1976, and in revised form 17 June 1977*)

Membranes prepared from *Torpedo californica* electroplax containing acetylcholine receptors have been studied by X-ray diffraction and electron microscopy. X-ray diffraction data suggest that acetylcholine receptor molecules traverse the endplate membrane, extending 15 ± 5 Å on one side of the bilayer and some 55 ± 5 Å on the other, with an overall length normal to the membrane of 110 Å.

Lattices of acetylcholine receptor have the symmetry of the crystallographic plane group $p1$, with one molecule per unit cell. A low-resolution projection of the surface structure of receptor arrays was determined by reconstruction of images from electron micrographs. The resolution of the image is ~ 20Å in the plane of the membrane. The electron density profile through the membrane, derived from X-ray diffraction of vesicle dispersions and of oriented membranes, has been analyzed to resolutions of 20 and 13 Å, respectively. The high-angle X-ray scattering pattern was observed to a resolution of 1·7 Å. Maxima in the scattering pattern were analyzed in terms of the state of the lipids and secondary structure in the membranes. Sharp maxima in the scattering pattern indicate that long stretches of secondary structure are present in the receptor-containing membranes. The receptor membranes contain repeating structural units of length 80 Å (5·2 Å repeat) oriented perpendicular to the membrane plane, and uninterpreted components greater than 90 Å in length with a basic repeat of 6·3 Å.

1. Introduction

Nicotinic acetylcholine receptor molecules provide one of several mechanisms found in nature for neural transmission. AcChR§-mediated synaptic transmission depends on pre-synaptic release of the low molecular weight transmitter, acetylcholine. After the transmitter diffuses across the synaptic space, it interacts with the membrane-bound receptor and effects depolarization.

The acetylcholine receptor has been shown to operate by increasing permeability to cations in the motor endplate (Takeuchi & Takeuchi, 1960). No permeability to anions was found. The ions are presumed to be conducted through a channel which spans the endplate membrane. The lifetime of this channel was estimated to be about

† Present address: The Biological Laboratories, Harvard University, Cambridge, Mass. 02138, U.S.A.

‡ Present address: Department of Biochemistry and Biophysics, University of California, School of Medicine, San Francisco, Calif. 94143, U.S.A.

§ Abbreviation used: AcChR, nicotinic acetylcholine receptor.

1 ms when excited by ac etylcholine; during this time about 5×10^4 sodium ions can pass from one side of the membrane to the other (Katz & Miledi, 1972). The channel is presumably at least 5 Å across, since it has been shown to conduct cations as large as isopropyl ammonium (Furukawa & Furukawa, 1959).

Membrane fragments rich in AcChR have been purified from several species of electric eel and skate (Cohen *et al.*, 1972; Duguid & Raftery, 1973). The fact that membranes containing AcChR, acetylcholinesterase, or ATPase can be separated by sucrose gradient centrifugation suggests that the different proteins are localized in different regions of the postsynaptic membrane. Further purification of AcChR isolated from membranes by detergent extraction has been accomplished and the molecular weight of these isolated molecules estimated at 330,000 for AcChR from the species *Torpedo marmarota* and *T. californica* by Edelstein *et al.* (1975) and 380,000 for AcChR from *T. californica* by Vandlen & Raftery (1977).

Gel electrophoresis in the presence of sodium dodecylsulfate and crosslinking experiments have established a tentative subunit structure for AcChR; four different subunits have been identified (Weill *et al.*, 1974; Vandlen & Raftery, 1977). The stoichiometry of these subunits is estimated as A_4B_2CD, where A has a molecular weight of 41,000; B, 51,000; C, 60,000; and D, 64,000 (Vandlen & Raftery, 1977).

Studies reported here are concerned with the structure and organization of a membrane-bound acetylcholine receptor from the electric skate *T. californica*. Three major questions are considered: (i) the distribution of protein relative to the lipid leaflet in AcChR membranes; (ii) the secondary structure present within the membrane proteins and the thermodynamic state of the lipids; and (iii) the structure of the molecules at low resolution.

2. Materials and Methods

(a) *Sample preparation*

Samples of AcChR membranes were prepared by M. A. Raftery, R. Vandlen and collaborators as described by Reed *et al.* (1975). Argon or nitrogen-saturated buffers, low temperatures and added anti-oxidants (e.g. 3,5-di-*tert*-butyl-4-hydroxy-benzyl alcohol) were used to minimize lipid oxidation; phenylmethanesulfonyl fluoride (10^{-4} M) and EDTA (10^{-3} M) were added to inhibit proteolytic degradation (Vandlen & Raftery, 1977).

(b) *X-ray diffraction*

The X-ray camera used for both low- and high-angle pictures was designed by two of us (M.J.R. and R.M.S.). The source was a rotating anode generator (Elliott Neutron Division GX-6) run at either 1·6 kW with a 2·0 mm × 0·2 mm focus, or 0·6 kW with a 1·0 mm × 0·1 mm focus. The anode was viewed through a nickel filter at a takeoff angle of 3° to 6° to provide an approximately square image of the target. The beam was focused on to the film plane by 2 perpendicular, elliptically bent silica mirrors (Franks, 1955), and passed through a 1-mm hole in the center of the film into the direct beam trap. The sample was kept at 2°C in an atmosphere of hydrated nitrogen (for wet samples) or dry helium (for dried samples). Two 0·001-in Mylar® windows were used to isolate the sample chamber from both the room atmosphere and the dry helium which filled the remainder of the camera length. The films (2 per pack) were flat and oriented perpendicular to the beam; camera lengths from 1·0 to 19·7 cm were used; exposure times varied from 4 to 48 h.

Samples for diffraction analysis included dispersions of membrane vesicles, oriented membrane pellets of varying degrees of hydration, and dried pellets. Membranes were concentrated by centrifugation into specially designed polycarbonate sample holders contained in celluose nitrate preparative ultracentrifuge tubes. The sample holders allow for

collection of circularly averaged in-plane (equatorial) diffraction from the membranes, or for recording lamellar (meridional) and sectioned equatorial diffraction data.

In attempts to generate oriented pellets of membrane fragments, samples containing about 0·2 mg of protein were added to argon saturated buffer and were centrifuged at 120×10^3 to 300×10^3 g for 2 to 48 h in either Beckman SW-65L-Ti or SW-41-Ti rotors. Some samples were subjected to 3 freeze–thaw cycles (between − 80°C and + 5°C) immediately before centrifugation. This empirical procedure was found to assist in close-packing the pellets by breaking up the vesicles in the dispersions. Excess buffer was removed from the pellet with absorbant paper. Omitting this step allowed the membrane pellet to swell, and the orientation of the bilayers was lost. This resulted in an unoriented membrane dispersion.

(c) *Densitometry of X-ray films*

Films were digitized on a Syntex AD-1 autodensitometer and optical density measurements were corrected for film non-linearity using a logarithmic correction (Morimoto & Uyede, 1963). Intensities were obtained by annular averaging of optical densities within sectors around either the meridian or equator (Ross & Stroud, 1977). During the process of data analysis, it proved necessary to locate the center of the film to within $\pm$ 100 μm, and when sharp reflections were present to within $\pm$ 20 μm. The center was refined using iterative calculations based on the positions of pairs of equivalent reflections located on opposite sides of the film center.

(d) *X-ray data reduction*

Continuous diffraction data were obtained from partially ordered membrane pellets (see section (b) above), and from vesicle dispersions. The scattering from vesicle dispersions should represent the square of the transform of a single AcChR membrane, $F(s)$, multiplied by the transform of the vesicle shape and distribution. The effects of vesicle size and curvature should be small perturbations only on the observed transform since the vesicles are quite large (~ 1 μm) (Lesslauer *et al.*, 1971; Moody, 1975). Meridional scattering (i.e. perpendicular to the membrane sheets) from partially ordered membrane sheets was corrected for background scatter by subtracting the equatorial from the meridional scattering. Observed intensities were then corrected for finite beam size, beam divergence and degree of orientation in the sample. The amount of orientation present in the sample was estimated from the angular width at half-maximum of peaks in the meridional scattering pattern. This angular width was typically $\pm$ 12° to $\pm$ 40°.

The background function for the unoriented vesicle data was more difficult to obtain and required a separate, shorter exposure from a much lower sample concentration. The scattering pattern from a more dilute vesicle dispersion should contain a smaller component of $F(s)$ in proportion to the background scatter $B(s)$, and the presumption is that the background scatter should be of the same form. In order to obtain a measure of $I(s) = |F(s)|^2$, the two scattering patterns $I_1(s)$ from the concentrated solutions and $I_2(s)$ from the dilute dispersions were scaled together. First, the constant density level on the films at high angles ($s^{-1} < 10$ Å) was subtracted both from $I_1(s)$ and from $I_2(s)$, on the assumption that such scattering contains little or no component from $F(s)$. After this background was subtracted, the scattering from the more dilute sample $I_2(s)$ was scaled up by a constant multiplicative factor c such that $I_1(s) \geq I_2'(s)$ for all values of s. $I_2'(s)$ equalled $I_1(s)$ at only one value of $s^{-1} = 22{\cdot}7$ Å, where $F(s)$ had its lowest minimum. The modulus of the transform, $|F(s)|$, was then approximated as $|F(s)| = \sin\theta\,(I_1(s) - cI_2(s))^{\frac{1}{2}}$. The appropriate geometric factor of $\sin\theta$ was derived by Levine & Wilkins (1971).

Fourier refinement of electron density profiles against $|F(s)|$ was carried out by the method of Stroud & Agard (1977) (see section (e)).

(e) *Determination of asymmetric membrane profiles*

An iterative Fourier refinement method was developed and used to calculate electron density profiles for asymmetric membranes, projected onto a line perpendicular to the membrane surface. The method is described in detail by Stroud & Agard (unpublished work) and a short description only is given here.

The method relies on Fourier refinement of an electron density function $\rho(r)$ against the continuous transform $F_0(s)$ derived from continuous X-ray scattering patterns. In this procedure an arbitrary starting model $\rho'(r)$ is used to calculate $F'(s)$ according to

$$F'(s) = \int_{r=-\infty}^{+\infty} \rho'(r) \exp(2\pi i r.s)\, dr \tag{1}$$

where r and s are perpendicular to the membrane surface and i is $\sqrt{-1}$. The phases of $F'(s)$ are associated with the observed $F_0(s)$ to give $F_0'(s)$ and back transformed according to

$$\rho''(r) = \int_{s=-s_1}^{s_1} F_0'(s) \exp(-2\pi i r.s)\, ds \tag{2}$$

where s_1 is the limiting maximum resolution to which the scattering pattern is observed. The function $\rho''(r)$ is constrained to lie within some estimated boundary thickness $a<r<b$ such that $\rho''(r) = 0$ for $a>r>b$, and the process is repeated beginning with equation (1) until convergence is achieved, which typically involved ~ 30 cycles.

The chosen boundary thickness $t = b - a$ is unimportant in determining the final solution, provided that it is greater than the true membrane thickness and less than ∞. No converged solution can be obtained if the boundary thickness is chosen to be smaller than the true thickness. The actual thickness of the membrane leaflet is determined by the solution obtained. This can be shown as follows. Any converged solution obtained will necessarily obey the normal Fourier inversion relationships

$$\rho(r) = \int_{s=-s_1}^{s} F_0(s) \exp(-2\pi i r.s)\, ds \tag{3}$$

and

$$F_0(s) = \int_{r=-\infty}^{+\infty} \rho(r) \exp(2\pi i r.s)\, dr. \tag{4}$$

The autocorrelation function

$$Q(r) = \int_{r'=-\infty}^{+\infty} \rho(r')\, \rho(r' + r)\, dr' = \rho(r) \widehat{\rho(-r)}$$

and the Patterson function

$$P(r) = \int_{s=-s_1}^{s_1} |F_0(s)|^2 \exp(2\pi i r.s)\, ds$$

(which is uniquely determined by the observables $|F_0(s)|$ will necessarily be exactly equivalent, $P(r) = Q(r)$ (Lipson & Taylor, 1958). Since the Patterson function $P(r)$ will be 0 for $r>w$, where w is the true thickness of the membrane, any solution $\rho(r)$ which is of less than infinite extent must be bounded within the thickness w. If $\rho(r)$ were of any other thickness, the convolution product $Q(r) = \rho(r) \widehat{\rho(-r)}$ could not match $P(r)$, and $\rho(r)$ could not be a converged solution to equations (3) and (4). Therefore, all refined solutions will necessarily be of the same thickness, w.

The imposition of a boundary thickness serves only: (a) to eliminate the trivial solutions for which $\rho(r)$ is of infinite extent, obtained by applying any random set of phases to $|F_0(s)|$; and (b) to accelerate convergence to a solution. If more than one solution, $\rho(r)$, exists which is compatible with a thickness of w, then these will form a set of possible solutions which cannot be eliminated without further information, by any method of treating $|F_0(s)|$ (Stroud & Agard, unpublished work). The choice of starting model $\rho'(r)$ in these instances will tend to select for the solution closest to the starting model. Consequently, this approach can be used to test hypothetical structures. Obviously, if only one $\rho(r)$ exists, this procedure will converge upon that structure regardless of the starting model used. In practice it seems that when multiple solutions do exist they are often qualitatively quite similar to one another. In most of the simpler membrane-like trial structures tested by Stroud & Agard (unpublished work) and in the case of acetylcholine receptor membranes considered here, it appears that the solution is unique. The method was also tested on the asymmetric purple membrane from *Halobacterium halobium* using the data of Blaurock & Stoeckenius (1971). Only two solutions were obtained which were identical to those of

Blaurock & King (1977). It was also tested on one set of myelin data of Worthington & McIntosh (1974) for the centrosymmetric myelin structure. In this case 4 solutions were obtained, 2 of which coincided with those of Worthington & McIntosh (1974).

Our considerations here have assumed that $|F_0(s)|$ contains no error. The effects of data errors are considered by Stroud & Agard (unpublished work). In practice the values of $|F_0(s)|$ should be extracted with care to try to achieve this condition. If there is independent evidence for the thickness of the leaflet, then imposition of the boundary thickness can serve to minimize possible errors introduced by certain kinds of data errors. These include the kind of errors which contribute to the Patterson function $P(r)$ at $r>w$. If such errors in the data exist, they will be assayed by the final agreement between $|F_0(s)|$ and $|F_c(s)|$. The agreement index

$$R = \frac{\int_{s=0}^{s_1} ||F_c(s)| - |F_0(s)|| \, ds}{\int_{s=0}^{s_1} |F_0(s)| \, ds}$$

was used as an index of the extent of convergence, and typically refined to a value of 0·3 to 1% for artificially created test data, or 1 to 5% for acetylcholine receptor membranes.

If the data $|F_0(s)|$ are cut off at some particular resolution, the final structure $\rho(r)$—and the Patterson function $P(r)$—will contain series termination ripples which could be potentially misleading. In any real case data to the highest observable resolution should be included, such that $|F_0(s)| \to 0$ at the resolution cutoff limit.

This method is efficient and can be applied to the continuous scattering profiles for symmetric or asymmetric membranes. Continuous scattering profiles may be derived either from dispersions of membranes, or extracted from a series of swelling experiments applied to close-packed sheets, as for example was carried out by Worthington & McIntosh (1974) for myelin. For asymmetric structures the X-ray scattering pattern from close-packed sheets is made only more complex by statistically ordered stacking. Since the overall scattering pattern is sampled by a statistical stacking function which is exceedingly difficult to derive, the transform of a single membrane sheet is equally difficult to derive. Therefore, continuous scattering patterns derived from membrane dispersions are intrinsically more manageable, and also contain a greater degree of information due to the continuity of the function $F(s)$.

This application of Fourier refinement is capable of determining and refining all possible solutions for the electron density function, although absolute certainty that all solutions have been obtained would require testing of a large number of possible alternatives. In practice, the number of real alternatives is limited to those consistent with the maximum and minimum electron density allowed by the chemical constituents of the system, i.e. to chemically reasonable alternatives which can in principle all be tested. The more difficult question is whether a determined solution is *necessarily* the correct one. If more than one solution is obtainable, it can be shown that identification of the correct one requires experimental evidence of a different type (Stroud & Agard, unpublished work), such as isomorphic replacement. Thus, in reporting membrane profiles many solutions should be sought and reported where obtainable.

(f) *Electron microscopy*

Negatively stained samples were prepared and imaged as described by Klymkowsky *et al.* (unpublished work). Images were also recorded on a tilting stage in a Philips EM301 electron microscope. This allowed for recording views of up to 60° from the normal to the membrane surface.

Thin sections of pellets used for X-ray diffraction were embedded, stained and analyzed by electron microscopy as follows: the pellets were glutaraldehyde/formaldehyde fixed (4% formaldehyde, 5% glutaraldehyde in 0·05 M-sodium/potassium phosphate buffer, pH 7·4) for 2 h and washed overnight in phosphate buffer. The pellets were further fixed in 1% osmium tetroxide also buffered in 0·05 M-phosphate buffer (pH 7·4) for 2 h, dehydrated and embedded in Epon 812 epoxy resin (Luft, 1961). Thin (silver gray) sections were cut parallel to the direction of sedimentation using a freshly made glass knife, and lead citrate post-stained before viewing (Reynolds, 1963). No change in pellet thickness

occurred during the fixation or embedding. Micrographs were taken on a Philips EM301 at 80 kV. Acetylcholine receptor protein was positively identified in the microscope by use of receptor-specific antibodies (Klymkowsky & Stroud, unpublished work).

(g) *Image reconstruction*

Well-ordered areas on the micrographs were identified by visual inspection and assayed for degree of perfection by optical diffraction or by computer transform. Optical diffraction was carried out on an optical diffractometer (Markham, 1968) using He–Ne laser illumination (Hughes, model no. 3599H) and an oil-filled film gate.

Areas of electron micrographs of negatively stained samples containing an ordered array were digitized using a Syntex AD-1 flatbed scanner. Data were collected using a 32 μm $\times$ 32 μm illuminating aperture and a 32 μm step-size. This step-size corresponds to a spacing of 2 to 4 Å in the micrographs of arrays that were analyzed.

Selected areas were densitometered and Fourier transformed using a 2-dimensional fast Fourier algorithm (Cooley & Tukey, 1965)†. For image reconstructions, the mean O.D. of the area was subtracted from all picture elements, and the digitized image was "floated" in borders equal to half of the original image size in all directions (DeRosier & Moore, 1970). After Fourier transformation, the reciprocal lattice parameters were refined by a weighted least-squares procedure, and the patterns indexed according to the distribution of intensities in the pattern, such that $F_{(10)} > F_{(01)} > F_{(1\bar{1})}$.

Each lattice chosen for reconstruction was checked by examining the deviation of the positions of the observed maxima in the Fourier transform from their expected positions. Any lattice with an overall standard deviation of greater than $\pm$ 0·75 (scan area)$^{-1}$ was rejected. The magnitudes of the Fourier coefficients at each diffraction maximum were examined and those lattices containing split peaks (indicative of a distorted lattice Klymkowsky *et al.*, unpublished work) were also rejected. Phases of the stronger reflections were examined for discontinuities within the region of a diffraction maximum. If phase incoherence was found, the lattice was rejected.

Two courses of action were taken with respect to the reconstruction of the final image. A digital process, formally identical to the optical filtering techniques developed by Klug & DeRosier (1966), was used to take the masked Fourier transform and back-transform it into real space. This pseudo-optical masking suffers from 2 disadvantages when applied to AcChR membrane lattices in that: (i) low frequency components of the noise, corresponding to repeats greater than the inverse of the mask aperture used around each diffraction spot, are not removed (Erickson, 1974); and (ii) whatever lack of phase coherence exists across each reflection remains. These low frequency terms are sometimes quite large and are mainly due to stain variations on the sample. Compared with stained 3-dimensional crystals (e.g. catalase) the signal-to-noise ratio in the diffraction pattern for AcChR membrane was about 5 times worse. In addition, the pseudo-optical process leads to an ordered image even when applied to an area of incoherent noise in the Fourier transform (Klug & DeRosier, 1966; Gibbs & Rowe, 1973). The test of phase consistency places a further constraint on the choice of acceptable intensities in the diffraction pattern, and consequently provides a measure of reliability for the image.

The second method was an averaging procedure where amplitudes $F_{(hk)}$ for each reflection were generated by integration of the peaks. Phases $\phi_{(hk)}$ were calculated as the weighted average across the peak. Weighting was according to the square of the amplitude at points in a 3 $\times$ 3 or 5 $\times$ 5 array surrounding the lattice points, thus

$$\phi_{(hk)} = \tan^{-1}\left(\frac{\sum_{ij} F_{ij}^2 \sin(\phi_{ij})}{\sum_{ij} F_{ij}^2 \cos(\phi_{ij})}\right)_{(hk)}.$$

The averaged structure factors were placed at the refined reciprocal lattice points.

† All calculations were done on a Data General NOVA800 computer with 32k words of core, a Syntex Analytical Instruments floating point processor, a 2·5 M byte disk, and two 800 BPI 9-track tape units. Times for transform calculations using the program written by one of us (M.J.R.) are: 128 $\times$ 128 transform, 3 min; 256 $\times$ 256 transform, 13 min; 512 $\times$ 512 transform, 1 h 10 min. If a real-hermite transform is calculated instead of a complex–complex transform, these times are halved.

As a quantitative measure of the quality of each reconstruction, the weighted average phase for each reflection was compared to each of the individual phases that went into calculating this average. The weighted mean phase angle discrepancy and the weighted mean cosine of this angle ("figure of merit") were calculated for each reflection according to

$$\Delta\phi_{(hk)} = \left(\frac{\sum\limits_{ij} F_{ij}^2 \, (\phi_{ij} - \bar{\phi})}{\sum\limits_{ij} F_{ij}^2} \right)_{(hk)}$$

$$m_{(hk)} = \left(\frac{\sum\limits_{ij} F_{ij}^2 \cos{(\phi_{ij} - \bar{\phi})}}{\sum\limits_{ij} F_{ij}^2} \right)_{(hk)}.$$

An overall figure of merit was also calculated for the entire diffraction pattern:

$$m = \frac{\sum\limits_{hk} F_{(hk)}^2 \, m_{(hk)}}{\sum\limits_{hk} F_{(hk)}^2}.$$

The possibility of reinforcing errors in the averaging procedure is perhaps greater than in the pseudo-optical case, since the reconstructed image is perfectly repeating by definition. Thus, the figure of merit becomes a very important measure of the validity of each reconstruction. A good AcChR reconstruction gave an overall figure of merit of 0·95 to 0·99 with no reflection below 0·80. In comparison the overall figure of merit for reconstruction on an unordered area or using incorrect lattice parameters ranged from 0·2 to 0·8 with individual figures of merit as low as 0·05 to 0·3.

3. Results

(a) *Membrane profile analysis*

In an attempt to characterize the distribution of protein and lipid in the membranes, the continuous X-ray scattering profiles from pelleted samples were analyzed. The X-ray scattering pattern shown in Figure 1 is typical of those generated from partially oriented pellets. There is no indication of regular stacking in the meridional direction, or of regular order in the plane of the membranes. Such order would give rise to equatorial diffraction (horizontal in Fig. 1). This is consistent with our observation that most of the sample ($> 99\%$) does not contain arrayed structures (Klymkowsky *et al.*, unpublished work). (Further close packing of the membranes results in a much more complex problem of analysis (Stroud & Agard, unpublished work) due to statistical sampling, therefore such patterns were not used for profile structure determination.)

The meridional pattern from hydrated pellets showed a continuous scattering profile, with the first minimum at $d = 110$ Å, and maxima at d spacings of about 76 Å and 37 Å. Meridional scattering from oriented dried pellets showed a broad maximum centred at $d = 59$ Å, presumably due to the scattering function of the denatured membranes (see Fig. 2). Oriented patterns provided a means of separating the meridional scattering pattern from the equatorial scattering. The meridional scattering function $|F(s)|$ was calculated.

In view of the possibility that the oriented patterns such as those shown in Figure 1 contain sampling due to close-packing within the pellet, $|F(s)|$ was also derived from vesicle dispersions.

Electron density profiles through the membrane were determined by Fourier refinement (see Materials and Methods, section (e)). In order to speed convergence, and to minimize the effect of data errors, a rough estimate of the membrane thickness was estimated as follows.

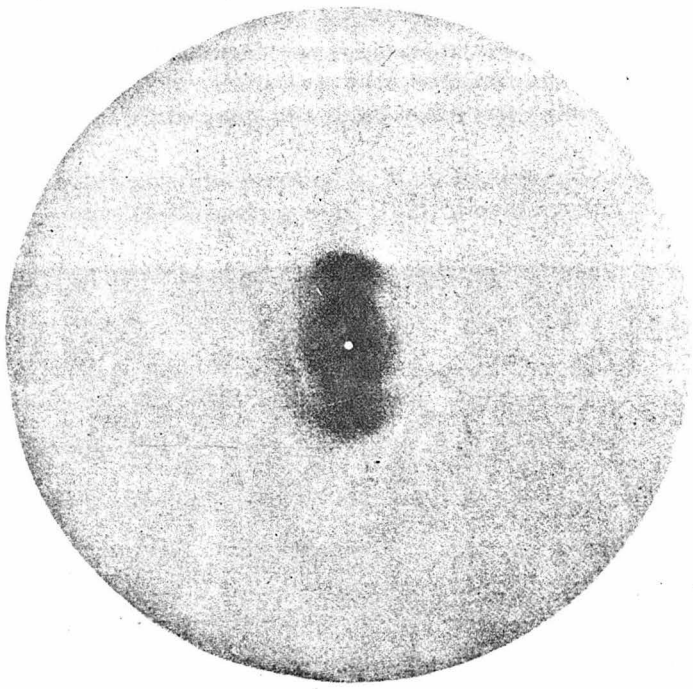


FIG. 1. Typical small-angle scattering pattern from partially oriented pellets of AcChR-rich membranes shows meridional diffraction with maxima at spacings of 76 Å and 37 Å. Angular dispersion of the peaks is about ± 22° (relative humidity 100%).

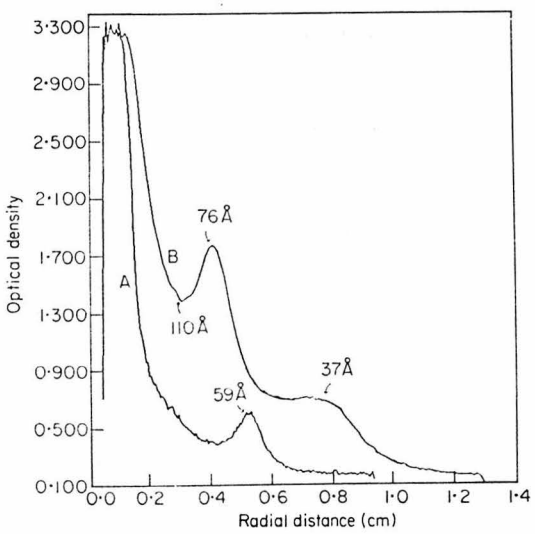


FIG. 2. Densitometer tracings of small-angle X-ray films of partially oriented pellets of AcChR membranes computed from annular integrations within an angular spread of ± 20° of the meridian. Curve A, tracing derived from a 2-h exposure of a dried pellet; curve B, integrated data from the film shown in Fig. 1.

(i) The Patterson function $P(r) = \int F^2(s) \cos(2\pi rs)ds$ calculated from vesicle dispersion data gave an indication of the largest vectors across the membrane leaflet, which indicated a minimum membrane thickness of about 110 Å.

(ii) Pellets used for X-ray diffraction were sectioned and analyzed by electron microscopy (Fig. 3). The thickness of a single leaflet was estimated to be about 100 $\pm$ 25 Å.

(iii) Isolated AcChR molecules prepared by M. A. Raftery and collaborators according to the procedures of Michaelson *et al.* (1974) were shadowed at 15° and at 45°

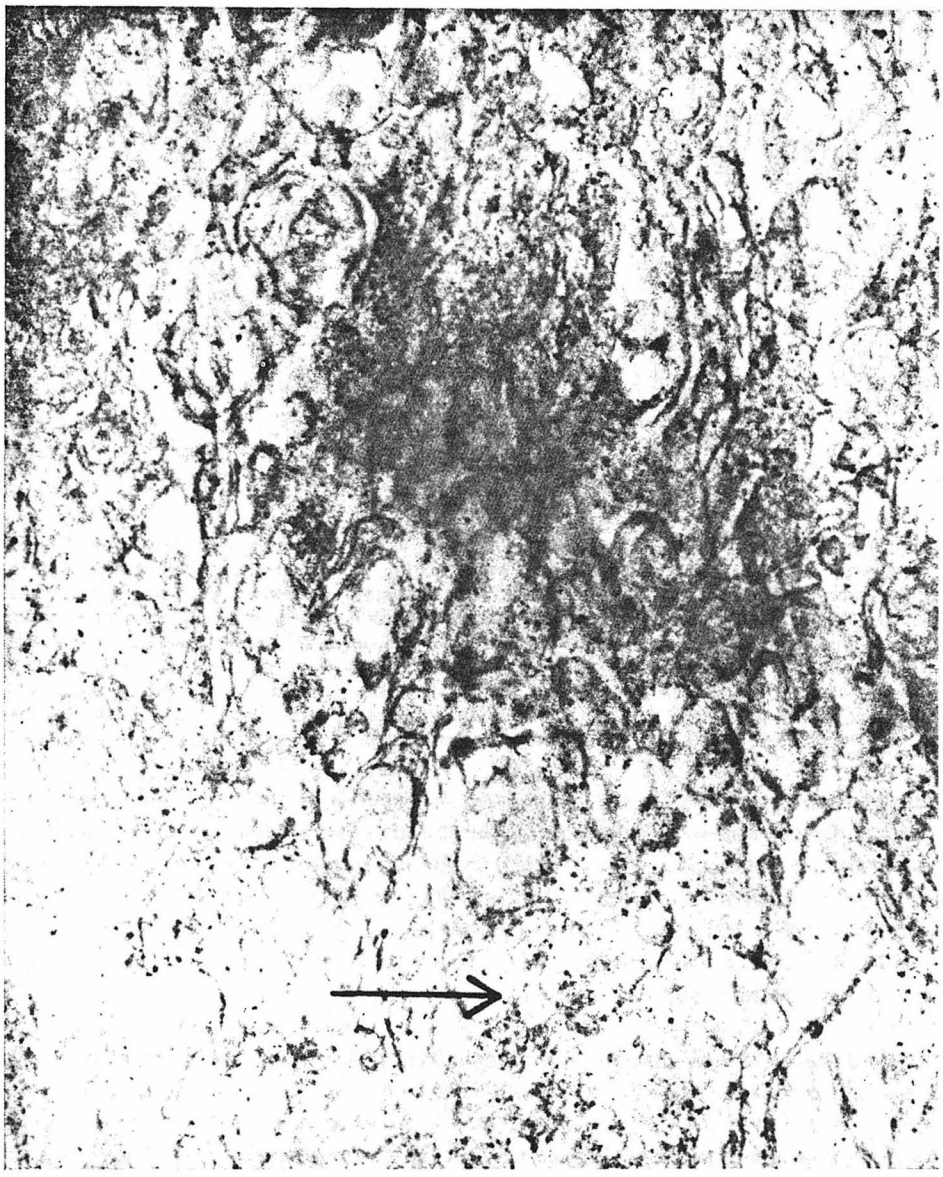


FIG. 3. Thin section of a partially oriented pellet of AcChR membrane vesicles. The direction of sedimentation in the pellet is indicated by the arrow. Membranes appear as dark lines with an average thickness of ~100 Å. The arrow represents a distance of 7600 Å on the micrograph.

with platinum (Kent & Stroud, unpublished results, 1974). Particles seen in the electron microscope were equidimensional with diameters of approximately 85 to 125 Å.

The corrected scattering function $|F(s)|$ from vesicle dispersions (Fig. 4(a)) and the corrected meridional scattering from partially oriented samples (Fig. 4(d)) were used as a basis for one-dimensional electron density refinement. After 40 cycles of refinement from many different starting models, the structures shown in Figure 4(b) and (e) were obtained. A boundary thickness of 115 Å was used to refine the electron density profile obtained from the vesicle data. Narrower boundaries do not permit a solution to be obtained, and wider boundaries slow convergence to the same solution.

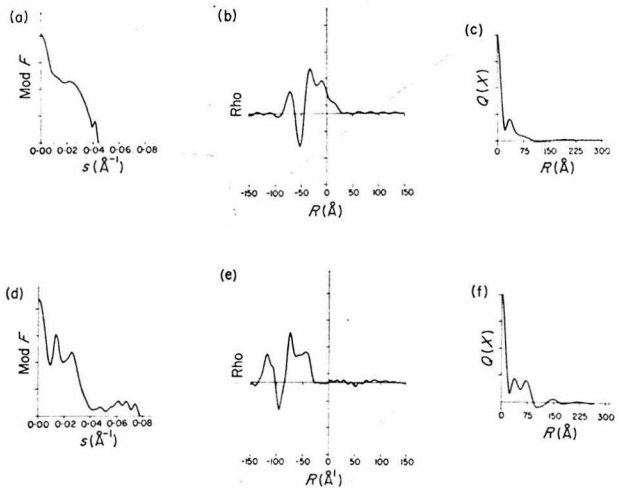


FIG. 4. Results of Fourier refinement of diffraction data from vesicle dispersions ((a) (b) and (c) to a resolution of 22Å, and from partially oriented membranes ((d), (e) and (f)) to a resolution of 13Å. Starting models included rectangular box functions, a delta function, and linear ramp functions. All gave the same results. Calculated and observed continuous scattering patterns for each of these data sets are shown superimposed in (a) and (d). The electron density profiles computed from these X-ray data are seen in (b) and (e). (c) and (f) Each contain superimpositions of the autocorrelation and Patterson functions ($R_P = 2{\cdot}3\%$ and $R_P = 1{\cdot}1\%$, respectively). (Solutions $\rho(r) = \pm\rho(\pm r)$ are mathematically equivalent. Only one for which $\tilde{\rho}(r) > 0$ is shown, since solutions where $\tilde{\rho}(r) < 0$ are chemically unreasonable.)

Application of the Fourier refinement method to the diffraction data from the partially oriented sample indicated that these data are also inconsistent with a structure narrower than 110 Å. Using a boundary width of 120 Å, the agreement between observed and calculated $|F(s)|$, and the Patterson and autocorrelation functions was considerably worse than found for the vesicle data. However, if the boundary was then relaxed to 300 Å, agreement was radically improved, and the results shown in Figure 4(e) and (f) were obtained. It is important to note that the membrane profile itself did not change significantly.

The agreement between observed and calculated scattering functions after refinement are indicated in Figure 4(a) ($R = 2{\cdot}3\%$) and (d) ($R = 1{\cdot}25\%$). The Patterson and autocorrelation functions in the two cases, as shown in Figure 4(c) and (f), are also in excellent agreement, and this provides a second indication that a converged solution has been obtained.

The two structures shown in Figure 4(b) and 4 (e) are surprisingly similar in general features, although they differ in nominal resolutions ($1/s_{max} = 22$ Å for vesicle data

and 13 Å for oriented patterns). Both profiles have characteristics of a bilayer structure in that the distance between the highest peaks on either side of the negative density region was 40 ± 3 Å. The negative density relative to solvent is interpreted as the center of a bilayer. Both profiles also indicate an extension of density on one side of the bilayer by some 55 ± 5 Å. The height of the peak for phosphatidyl head groups on the other side is lower, and may be due to insertion of a greater proportion of lower density material, i.e. protein or solvent, on that side. It therefore seems that protein extends mostly on one side of the membrane (~55 Å) and very little (~15 Å) on the other (see Discussion).

It must be noted that there is a difference between the oriented and vesicle-scattering profiles, and between the Patterson syntheses calculated in the two cases. This is primarily reflected in the peak at $d = 76$ Å, which is a shoulder in the vesicle profile (see Fig. 4(a) and (d). The difference may be due to the lower intensity, and therefore lower accuracy, of the radially smeared vesicle-scattering function, or may be due to a stacking disorder in the oriented pattern. The second explanation seems most reasonable since the refined electron density function from oriented sample seems to contain a second "ghost" membrane profile of much weaker amplitude, as would be expected if there was a small amount of close packing in the specimen (Stroud & Agard, 1977).

A thin section of partially ordered membrane pellet shows a degree of ordering in the pellet qualitatively consistent with the small-angle X-ray results (Fig. 3). The average intermembrane distance (in the pelleting direction) is ~800 Å; however, the membranes occasionally appear as pairs with much closer spacings between the two sheets in a pair. The bilayers in each close pair of membranes are an average of 225 Å apart (center to center) with a standard deviation of ± 90 Å, and approach as close as ~105 Å. This could account for the small amount of statistical sampling implied in the X-ray pattern of partially ordered pellets.

(b) *Image enhancement*

The nature of negative staining makes interpretation of stained images less than straightforward. According to current models (Horne & Whittaker, 1962), the heavy metals form an amorphous glass over the specimen, filling in uneven features on the surface of the membrane. Stain density should therefore be inversely proportional to the surface relief of the membrane-bound components. Multiple-tilted views of each specimen are required to obtain unequivocal information about the distribution of stain in the third dimension.

Some membrane fragments contained areas of extended lattice organization which allowed the application of image enhancement techniques to certain areas (Klymkowsky *et al.*, unpublished work; and Fig. 5). The contrast transfer function (Erickson & Klug, 1971) was evaluated from the image transforms. All images were underfocused to achieve maximum contrast. The first phase change in the transfer function occurred at about 15 to 18 Å resolution. All maxima in transforms used for reconstruction were of lower resolution than the first node in the transfer function, thereby eliminating the need for phase correction.

The transform to 20 Å resolution contained 32 independent (hk) reflections out to the fourth order ($h = 4$) for each latticed array (see Fig. 6). Typically 18 to 23 reflections had enough significant intensity and phase coherence for inclusion in the reconstruction.

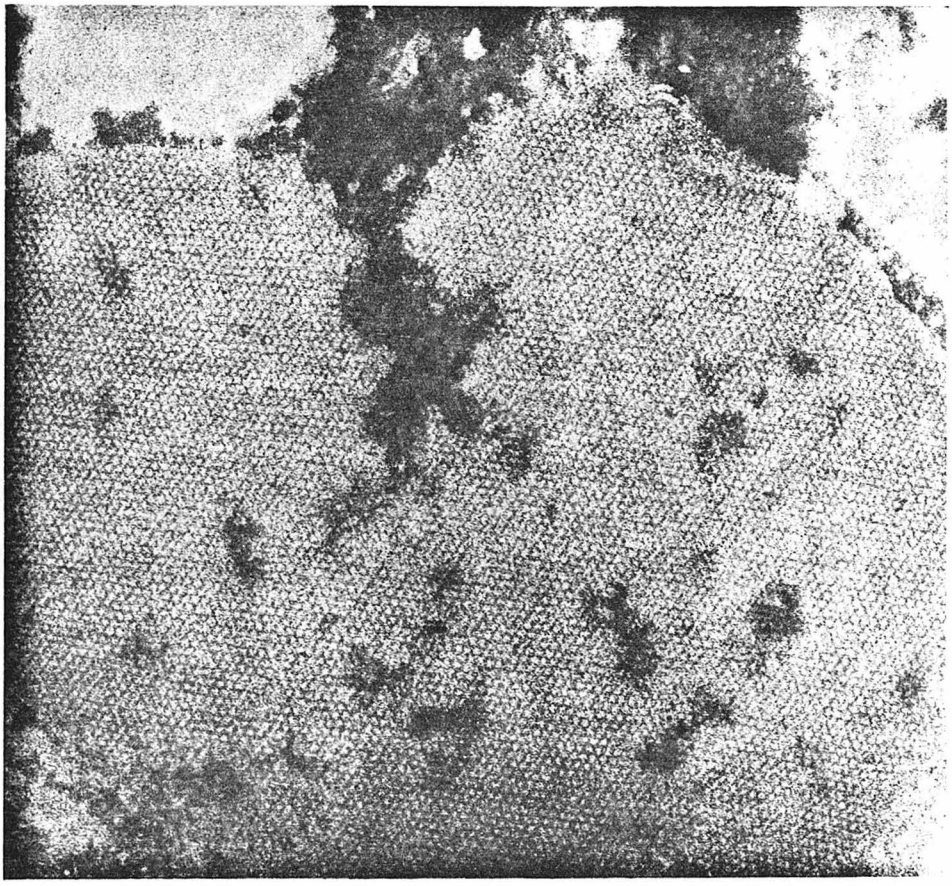
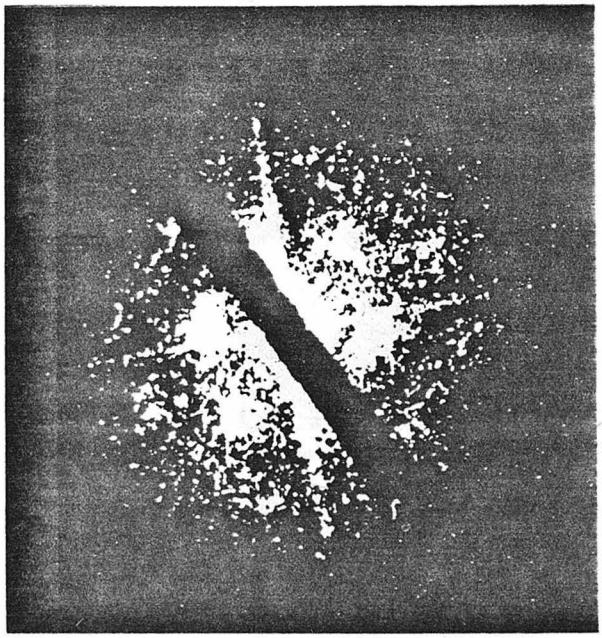


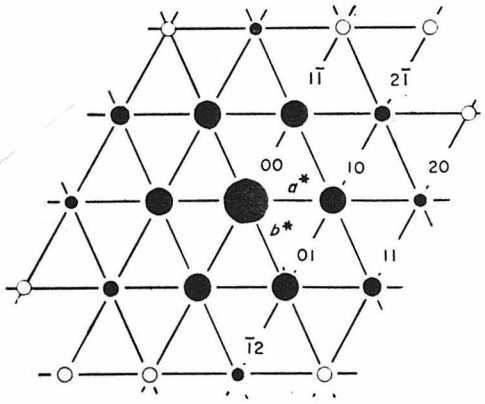
FIG. 5. Negatively stained (1% phosphotungstate, 0·1% uranyl acetate, pH 6) AcChR-rich membrane with a high degree of ordering. Electron optical magnification 98,000×.

Many images contained two or more ordered arrays. These were separated in the Fourier transform and treated separately. Reconstructed images from the separated lattices of two-layer structures (stained with uranyl acetate) consistently gave either of two different views of the receptor ((a) and (b) in Figs. 7, 8 and 9). One of these views indicated that the stain penetrated a well in the center of the molecule. The reconstructed molecule looked like the isolated particles seen in vesicles (Klymkowsky *et al.*, unpublished work; also (a) in Figs. 7, 8 and 9). The alternative view consistently showed a groove part of the way across the molecule, with a shallower central well ((b) in Figs. 7, 8 and 9). The presence of these two different views from alternate layers of moiré patterned images suggests a different distribution of stain in the upper layer and the layer in contact with the grid. The particles seen in reconstructed images (with either phosphotungstate or uranyl acetate staining) are not centrosymmetric, even at lower resolution (90 Å), indicating that the phases are inconsistent with the oblique plane lattice $p2$. The lattice therefore has $p1$ symmetry.

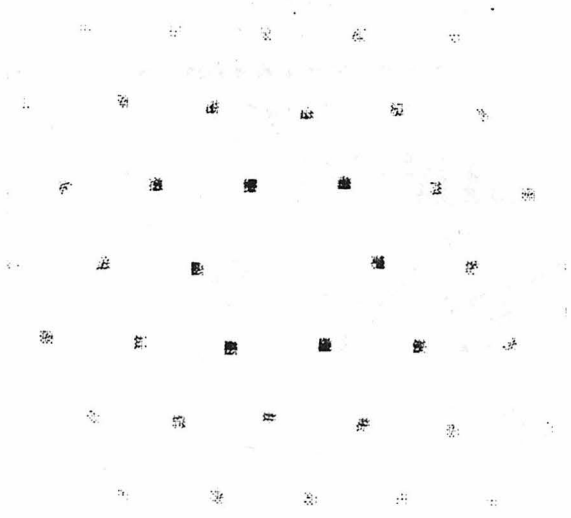
Reconstructed images from phosphotungstate-stained material indicated much weaker staining of the central well than was seen with uranyl acetate, and this may be due to some degree of positive staining with uranyl cations in this area, which is



(a)



(b)



(c)

FIG. 6. (a) Optical diffraction pattern showing intensities from an array.
(b) Schematic of the reciprocal lattice in (a).
(c) A computed transform showing amplitudes $|F_{hk}|$ masked according to the aperture sizes used in Fig. 7.

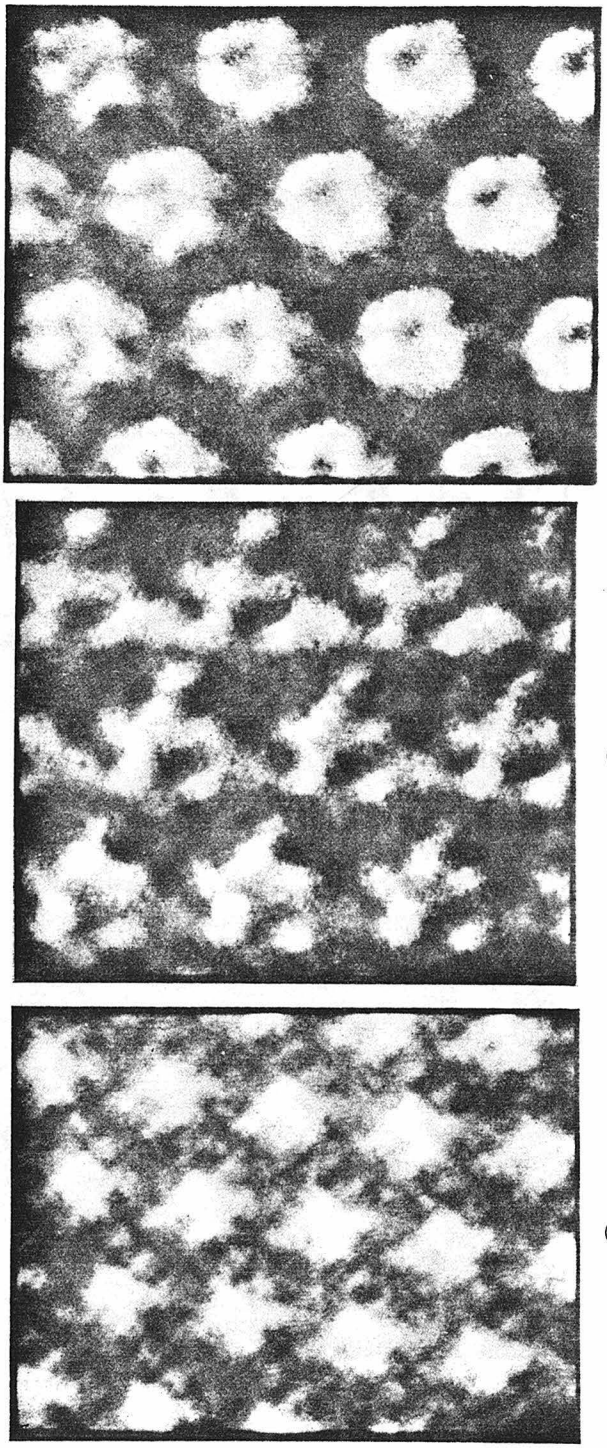


FIG. 7. Pseudo-optically enhanced images. Stain is dark.

(a) and (b) Typical uranyl acetate stained images from alternate sheets of 2 overlaid AcChR membranes. Separate reconstructions were carried out on each of the moiréd lattices by masking of the 32 independent reflections from each lattice (resolution 20 Å).

(c) Phosphotungstate-stained image of one sheet of AcChR membrane. 23 independent reflections were masked and used in reconstruction (resolution 20 Å).

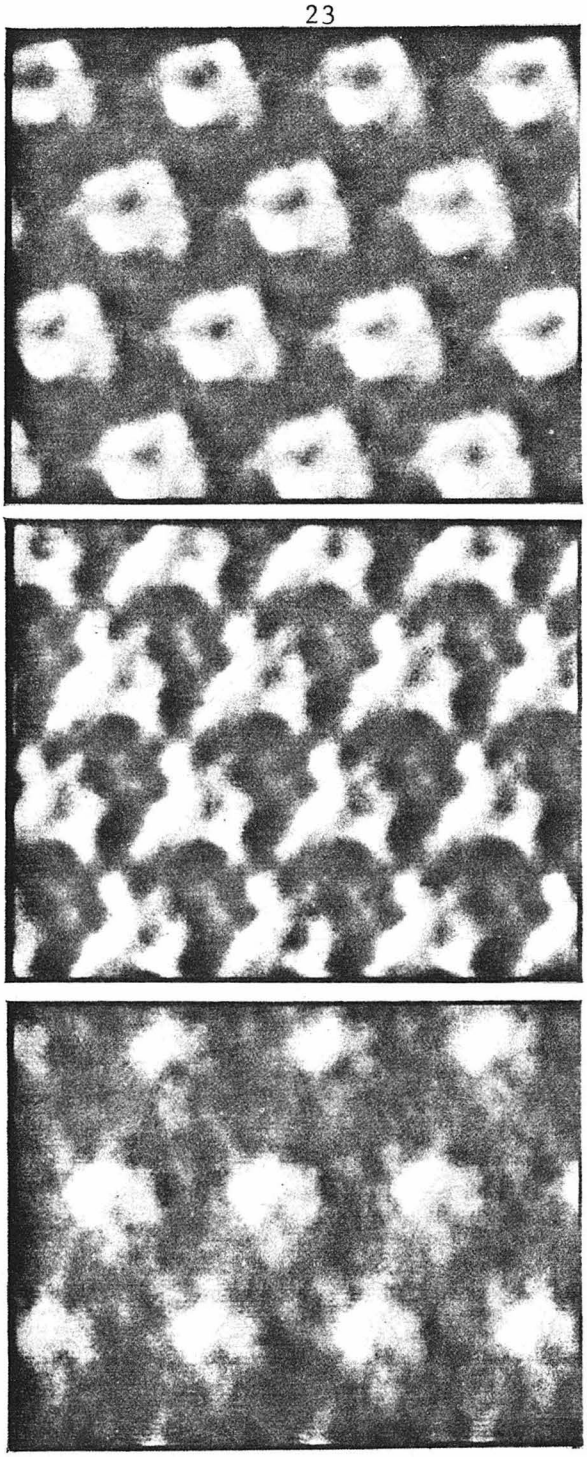
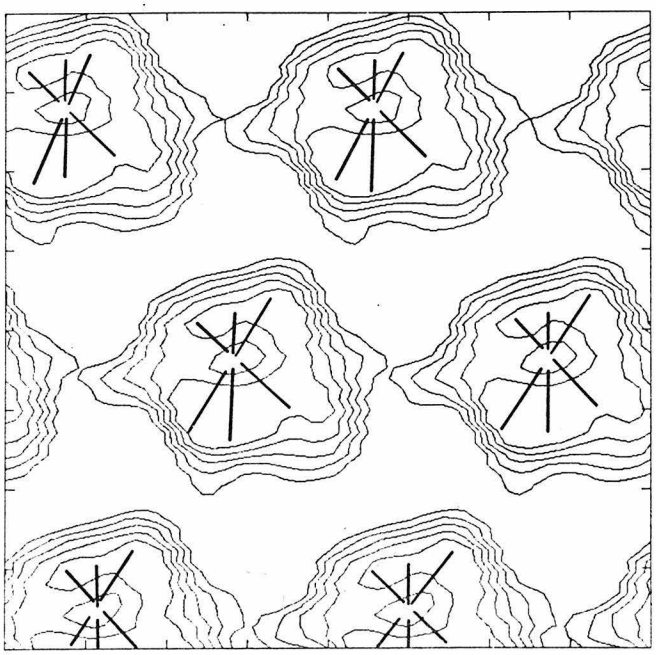


FIG. 8. Images enhanced by phase averaging show: (a) and (b) the 2 characteristic images from alternate layers of double-layered structures, stained with uranyl acetate; (c) the characteristic pattern seen with phosphotungstate stain (stain is dark).

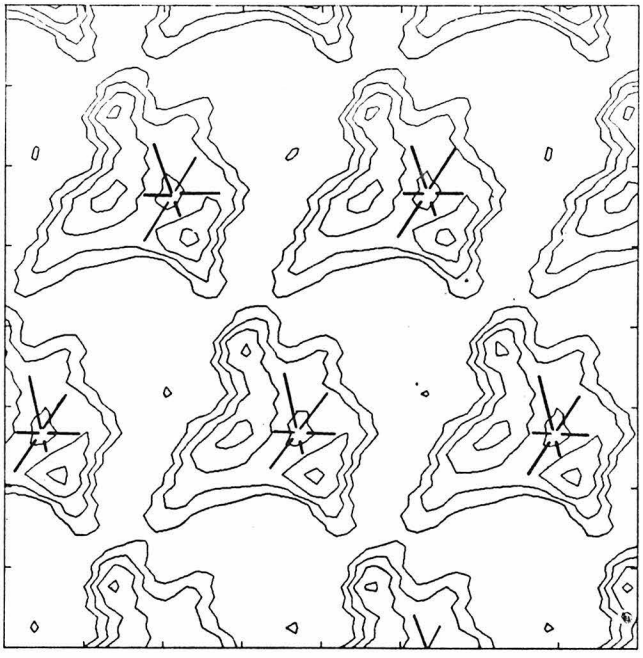
(a) 18 independent reflections phase-averaged. Average overall positional error in diffraction centers was $x = 0{\cdot}57$, $y = 0{\cdot}41$ (scan area)$^{-1}$ from calculated lattice positions. First-order maxima were at a spacing of $\sim$25 (scan area)$^{-1}$. Overall figure of merit = 0·96.

(b) 22 independent reflections used. Averaged overall error in $x = 0{\cdot}47$, $y = 0{\cdot}43$ (scan area)$^{-1}$ from calculated lattice positions. Overall figure of merit = 0·90.

(c) 18 independent reflections used. Average overall error $x = 0{\cdot}54$, $y = 0{\cdot}60$ (scan area)$^{-1}$. Overall figure of merit = 0·96.

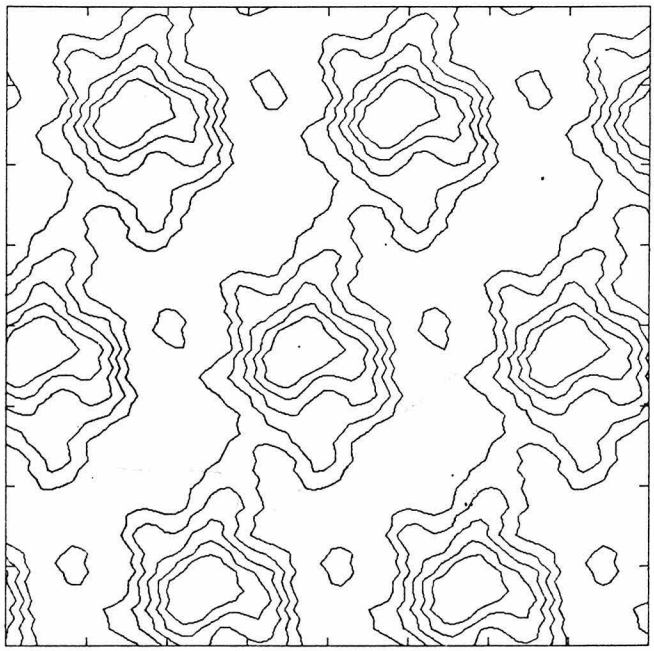


(a)



(b)

FIG. 9



(c)

FIG. 9. Contoured plots of phase-averaged images. The images shown in Fig. 8(a), (b) and (c) were contoured at isodensity levels to indicate the overall molecular shape and lattice contacts present in AcChR membranes. (a) and (b) Uranyl acetate; (c) phosphotungstate.

not matched by phosphotungstate anions. This is not unreasonable if the central well constitutes an ion channel, since the channel transports only positive ions.

(c) *Secondary structure*

High-angle X-ray diffraction photographs of AcChR-rich membrane vesicles reveal several broad maxima characteristic of lipid or water spacings (Fig. 10(a) and (b)). A broad band centred at d-spacing of 4·6 Å is characteristic of the inter-hydrocarbon chain spacings in lipids above the fluid–crystalline phase transition (Luzzati *et al.*, 1960). A sharper maximum at $d = 4{\cdot}2$ Å is expected for the crystalline lipid phase (Dervichian, 1964). High-angle vesicle patterns recorded at either 2°C or 20°C (relative humidity 100%) indicate that a small proportion of the lipids are in the crystalline phase. The phase transition is broad, and this is not surprising in view of the temperatures of the natural habitat of *Torpedo*.

As a quantitative assay for the orientation of these rings, a difference plot of the equatorial pattern subtracted from the meridional pattern was calculated (Fig. 11). 4·2 Å diffraction appeared in both meridional and equatorial scans; however, the diffraction from fluid phase lipids at 4·6 Å was strongly equatorially oriented. This would suggest that most of the lipids contained in the oriented vesicles are above their phase transition temperature (at 2°C), but that part of the sample contains crystalline lipids. These are presumably not in vesicles or sheets and thus do not orient during pelleting.

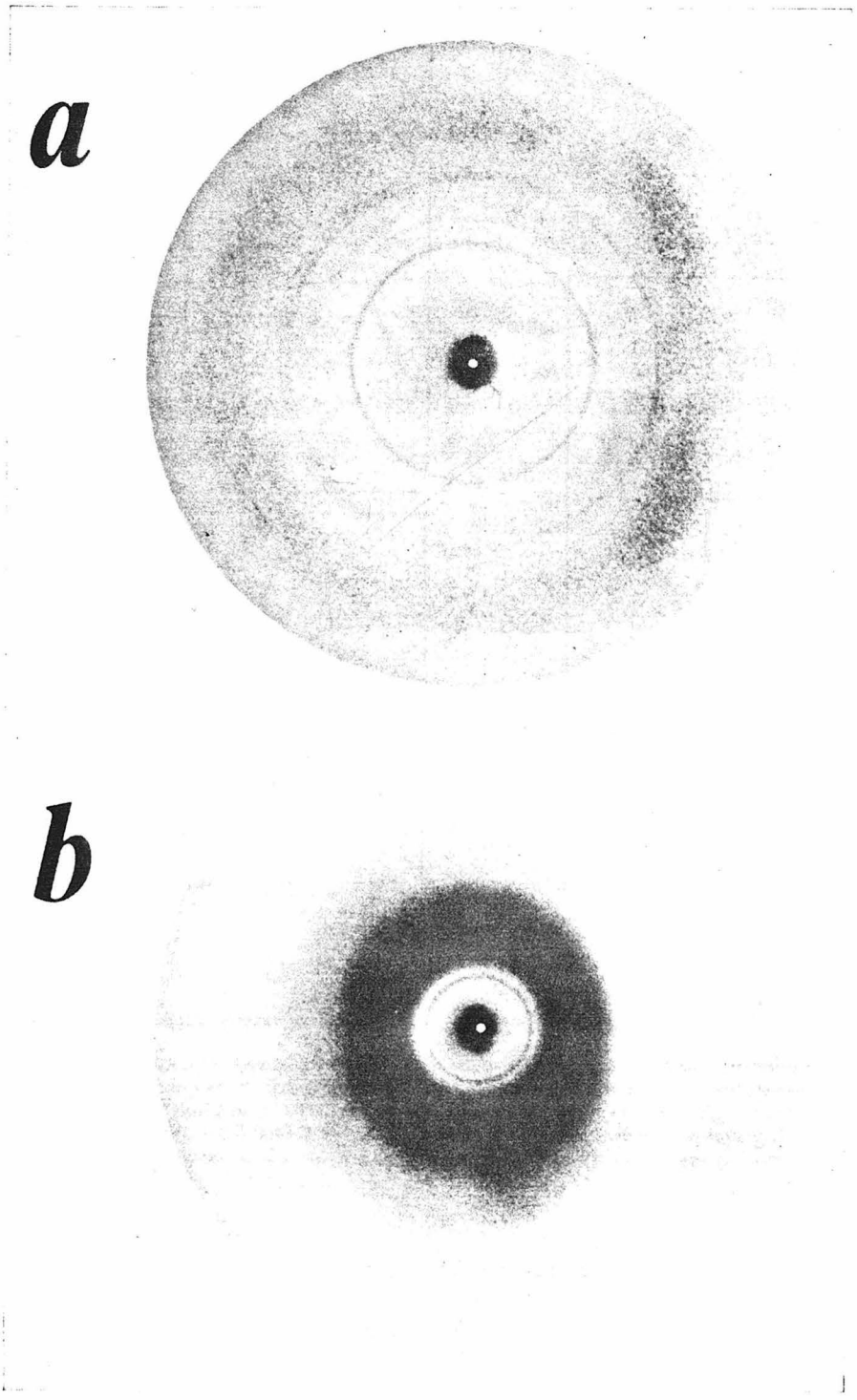


FIG. 10. High-angle X-ray diffraction from partially oriented membrane samples (meridian vertical).

(a) Camera length was 4·66 cm. Exposure time was 15 h. X-ray focus 0·2 mm × 2 mm.

(b) Camera length was 2·0 cm. Exposure time was 20 h. X-ray focus 0·1 × 1 mm.

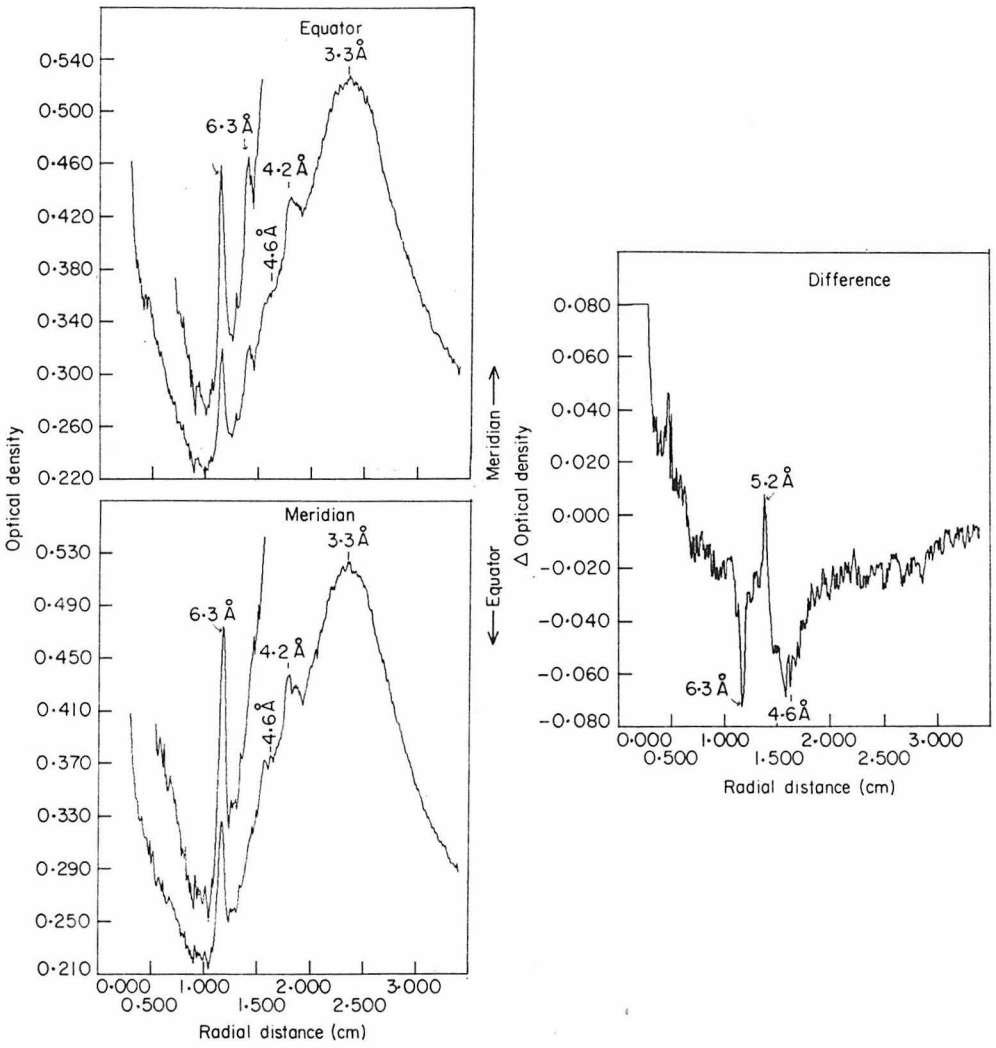


FIG. 11. Densitometer tracings of high-angle scattering from AcChR-rich membranes. Equatorial (a) and meridional (b) integrations from the film shown in Fig. 10 were carried out with angular acceptance limits of ± 50°. Insets on the equatorial and meridional figures are expansions which show the sharp 6·3 Å and 5·2 Å reflections. A difference curve (c) displaying the meridional minus equatorial density is shown. Peaks with meridional orientation are positive; those with equatorial are negative on this plot.

There is a broad peak centred at $d = 3{\cdot}3$ Å characteristic of water scattering. The degree of hydration of the sample can be estimated from the height of the water peak. There are two sharp reflections at spacings $d = 5{\cdot}2$ Å and $d = 6{\cdot}3$ Å in the high-angle pattern of hydrated AcChR membranes. In addition there is a maximum at $d = 4{\cdot}06$ Å (Fig. 11) and a broad maximum at $d = 2{\cdot}2$ Å (Fig. 10).

The maximum at $d = 5{\cdot}2$ Å is highly oriented towards the meridian, while the 6·3 Å reflection is slightly oriented toward the equator. Both the 5·2 Å and the 6·3 Å reflections are extremely sharp. The ratio of the width of these rings at half-height

to their radial position from the film center is an index of the length of the structural feature giving rise to the diffraction. These ratios are 1/18 for the 5·2 Å reflection, and 1/17 for the 6·3 Å reflection, indicating that the 5·2 Å reflection is caused by a stretch of secondary structure ~ 80 Å in length running perpendicular to the membrane, and that the 6·3 Å reflection is caused by structures of ~ 90 Å in length. The angular reflection width of the 5·2 Å reflection was analyzed and compared to the angular width of the small-angle diffraction maxima in the same pattern; the 5·2 Å reflection had an angular peak width about twice that of the low-angle maxima.

4. Discussion

(a) *Contents of the unit cell*

The subunit stoichiometry of this acetylcholine receptor has been estimated to be $A_4B_2C_1D_1$ (Vandlen & Raftery, 1977), which is inconsistent with a three- or sixfold symmetry within the molecule. Therefore, any symmetry higher than that of a primitive lattice cannot be assumed. A careful analysis of likely errors in the intensities and phases of the transform, and comparison with similar studies of the hexagonal arrays found in gap junctions (Klymkowsky *et al.*, unpublished work), render our results inconsistent with any type of lattice other than a plane lattice of oblique symmetry (plane group $p1$). The lattice type may be important to the function of this receptor, if it were shown to be present at the synapse.

The averaged values of unit cell parameters were obtained from ten different arrays, and were found to be $a = 90{\cdot}8 \pm 4{\cdot}1$ Å, $c = 91{\cdot}0 \pm 4{\cdot}3$ Å, and $\beta = 118 \pm 4°$. The average area of one projected unit cell was found to be 7300 ± 200 Å^2. While the unit cell angles are close to 120°, the lattice cannot be described as a hexagonal or trigonal arrangement of molecules, since both intensities (see Fig. 6) and phases in the lattice transforms are far from symmetric. The unit cell contains one molecule, and a symmetric lattice arrangement would require that the molecule had internal symmetry. The unit cell area would imply a volume of 805,000 Å^3 for a 110 Å thick "unit cell". Each cell contains one molecule of AcChR oligomer, of estimated molecular weight 370,000. Assuming a $\bar{v}$ for the protein of 0·74 cm^3 g^{-1} (Matthews, 1968), the protein would occupy a volume of 450,000 Å^3.

Based on the image analyses (Fig. 9), we estimate that no more than half of the area of each unit cell may be lipid. The number of lipid molecules present in such an area can be estimated by dividing the lipid area of each unit cell (less than 3700 Å^2) by the estimated area per lipid molecule. Assuming a value of 62·7 Å^2 per lipid molecule (obtained by Levine & Wilkins (1971) for lecithin bilayers at 100% relative humidity), 60×2 lipid molecules would be contained in bilayer structure per unit cell. The volume occupied by the lipids would be $3700 \times 40 = 148{,}000$ Å^3 (taking 40 Å as the bilayer thickness in hydrated lecithin bilayers (Levine & Wilkins, 1971)). Thus the protein and lipid would account for a total of 600,000 Å^3 or about 74% of the unit cell.

It must be emphasized that the three unit cell parameters, a, b, and c, are never observed simultaneously, since no estimate of the thickness of one layer b is obtained from the microscopy of single or multilayered arrays used to define a and c. Conversely, since the bulk of the sample contains membranes with close-packed, but not highly-ordered arrays of molecules, the X-ray diffraction studies used to define the b dimension do not allow for an estimate of the in-plane lattice dimensions.

(b) *Receptor arrays*

It seems likely that the acetylcholine receptor exists as an arrayed structure *in vivo*, since a wide range of preparative conditions has been used, and these are certainly not expected to be conducive to "crystallization" of the membrane-bound protein. Nor have we been able to alter the frequency with which crystalline arrays are observed by changing conditions of pretreatment. The lateral motion of AcChR in membranes of developing muscle fibers has been studied by fluorescence photobleaching recovery (Axelrod *et al.*, 1976). In this system it was found that there were two coexisting classes of AcChR on non-innervated rat myotubes. One class was relatively mobile with a diffusion constant of 5×10^{11} cm^2/s at 22°C, while the other class was immobile and occurred in dense patches. It may be that the immobile patches detected in these experiments correspond to the arrayed structures seen in our studies. This kind of organization *in vivo* might simply represent an energetically favorable system for concentrating receptor activity at the tips of postsynaptic membranes, or might be functionally important for molecule–molecule co-operativity (Levitski, 1974). Such mechanisms offer attractive hypotheses for the efficient and error-free repetitive action of neuroreceptors.

(c) *Distribution of lipid and protein*

The electron density profile perpendicular to the membrane surface indicates that the membranes are 110 Å thick. The resolution of the profiles are nominally 22 Å and 13 Å, although by the Rayleigh criterion actual resolution should be 11 Å and 6·5 Å, respectively. From the solutions indicated in Figure 4, we presume that the main minimum in the function lies at the center of a lipid bilayer. Thus, it appears that the protein extends considerably on one side, ~55 Å, and little on the other, ~15 Å. The two maxima in the electron density profile on either side of the lowest minimum were ~40 ± 3 Å apart, i.e. about equal to the separation between the electron-dense phosphatidyl head groups in artificial lipid bilayers (Levine & Wilkins, 1971; Lesslauer *et al.*, 1972). Many different model profiles were tested using the method of Stroud & Agard (unpublished work), and no other models were found which were compatible with the continuous scattering profiles.

The profile solutions shown in Figure 4 represent the averaged profile for all membranes in the specimen. Thus, the density of AcChR protein within the membranes will affect the relative scale of those features of the profile due to protein, with respect to those due to a lipid bilayer. Also, any membrane-bound protein other than AcChR in the preparations will be represented according to its relative contribution of electron density.

These membranes have been chemically characterized by Reed *et al.* (1975), who showed that the protein subunits and their relative stoichiometry in the membranes are closely similar to that of Triton-extracted AcChR from the membranes after purification by affinity chromatographic procedures.

The molecular weights of subunits found in the membranes were the same as for AcChR, with the addition of a small amount of a 105,000 molecular weight component which appears in varying proportions between preparations. The stain density for the A subunit of AcChR (M_r~41,000) is also increased by the presence of actin monomers (M_r~42,000) which are also found in the solubilized membranes (M. Raftery, personal communication). Actin filaments were also observed occasionally in electron micrographs, however it is unlikely that the presence of randomly oriented

actin filaments would contribute significantly to the profile structure since they are not integral to the membranes. While the total electron content of proteins other than AcChR is relatively quite small, they could cause perturbations in the final profile if they were membrane bound. In fact, the differences between electron density profiles from different preparations were very small.

In the electron microscope, the AcChR membrane fragments typically occurred as vesicles several microns across. The structures visible in the vesicles appeared as "doughnut-like" structures which were densely close-packed (although generally not arrayed) in the membranes. These structures resemble the structures seen in negatively stained fields of isolated AcChR (Kent & Stroud, unpublished data) and are easily distinguished from the particles seen in membranes enriched in AcCh esterase from the same source (Reed *et al.*, 1975). Thus almost all discernible structures within the AcChR membranes appear to be the same doughnut-like particles, generally held to be AcChR molecules (Nichol & Potter, 1973; Cartaud *et al.*, 1973; Reed *et al.*, 1975), and positively identified as such immunologically (Klymkowsky & Stroud, unpublished work).

Some membrane vesicles seen in the AcChR-rich fraction do not contain any discernible structures (10 to 20%). It seems unlikely that these vesicles contain phospholipid alone, since they band at the same density as the AcChR membranes (1·17 g/ml). However, if they were lipid vesicles, they would perturb the "average" profile, de-emphasizing the features due to protein alone. More likely is the possibility that these are smooth-side-out AcChR vesicles sealed to negative stain. In this case the electron density profile would be unaffected, although little contrast would be seen in the micrographs.

The electron density profile can best be analyzed in terms of a lipid bilayer plus protein (which may or may not be 100% AcChR) plus solvent. The electron density of protein ($\rho \sim 0{\cdot}40$ eÅ^{-3}) is close to that of phosphatidyl head groups ($\rho \sim 0{\cdot}45$ eÅ^{-3}). Therefore, the highest positive density in the profile should be due to the densest arrangement of phosphatidyl head groups plus protein, and the lowest negative trough due to terminal methyl groups in the center of the bilayer.

The electron density of water is 0·334 eÅ^{-3}. Electron densities for hydrated protein are about 0·40 eÅ^{-3}, or 0·44 eÅ^{-3} for anhydrous protein. Electron densities estimated for phosphatidyl head groups are typically $\rho \sim 0{\cdot}45$ eÅ^{-3}; close to that of protein. For methylene groups $\rho \sim 0{\cdot}32$ eÅ^{-3} is close to that of water. Densities for terminal methyl groups in the center of a bilayer vary from about 0·18 eÅ^{-3} (Engleman, 1971) to about 0·27 eÅ^{-3} (Caspar & Kirschner, 1971).

The electron density scale for AcChR membranes is relative, but can be scaled assuming that the highest peak corresponds to protein plus phosphatidyl head groups $\rho \sim 0{\cdot}43$ eÅ^{-3}, the constant density outside the membrane being that of water, 0·334 eÅ^{-3}. The density at the center of the bilayer would be $\rho = (0{\cdot}26)\dagger\ 0{\cdot}27 \pm 0{\cdot}01$ eÅ^{-3}, which could represent 0 to 40% protein at the bilayer center (depending on which methyl group density is assumed). The protein density on the right of the profile is $\rho \sim (0{\cdot}40)\ 0{\cdot}39 \pm 0{\cdot}01$ eÅ^{-3}, and indicates that hydrated protein is reasonably close-packed immediately above the membrane surface, and this is consistent with electron micrographs which show densely packed particles in the plane of the membrane.

† Values in parentheses are from the membrane dispersion profiles (Fig. 4(b)); other values are for the higher resolution profiles (Fig. 4(e)) from partially oriented membranes.

The lower head group peak on the left side of the profile $\rho\sim(0{\cdot}38)$ $0{\cdot}39 \pm 0{\cdot}01$ eÅ^{-3} could be explained by a higher protein concentration at that surface of the bilayer, with the possibility that solvent trapped in a protein pore could also contribute to the lowered density there. Thus, the profile suggests that protein extends ~55 Å on one side of the bilayer and little, ~10 to 15 Å, on the other; that protein is present on both sides; and most probably in the center of the bilayer. Stronger evidence that AcChR molecules indeed span the bilayer derives from the 80 Å long stretches of secondary structure (most probably α helices) which run perpendicular to the membrane surface. Thus, the X-ray evidence suggests the AcChR is an integral membrane protein which spans the endplate membrane, and this is consistent with its operation as an ionophoretic channel.

The membrane thickness (110 Å) determined from this X-ray analysis is closely similar to that found by Rosenbluth (1975) by electron microscopy of thin-sectioned and freeze-fractured electrocyte membranes from *Torpedo* (~120 Å). Rosenbluth (1975) also found that particles within these membranes project (~60 Å) into the junctional cleft, and little on the other side. Thus, the side which contains peripheral protein is presumably the synaptic side of the endplate, and might therefore be reasonably expected to contain the ligand, or toxin-binding sites, located on the A_4 subunits.

(d) *Secondary structure*

Henderson (1975) discussed evidence for α-helical structure in other transmembrane proteins, and argued that the α-helix satisfies the hydrogen-bonding requirements of a polypeptide chain in a hydrophobic environment. It is notable that AcChR membranes give rise to a sharp reflection at $d = 5{\cdot}2$ Å, a spacing characteristic of α helices in the coiled-coil conformation. Whatever this arises from, the corresponding structural features are of average length ~80 Å, and oriented perpendicular to the membrane surface. The most probable explanation is that these are α helices.

Two other structures which might represent an energetically acceptable way to define a channel of dimensions ~5 to 10 Å would be: (i) a large diameter coil of polypeptide, crosslinked as a parallel β-sheet structure, and (ii) a barrel formed by twisted antiparallel β sheet. This latter structure has been found in several proteins. Either of these two structures might account for the 6·3 Å reflection.

The antiparallel-pleated sheet gives rise to a chain repeat of 7 Å, with 4·75 Å between chains running in alternate directions (as found for silk (Marsh *et al.*, 1955)). A twisted-pleated sheet might reduce the chain repeat to 6·3 Å.

The parallel β-sheet arrangement was suggested for β-keratin (Pauling & Corey, 1951), and gives rise to a 6·5 Å chain repeat, with 4·85 Å separation between chains. The sharpness of the 6·3 Å reflection is nevertheless surprising, and it is difficult to see how a coiled chain could account for the apparently large number of repetitions. The 6·3 Å reflection was observed in the X-ray patterns of other membranes prepared from *Torpedo* and *Electrophorus electricus* including those enriched in acetylcholine esterase, or ATPase. Therefore, there is at least the possibility in this case that the 6·3 Å reflection arises from some regular lipid phase in the membranes.

5. Conclusion

The acetylcholine receptor from *T. californica* is an integral membrane protein, which traverses the endplate membrane. The protein extends some 55 Å on one side

of the lipid bilayer and little on the other. This receptor occurs in an ordered lattice which is maintained by protein–protein interactions, and contains long 80 Å stretches of secondary structure tentatively identified as α helices, oriented perpendicular to the membrane surface. The center of each molecule is more accessible to uranyl stain than other parts of the molecule, and this well is tentatively identified as the ionophoretic channel. Further low-resolution studies are aimed at: (i) locating binding sites for macromolecular toxins such as α-Bungarotoxin which bind tightly to the receptor; and (ii) assaying for ligand-induced conformational change. The single crystal structure analysis of α-Bungarotoxin is nearing completion in our laboratory, and it is hoped that details of toxin binding may be obtained from the high resolution structure of the α toxin.

This work was carried out with the support of the National Institutes of Health grant no. GM-19984 and the National Science Foundation grant no. BMS75-04105, whose help is gratefully aknowledged. One of us (R.M.S.) is the recipient of a National Institutes of Health Career Development Award, and is a Sloan Foundation Fellow. Another author (M.J.R.) is the recipient of a National Institutes of Health Predoctoral Traineeship, a third author (D.A.A.) is the recipient of a National Science Foundation Predoctoral Fellowship, and the fourth author (M.W.K.) is the recipient of a California Foundation Fellowship for Biochemical Research. This is contribution no. 5370 from the Norman W. Church Laboratory of Chemical Biology, California Institute of Technology. We are grateful to Dr M. A. Raftery for valuable discussion and advice.

REFERENCES

Axelrod, D., Ravdin, P., Koppel, D. E., Schlessinger, J., Webb, W. W., Elson, E. L. & Podleski, T. R. (1976). *Proc. Nat. Acad. Sci., U.S.A.* **73,** 4594–4598.

Blaurock, A. E. & King, G. I. (1977). *Science,* **196,** 1101–1104.

Blaurock, A. E. & Stoeckenius, W. (1971). *Nature New Biol.* **233,** 152–157.

Cartaud, E. L., Benedetti, L., Cohen, J. B., Meunier, J-C. & Changeux, J-P. (1973). *FEBS Letters,* **33,** 109–113.

Caspar, D. L. D. & Kirschner, D. A. (1971). *Nature New Biol.* **231,** 46–52.

Cohen, J. B., Weber, M., Huchet, M. & Changeux, J-P. (1972). *FEBS Letters,* **26,** 43–47.

Cooley, J. W. & Tukey, J. W. (1965). *Math. Comput.* **19,** 297–301.

DeRosier, D. J. & Moore, P. B. (1970). *J. Mol. Biol.* **52,** 355–369.

Dervichian, D. B. (1964). *Prog. Biophys. Mol. Biol.* **14,** 263–342.

Duguid, J. R. & Raftery, M. A. (1973). *Biochemistry,* **12,** 3593–3597.

Edelstein, S. J., Beyer, W. B., Edelfrawi, A. T. & Edelfrawi, M. E. (1975). *J. Biol. Chem.* **250,** 6101–6106.

Engleman, D. M. (1971). *J. Mol. Biol.* **58,** 153–165.

Erickson, H. P. (1974). *Eighth Internat. Congr. Electron Microscopy, Canberra,* pp. 310–311.

Erickson, H. P. & Klug, A. (1971). *Phil. Trans. Roy. Soc. ser. B,* **261,** 105–118.

Franks, A. (1955). *Proc. Phys. Soc. (Lond.) B,* **68,** 1054–1064.

Furukawa, T. & Furukawa, A. (1959). *Jap. J. Physiol.* **9,** 130–142.

Gibbs, A. J. & Rowe, A. J. (1973). *Nature (London),* **246,** 509–511.

Henderson, R. (1975). *J. Mol. Biol.* **93,** 123–138.

Horne, R. W. & Whittaker, V. P. (1962). *Z. Zellfor. Microsk. Anat.* **58,** 1–22.

Katz, B. & Miledi, R. (1972). *J. Physiol. (London),* **224,** 665–699.

Klug, A. & DeRosier, D. J. (1966). *Nature (London),* **212,** 29–32.

Klymkowsky, M. W., Ross, M. J. & Stroud, R. M. (1977). *J. Cell Biol.,* submitted.

Lesslauer, W., Cain, J. & Blasie, J. K. (1971). *Biochim. Biophys. Acta,* **241,** 547–566.

Lesslauer, W., Cain, J. E. & Blasie, J. K. (1972). *Proc. Nat. Acad. Sci., U.S.A.* **69,** 1499–1503.

Levine, Y. K. & Wilkins, M. H. F. (1971). *Nature New Biol.* **230,** 69–72.

Levitski, A. (1974). *J. Theoret. Biol.* **44,** 367–372.

Lipson, H. & Taylor, C. A. (1958). *Fourier Transforms and X-ray Diffraction*, G. Bell and Sons, Ltd., London.

Luft, J. H. (1961). *J. Biophys. Biochem. Cytol.* **9,** 409–414.

Luzzati, V., Mustacchi, H., Skoulos, A. & Husson, F. (1960). *Acta Crystallogr.* **13,** 660–667.

Markham, R. (1968). *Meth. Virol.* **4,** 503–529.

Marsh, R. E., Corey, R. B. & Pauling, L. (1955). *Biochim. Biophys. Acta*, **16,** 1–34.

Matthews, B. W. (1968). *J. Mol. Biol.* **33,** 491–497.

Michaelson, D., Vandlen, R., Bode, J., Moody, T., Schmidt, J. & Raftery, M. A. (1974). *Arch. Biochem. Biophys.* **165,** 796–804.

Moody, M. F. (1975). *Acta Crystallogr. sect. A*, **31,** 8–15.

Morimoto, H. & Uyeda, R. (1963). *Acta Crystallogr.* **16,** 1107–1119.

Nichol, E. & Potter, L. T. (1973). *Brain Res.* **57,** 508–517.

Pauling, L. & Corey, R. B. (1951). *Proc. Nat. Acad. Sci., U.S.A.* **37,** 729–740.

Reed, K., Vandlen, R., Bode, J., Duguid, J. & Raftery, M. A. (1975). *Arch. Biochem. Biophys.* **167,** 138–144.

Reynolds, E. S. (1963). *J. Cell Biol.* **17,** 208–212.

Rosenbluth, J. (1975). *J. Neurocytol.* **4,** 697–712.

Ross, M. J. & Stroud, R. M. (1977). *Acta Crystallogr. sect. A*, **33,** 500–508.

Takeuchi, A. & Takeuchi, N. (1960). *J. Physiol. (London)*, **154,** 52–67.

Vandlen, R. & Raftery, M. A. (1977). *Arch Biochem. Biophys.*, in the press.

Weill, C. L., McNamee, M. G. & Karlin, A. (1974). *Biochem. Biophys. Res. Commun.* **61,** 997–1003.

Worthington, C. R. & McIntosh, T. J. (1974). *Biophys. J.* **14,** 703–729.

CHAPTER THREE

IMMUNOSPECIFIC IDENTIFICATION AND RECEPTOR STRUCTURE

Clouds, now and then
giving men relief
from constant moon-viewing.

-Basho

INTRODUCTION:

After moving in advance of Dr. Stroud to the University of California at San Francisco in May 1977, I began a series of experi- designed to identify the membrane-bound acetylcholine receptor under negative stain electron microscopy conditions and to analyze the x-ray diffraction derived electron density profiles of receptor membranes (Chapter Two) in terms of direct electron microscopic observations of the identified receptor. The large portion of the receptor projecting above the membrane surface was directly visualized and confirms and extends the analysis used in phasing the continuous x-ray diffraction patterns.

The immunospecific identification of the receptor in negative stain condition with colloidal gold was the first use of the technique under negative stain conditions. The electron dense gold spheres may also be useful as a focussing aid in low-dose, unstained electron diffraction and image studies.

Also, we sought to determine whether or not the large crystalline arrays sometimes found in receptor enriched fractions (Chapter Two) were made up of receptor. Three observations indicate that they are not receptor, (i) they appear different from the receptor in tungstate and uranyl negative-stains (Chapter Five), (ii) they are not labeled by anti-receptor antibodies, and (iii) they occur in membranes of distinctly different overall morphology from the receptor vesicles (Chapter Five). However, it remained a possibility that they preferentially adhered to the carbon support

film and that the substantial asymmetry between the intracellular and extracellular surfaces gives rise to these observed discrepancies.

A closer look at folded membrane sheets (Appendix III) in which both intra- and extracellular membrane surfaces are visualized indicates that this is not the case and the crystalline sheets are not made up of the receptor.

J. Mol. Biol. (1979) **128**, 319–334

Immunospecific Identification and Three-dimensional Structure of a Membrane-bound Acetylcholine Receptor from *Torpedo californica*

MICHAEL W. KLYMKOWSKY AND ROBERT M. STROUD

Department of Biochemistry and Biophysics
University of California at San Francisco
San Francisco, Calif. 94143, U.S.A.

(Received 18 September 1978)

Antibodies, raised against affinity column-purified acetylcholine receptor from *Torpedo californica*, were used as a basis for immunospecific identification of the receptor in membrane fragments. Rabbit and goat anti-receptor antibodies were coupled directly or indirectly *via* goat anti-rabbit antibody to colloidal gold spheres or to ferritin. The labeled membranes were visualized by negative stain electron microscopy, and show that the receptor corresponds to the 85 Å diameter rosette seen in membranes derived from electroplaques.

Electron micrographs of immunospecifically labeled receptor, in the plane perpendicular to the membrane surface, confirm and extend our previous conclusions based on X-ray diffraction analysis, that the molecule extends above the extracellular membrane surface by approximately 55 Å, and little on the cytoplasmic side. Calculated molecular volumes based on X-ray diffraction and electron microscopy indicate that the membrane receptor has a molecular weight in the range of 250,000 to 310,000, a range consistent with current estimates of detergent-solubilized monomer molecular weight.

1. Introduction

Acetylcholine receptors from the nerve–electrocyte synapse of electric fish and the neuromuscular junction of mammals are currently the subject of intensive biochemical characterization (for reviews see Raftery *et al.*, 1975; Karlin *et al.*, 1975; Changeux *et al.*, 1975; Heidmann & Changeux, 1978). The primary basis for the identification of AcChR† has centered on two functional properties; (1) the receptor ligand binding site and (2) the ionophoretic channel. Membrane fragments isolated from *Torpedo marmarota* (or *Electrophorus electricus*), purified by density gradient centrifugation have been shown to respond *in vitro* to cholinergic agonists, increasing permeability to radioactive cations such as ^{22}Na much like the *in vitro* response of post-synaptic membranes (Kasai & Changeux, 1971; Sugiyama *et al.*, 1976; Popot *et al.*, 1976; Hess & Andrews, 1977). These functional membranes have been the subjects of X-ray diffraction analysis (Dupont *et al.*, 1974; Raftery *et al.*,

† Abbreviations used: AcChR, nicotinic acetylcholine receptor; AcChRm, membrane-bound acetylcholine receptor; AcChRp, Triton X100-solubilized and affinity-purified acetylcholine receptor; AbAu, antibody–gold sphere complex; GARF, goat anti-rabbit ferritin conjugate; SDS, sodium dodecyl sulfate; IgG, immunoglobulin G.

© 1979 Academic Press Inc. (London) Ltd.

1974; Ross *et al.*, 1977) and electron microscopy (Nickel & Potter, 1973; Cartaud *et al.*, 1973,1978; Raftery *et al.*, 1974; Ross *et al.*, 1977; Potter & Smith, 1977) in attempts to characterize the three-dimensional structure and organization of the AcChR.

We previously reported electron density profiles perpendicular to the membrane plane for AcChR membranes from *Torpedo californica*, obtained by analysis of X-ray scattering patterns from vesicle suspensions and partially oriented membranes (Ross *et al.*, 1977). Such profiles represent the average distribution of electron density for all of the material present in the sample. SDS/polyacrylamide gel electrophoretograms of membrane material closely resemble patterns derived from detergent-extracted and affinity-purified AcChR (here termed AcChRp) from the same source (Raftery *et al.*, 1975). The other protein impurities are a heterogeneous mixture in low concentrations. Their effect on the X-ray profile is likely to be a second order perturbation since no single component seems to be present at a significant fraction of AcChR density.

The identification of AcChR in electron micrographs of membranes (termed AcChRm) has been open to possible ambiguity. In previous studies the identification of AcChRm under negative stain conditions has been based on circumstantial evidence: (1) a correlation between the number of particles found per square μm of membrane and toxin or ligand site density as measured on postsynaptic membranes; (2) the increasing frequencies of these particles with purification; and (3) the similarities between electron micrographic views of membrane particles and AcChRp particles (Meunier *et al.*, 1974). But specific activities of receptor in purified membranes are rarely greater than 50%, and frequently substantially lower than those found for purified receptor. Either substantial impurities remain unaccounted for in the membranes, even though such fractions are described as being more than 99% rosette filled membranes (Sobel *et al.*, 1977), or the "purified receptor" consists of only a part of the functional molecule as it exists in the membranes. The possibility that 50% of the toxin-binding sites are unavailable in AcChRm or that half of the membrane fragments are inside out and therefore unable to bind toxin can be discounted since toxin-binding activities per unit weight of protein are essentially identical for membranes before and after treatment with detergents (Duguid & Raftery, 1973), a result we have routinely confirmed in our own preparations.

Heidmann & Changeux (1978) have raised the possibility that the solubilized receptor may contain unrelated polypeptides which aggregate with the minimal functional AcChR upon detergent solubilization, and so could explain the differences in observed subunit patterns. Thus comparisons between membrane-bound receptor and solubilized receptor are less than straightforward. Additionally, patterns of affinity labeling differ between membrane-bound and solubilized receptor (Witzemann & Raftery, 1977) indicating that some rearrangement may occur upon solubilization.

This paper reports the use of antibodies directed against solubilized affinity-purified receptor to identify those same components of the receptor molecule in membrane fragments. The antibody–colloidal gold method of Faulk & Taylor (1971) has been adapted for use in negative stain electron microscopy. Its advantages and disadvantages over conventional ferritin conjugate techniques are discussed.

Identification and visualization of the cross-sectional projection of the receptor molecule confirm and extend our earlier conclusions as to receptor shape and molecular volume.

2. Materials and Methods

(a) *Sample preparation and analysis*

Membranes were prepared by the methods of Reed *et al.* (1975) and Sobel *et al.* (1977) from *T. californica* electroplaques. Organ (perfused, frozen and stored as described by Carlson *et al.* (1978)) was supplied by Dr R. Kelly. Organ (10 to 20 g) was broken into small pieces while still frozen and was homogenized at full speed for 5 min at 4°C in a Virtis model 23 homogenizer, modified to allow continuous purging with argon. Phenylmethanesulfonyl fluoride (0·1 mM) and EDTA (1 to 10 mM) were added to all buffers to minimize proteolytic degradation (Raftery *et al.*, 1975). Limited proteolysis still occurred however, as judged by the presence of Coomassie brilliant blue staining material close to the dye-front on SDS/polyacrylamide gel electrophoretograms.

Protein concentrations were measured by the method of Lowry *et al.* (1951) using bovine serum albumin as a standard. A modified Lowry assay (Markwell *et al.*, 1978), designed to be used with membrane proteins and which avoids the interfering effects of sucrose and EDTA, gave protein values 5% above those of the standard procedure. Sucrose (density gradient grade, Schwartz-Mann) concentrations were measured with a Zeiss refractometer. Acetylcholine esterase activity was measured by the method of Ellman *et al.* (1961). SDS/polyacrylamide 10% electrophoretic gels were run following the procedure of Laemmli (1971) and stained with Coomassie brilliant blue R.

Alpha-bungarotoxin (abutx) was purified from crude *Bungarus multicinctus* venom (Sigma or Miami Serpentarium) by the method of Clark *et al.* (1972) as modified by Spencer (1977). [^{125}I]abutx was prepared by lactoperoxidase (Calbiochem) iodination (Marchalonis, 1969). Specific activities ranged from 10^5 to 10^7 cts/nmol toxin. Receptor activity was measured by [^{125}I]abutx binding using the DEAE-disk (Whatman DE52, 2·5 cm diam.) filter assay of Schmidt & Raftery (1973). Dilute toxin solutions had 0·1 mg bovine serum albumin/ml added to prevent toxin adsorption onto glass or plastic tubes. Adsorption was reversible by Triton X100 at concentrations above 0·0025%. Membranes were routinely prepared with specific activities ranging from 2 to 5 nmol toxin bound/mg protein. All membranes were stored at 4°C and used within a period of one to two weeks for microscopy.

Light scattering is inversely proportional to vesicle size (Bangham *et al.*, 1967) and osmotic activity upon the addition of salt was measured as described in Michaelson & Raftery (1974).

Unless otherwise stated all chemicals used were of the highest purity commercially available and were used without further purification. All solutions were filtered through 0·22 μm Millipore type GS filters to sterilize and remove aggregates.

(b) *Electron microscopy*

Electron microscopy was carried out on a Philips EM300 microscope using a liquid nitrogen anti-contamination stage. The accelerating voltage was 80 kV. Samples were placed on thin carbon films prepared by evaporation onto freshly cleaved mica. Carbon films on 400-mesh copper grids were prepared for use by dipping into 95 to 100% ethanol, dried on filter paper and used immediately. Negative staining was done by placing 10 μl of membrane solution onto a grid and allowing it to sit for 1 min. The solution was removed with a piece of torn filter paper touched to the edge, and 20 μl of a negative stain (one of the following: 1% uranyl acetate, pH 4·8; 1% uranyl oxalate, pH 6·5; 2% ammonium molybdate, pH 7; 2% phosphotungstate, pH 7·4, as described in Haschmeyer & Meyers, 1972) was applied, allowed to sit for 1 min, and removed as before. The grids were then dried thoroughly.

(c) *Antibodies and antibody conjugates*

Rabbit antisera raised against AcChRp were kindly provided by Dr S. Froehner. Rabbit anti-AcChRp IgG and pre-immune IgG were provided by Dr M. A. Raftery and T. Claudio (Claudio & Raftery, 1977). Normal rabbit sera was provided by Dr J. Sanes. AcChRp was kindly supplied by Drs G. Reiness, S. Rowe and Z. Hall. Goat anti-AcChRp was the gift

of Drs A. Gordon, C. G. Davis, and I. F Diamond (Gordon *et al.*, 1977). Rabbit anti-mouse IgG was supplied by Dr E. Linney. Normal rabbit and goat sera, goat anti-rabbit sera and goat anti-rabbit IgG ferritin conjugate were purchased from Cappel Labs. All sera were incubated at 60°C for 20 min in order to inactivate complement.

Colloidal gold beads were formed by the reduction of chlorauric acid (J. T. Baker) with trisodium citrate as described by Turkevich *et al.* (1953). Beads with diameters in the range of 20 to 30 nm were formed and stored at 4°C until use. Colloidal gold solutions were filtered through 0·22 μm filters and used directly for antibody–gold complexation. It was noted that while the gold solution passed readily through Millipore filters, it is retained by 0·2 μm Amicon microporous filters. The optimal amount of protein for gold solution stabilization was determined using the method of Horisberger *et al.* (1975) in which a portion (1 to 10 μl) of antibody was added to 100 μl of gold solution and after 1 min 10 μl of 5 M-NaCl was added. If the solution remained red, the beads were stabilized, but *any* bluish-purple color indicated an aggregation of gold particles, due to an insufficient amount of protein. The assay was repeated until the amount of protein needed was determined to within 0·5 μl/100 μl of gold solution (i.e. to within about 1 part in 10).

Large batches (1 to 5 ml) of AbAu were made up by adding gold solution to protein solution. After 1 min the solution was made 1% in polyethylene glycol (20,000 average molecular weight, Sigma) and 0·02% in NaN_3. The solution was refiltered and stored at 4°C until use. After prolonged storage (1 week) the solution was refiltered before use.

All pH adjustments were made with 0·2 M-K_2CO_3 and pH was monitored with Color-pHast^R (Merck, Darmstadt) pH paper. Titration curves were made by stabilizing the gold solution with 1% polyethylene glycol and measuring pH change with added K_2CO_3. Citrate was removed by dialysis against distilled water.

The stability of the antibody–colloidal gold complex was determined by pre-incubating the membranes to be labeled with the same antibody as used to form the AbAu complex. All labeling of membranes by AbAu is abolished when the complex is stable, but labeling is unaffected in cases where the beads are not fully stabilized, i.e. where the protein on-off rate from the gold spheres is significant (see Discussion).

(d) *Membrane tagging*

Double antibody labeling experiments were carried out by first applying membranes to ethanol-prepared grids. Excess membrane solution was removed and a 10-μl drop of the first antibody was added. After standing at room temperature for 10 min this solution was removed, and the grid was washed with 10 mM-phosphate buffer (pH 7·4). Either GARF or AbAu was then applied and allowed to stand at either room temperature or 37°C for 30 min. After this time the grid was washed thoroughly with buffer as before and negatively stained.

For direct labeling experiments the sample was applied to the grid as above, but the AbAu was applied onto a fresh sheet of Parafilm^R (American Can Corp.). The grid was then placed on top of the AbAu drop, covered with a Petri dish, and incubated at room temperature or 37°C for from 30 min to 4 h.

3. Results

(a) *Antibody labeling, specificity and saturability*

Immunospecific activity of the labels was assayed in parallel sets of experiments and controls. Any instability of the AbAu complex or incomplete saturation of the gold spheres was detected in the controls. In experiments where the label-receptor linkage was *via* rabbit anti-receptor antibody, and then through goat anti-rabbit antibody to the electron dense label, the control was to substitute non-immune (rabbit) sera for immune sera in the first membrane labeling step. This eliminated the possibility that normal rabbit serum contains any antibody toward components of the sample. The density of immune labeling by ferritin was typically 10^2 to 10^3 per square μm of membrane. Non-immune controls showed less than one ferritin per square μm

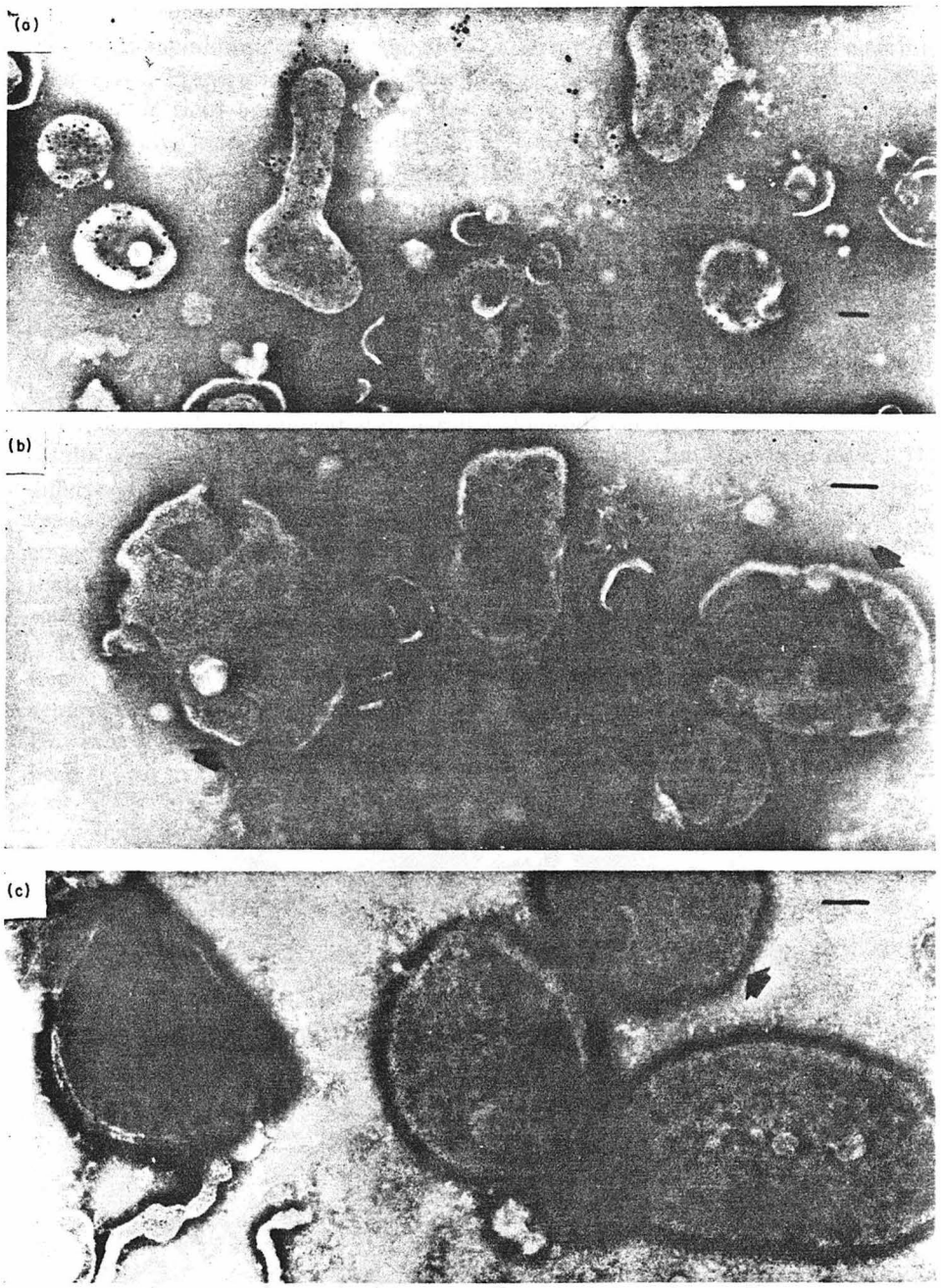


FIG. 1.(a) Negatively stained AcChR vesicles labeled with anti-AcChRp–gold complex. AcChRm-containing vesicles are labeled whereas other membranes are not. The antibody used for labeling in the Figures shown was supplied by Dr S. Froehner. All of the antibodies described in the text gave essentially identical results. Final magnification, 37,500×. Bar represents 100 nm, as it does in all the Figures.

(b) A control experiment in which non-immune serum has been substituted for immune serum in the AbAu complex. Arrows point out the distinctive edge structure of receptor vesicles. Final magnification for (b) and (c) is 60,000×.

(c) Preblocking of membranes with immune sera eliminates subsequent binding of AbAu. Arrow points to the decorated receptor vesicle edge; note the difference upon comparison with the edge in (b).

of AcChR membrane giving a signal-to-noise ratio of >1000:1 on the membranes themselves. Preparations of gold spheres were rejected if the non-immune labeling was greater than one gold sphere per square μm. Properly stabilized AbAu was found to give reproducible results for at least one week after preparation. Goat anti-rabbit conjugates to ferritin or gold showed no labeling of membranes without prior incubation of the membranes with rabbit anti-receptor sera. In direct labeling experiments where the linkage was *via* anti-receptor antibody, specificity and labeling efficiency were assayed in two ways: (1) by the substitution of normal for immune sera (see Fig. 1(a) and (b)) and (2) by pre-incubation of the membranes with immune sera which blocks subsequent labeling by specific conjugates (Fig. 1(c)). Pre-incubation of membranes in normal sera, or immune serum raised against an unrelated antigen had no effect on subsequent immunospecific labeling efficiency.

These controls were repeated in parallel alongside each labeling experiment and no results were accepted unless both controls were satisfied, and showed at least a 100:1 difference between specific and non-specific labeling efficiency. In addition, immunospecific labeling of AcChRm was completely abolished by pre-incubation of AbAu complex with a tenfold excess of AcChRp for 10 hours at 4°C. This demonstrated that there was no significant exchange of antibody–antigen complexes once antibody was bound to gold spheres.

The question as to whether labeling in a membrane can be correlated with a particular structure requires a one-to-one labeling of the structures. This can rarely be achieved due to the physical size and electron dense nature of the antibody conjugates. However, tagging levels approaching total coverage of the membrane surface have been shown in this system in three different ways. (1) By the direct visualization of

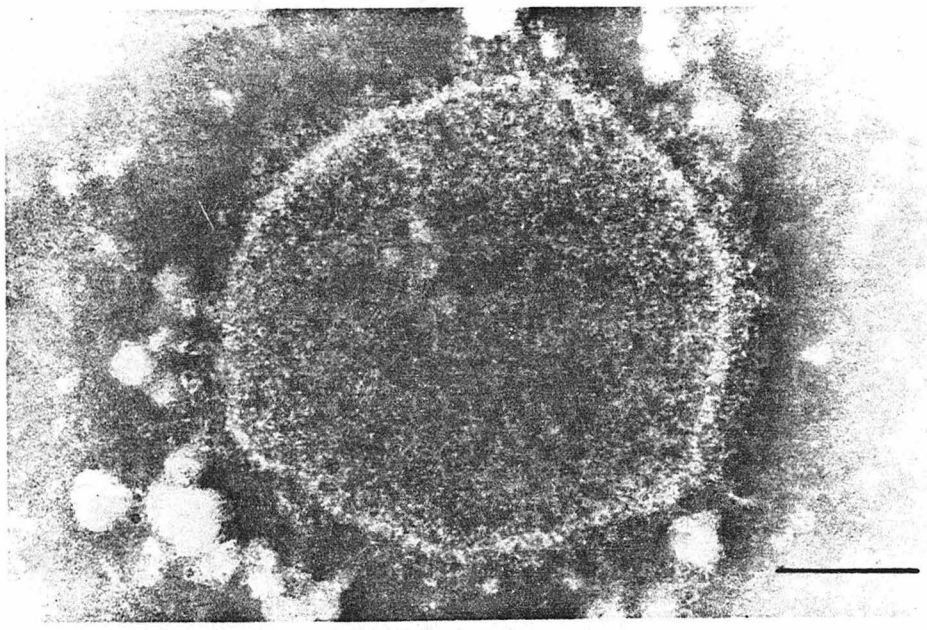


FIG. 2. Receptor vesicle heavily labeled with rabbit anti-AcChRp/GARF. AcChRm images are confused by the presence of antibody and antibody ferritin. Ferritin is 12 nm in diameter. Final magnification, 185,000 ×. Bar represents 100 nm.

antibody totally covering rosette filled membranes (see Fig. 1(c)). Image confusion caused by the antibody, through which receptor rosettes can be seen, is not found on other membrane types. (2) GARF indirect labeling of membranes shows high labeling densities, but the surface is difficult to see clearly, due to the first antibody layer and the similarity in the contrast developed by the negative stain around AcChRm and ferritin (Fig. 2). (3) Using antibody–gold complex, which had first been concentrated in phosphate buffered, polyethylene glycol prewashed S-125 Amicon serum concentrators, in which high levels of gold labeling are attainable (Fig. 1(a)). The labeling density for AbAu is substantially lower than for GARF–antibody conjugate because of the lower concentration of gold spheres, 5×10^{10} per ml or 8×10^{-14} moles per ml (Enüstün & Turkevich, 1963), compared with 10^{-7} to 10^{-9} moles per ml for GARF, as derived from protein concentrations. Nevertheless, the saturability of AcChRm-binding sites by the labels, and the fact that only the rosette structures are labeled, identifies them as the only structures containing AcChRp antigenic determinants (Figs 1(a) and 3).

Heterogeneity in different antisera was shown in preblocking experiments using the three different antibody preparations. Membranes were first incubated for 10 minutes with one of the sera, and then incubated with AbAu. When the same antibody was used in both steps, labeling was abolished ($<0{\cdot}5$ beads per square μm). When both antibodies were from the same species (i.e. rabbit), labeling was reduced significantly (<10 beads per square μm), however, in the case of interspecific antibodies,

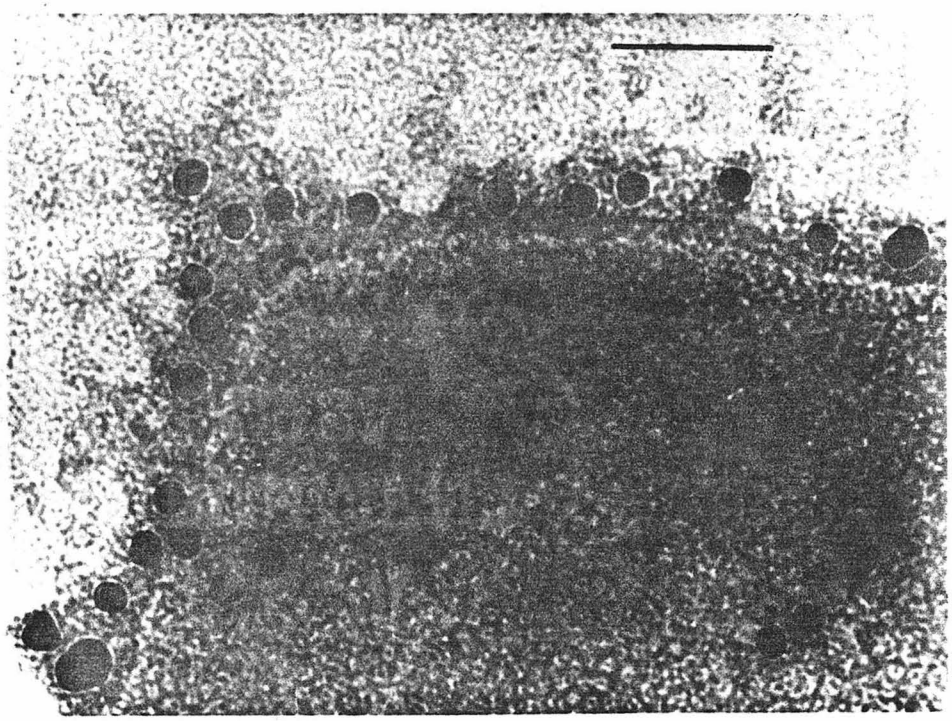


FIG. 3. Higher magnification view of an anti-AcChRp–gold-labeled vesicle, which shows the specific attachment of gold spheres to the AcChRm rosettes. Final magnification, 212,000 ×. Bar represents 100 nm.

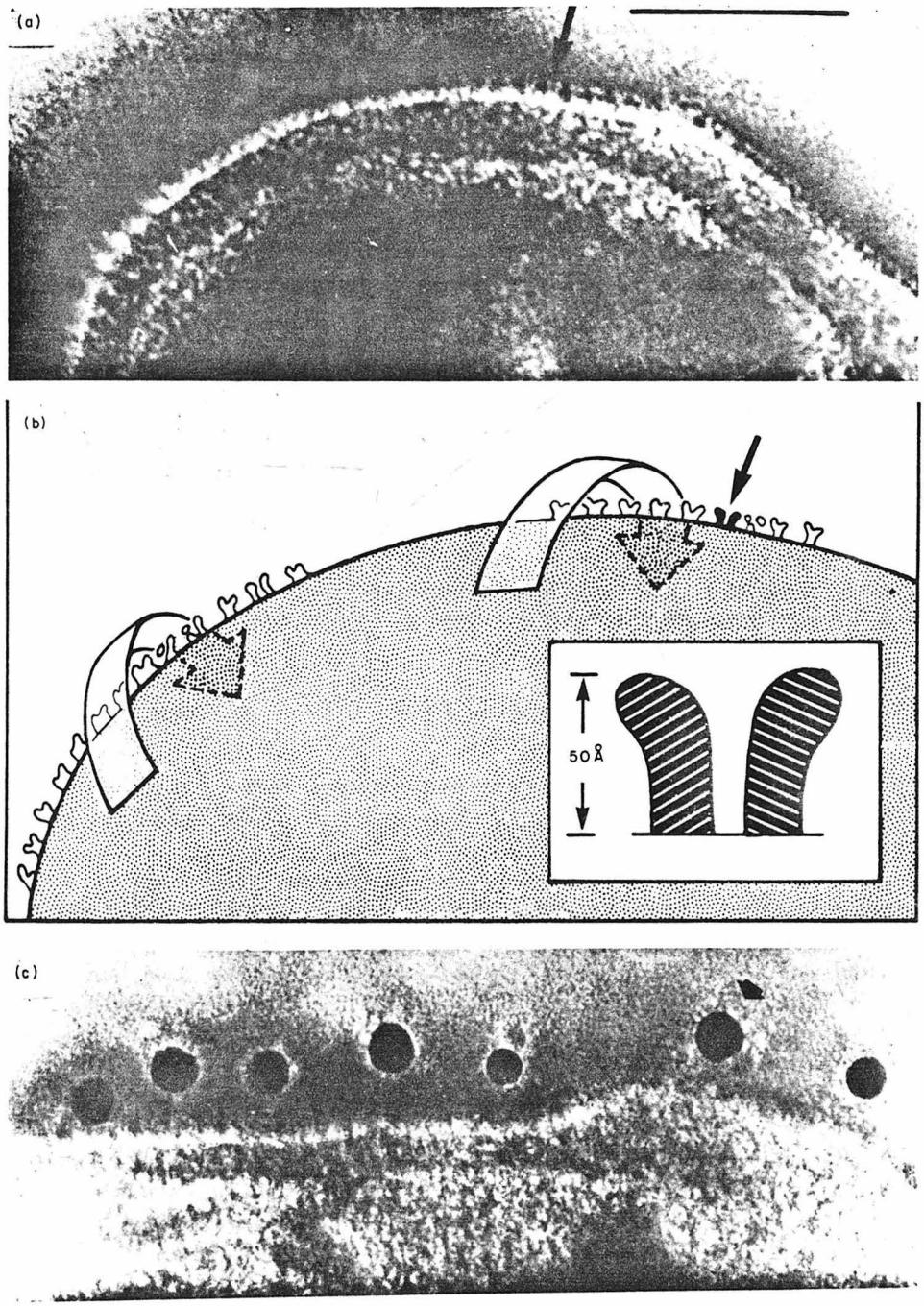


FIG. 4. (a) Negatively stained AcChR vesicle shows the protrusion of AcChRm on one (the synaptic) side of the membrane. Lines of AcChRm are twisted across the vesicle's edge allowing for multiple tilted views of the molecule. At 2 locations (short arrow and the 3 molecules underneath the long arrow) AcChRm molecules are seen oriented so that their axis perpendicular to the membrane surface lies in the microscope's focal plane. Final magnification, 294,000 × for both (a) and (c). Bar represents 100 nm.

(b) A schematic representation of the coiled lines of AcChRm in (a) along with the

(i.e. goat *versus* rabbit and rabbit *versus* goat) the labeling remained high, approximately 100 beads per square μm.

(b) *Cross-sectional projections*

Almost all of the receptor-filled vesicles have a clearly defined edge structure distinct from those of other vesicle types (Figs 3 and 4). These structures are seen with all the negative stains used. Antibody–gold labeling of these structures (Figs 3 and 4(c)) unequivocally identifies the characteristic grommet-like structures as AcChRm. Both the antibody halo surrounding the gold particles and the projecting connection to AcChRm are visible in Figure 4(c). The distances between gold and receptor were typically 100 to 200 Å, consistent with a 180 Å length for antibodies (Sarma *et al.*, 1971). AcChRm extends 55 ± 10 Å above the membrane on the antibody-labeled side in Figure 4.

The labeled side in Figure 4(c) was also labeled by anti-abutx antibody–gold, when the membranes had been pre-treated with abutx. This demonstrates that the receptor extension of 55 Å is on the extracellular surface of the electrocyte, the side to which ligands bind. This is consistent with the thin section studies of Rosenbluth (1975), which showed protrusion of protein by about 60 Å into the synaptic cleft in *T. californica*. The observation of side-view projections, taken with immunospecific labeling provide a direct visualization of the AcChRm profile structure, and confirm the electron density profile previously determined from X-ray diffraction studies (Ross *et al.*, 1977).

(c) *Molecular volume and molecular weight of AcChRm*

The previously reported electron density profile for AcChR membranes was derived by the method of Stroud & Agard (1978) from continuous X-ray scattering from vesicles in solution, and from partially oriented membranes (see Fig. 4 of Ross *et al.*, 1977). The density profiles were previously scaled using the known electron density of water (0·334 e/Å^3), and assuming that the highest peak in the profile corresponded to hydrated protein $\rho\sim0{\cdot}40$ e/Å^3) and phospholipid head groups $\rho\sim0{\cdot}45$ e/Å^3. Thus the highest peak was taken to be $\rho\sim0{\cdot}43$ e/Å^3 (Ross *et al.*, 1977). This basis for scaling led to an electron density of $0{\cdot}38\pm0{\cdot}01$ e/Å^3 immediately above the membrane surface on the synaptic side, corresponding to AcChRm protein and solvent.

Electron micrographs of the edge coupled with a measure of the density of AcChRm on this surface provide an alternate experimental basis for scaling the density profile, which obviates the use of an assumed phospholipid head group electron density. Electron micrographs of the edge view of molecules on the synaptic surface (Fig. 4(a)) were densitometered across the structure and diameters were averaged for several particles. The average external and internal diameters of AcChRm above the membrane were found to be 85 ± 5 Å and 25 ± 5 Å, respectively, in good agreement with those obtained by two-dimensional image reconstructions (Ross *et al.*, 1977), and those obtained by photographic superposition of AcChRm rosettes in unordered membranes, without regard to orientation.

---

molecular projection (insert) of the single AcChRm directly beneath the long arrow in (a) and (b).

(c) This edge-view of AcChRm is immunospecifically labeled by AbAu complex establishing the identity of the characteristic structures schematized in (b). Arrow points out the antibody halo surrounding the gold beads. The connections between gold and membrane can be seen clearly.

The density of receptors in these AcChR membranes has been estimated by counting of particles in electron micrographs (Cartaud *et al.*, 1973,1978), quantitative autoradiography (Salpeter & Eldefrawi, 1973; Fertuck & Salpeter, 1976) and by physiological recording of maximal response to agonists compared with individual AcChR channel conductance (Katz & Miledi, 1972; Anderson & Steven, 1973; Peper *et al.*, 1975) to be 10,000 per square μm or one molecule per 10^4 Å^2. The electron density profile (Fig. 5(c)) was then scaled using this value for the packing density of receptors, the size estimate (above) for single receptors above the membrane surface, and assuming that the electron density outside of the bilayer is due to protein + solvent. The electron density for hydrated protein was taken as $\rho \sim 0{\cdot}40$ e/Å^3; solvent density was 0·334 e/Å^3. The calculated average electron density for protein and solvent above the bilayer was $0{\cdot}367 \pm 0{\cdot}007$ e/Å^3: the phospholipid head group densities are 0·37 and 0·39 and the terminal methyl group region in the center of the bilayer has a density of 0·30 e/Å^3.

The scaled profiles were analyzed in terms of a rotationally symmetric model for AcChRm. The electron densities were analyzed as a linear combination of protein and solvent outside the bilayer, or lipid and protein inside the bilayer, to derive the models shown in Figure 5. The central ionophoretic channel was assumed to narrow from the observed value of 25 Å on the extracellular side to 10 Å diameter inside the bilayer in order to account for the experimentally observed size selectivity of the channel which has been shown to pass ions as large as isopropylammonium, requiring an approximately 10 Å diameter channel (Furukawa & Furukawa, 1959).

The expression relating electron density to radii in Å of the cross section of protein $R_0(h)$. $R_i(h)$ parallel to the membrane was:

$$10^4 \frac{(\rho_0(h) - \rho_s)}{(\rho_p - \rho_x(h))} = (R_0(h)^2 - R_i(h)^2)\pi ,$$

where h is the location normal to the membrane plane, ρ_x is 0·334 e/Å^3 outside the

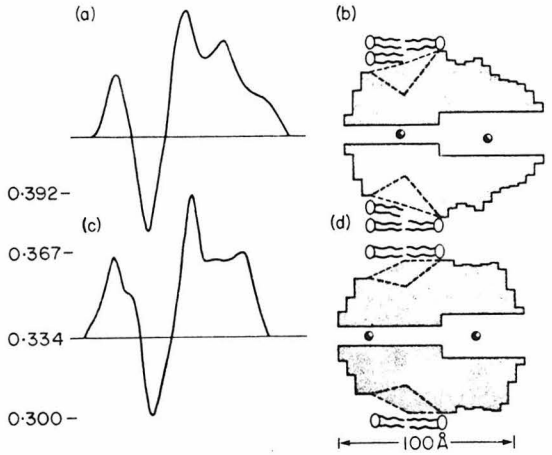


FIG. 5. Electron density profile structures determined from vesicles in solution (a) to a resolution of 11 Å and from partially oriented membranes (c) to a resolution of 6·5 Å as shown alongside cylindrically symmetric models derived from the diffraction data. Spheres in (b) and (d) represent hydrated sodium ions drawn to scale. Density profiles and models and shown in the same orientation and at the same scale.

bilayer, and equal to lipid electron densities within the bilayer, ρ_s is the solvent density of 0·334 e/Å^3, ρ_p is the hydrated protein density taken as 0·40 e/Å^3, and ρ_0 is the observed density. Radii were calculated at 5 Å intervals perpendicular to the membrane surface to obtain the models shown in Figure 5(b) and (d).

Densities for terminal methyl groups in membranes vary from about 0·18 e/Å^3 (Engelman, 1971) to 0·27 e/Å^3 (for myelin: Caspar & Kirschner, 1971). The variability of this value makes the actual protein/lipid ratio in the center of the bilayer somewhat uncertain. The dotted lines represent the radii derived from using these two values for lipid terminal groups, with the observed density of 0·30$\pm$0·01 e/Å^3 for AcChR membranes.

The molecular volumes of AcChRm calculated from the two profiles shown in Figure 5(b) and (d) are 380,000$\pm$51,000 and 347,000$\pm$47,000 Å^3, respectively. The value for partial specific volume of AcChR, from the known amino acid composition was calculated to be 0·74 cm^3/g (Changeux *et al.*, 1975) in agreement with the value derived by Matthews (1968) from crystallographic data for soluble proteins. Thus the molecular weight of the AcChRm particle must lie in the range of about 250,000 to 310,000, of which about half lies above the membrane surface on the synaptic side.

4. Discussion

(a) *Immunospecific labeling*

The two methods used for the immunospecific identification of AcChRm both involved the use of electron dense particles, either the iron storage protein ferritin or colloidal gold beads, and anti-AcChRp antibodies. Both labels have distinct drawbacks. Ferritin must be covalently coupled to the antibody molecule and this chemical reaction results in a substantial loss of activity, a severe drawback with scarce material. Ferritin tends to bind non-specifically to carbon support films. In addition, the contrast from ferritin's iron oxide core can be closely matched by that produced by negative staining of highly reliefed surfaces, such as that of receptor membranes (see Fig. 2). Antibody inactivation can be avoided by using an indirect method, i.e. recognizing the first antibody with a second, more readily available antibody coupled to ferritin. The indirect method, however, suffers from both resolution and imaging limitations. The effective length of the antibody label is doubled and the molecule to be identified is obscured by an additional layer of antibody (see Fig. 2).

Colloidal gold beads overcome the problem of chemical inactivation. They are easily recognized, and have very low affinity for carbon films. However, the ionic nature of the protein attachment to the gold particle results in an inherently less stable label. In their model for the stabilization of gold sols by protein, Enüstün & Turkevich (1963) postulate that the hydrophobic surface of the gold spheres is covered by a layer of citrate ion which, in turn, produces an electrical double layer in the solvent around each sphere. Adsorbed protein acts as the double layer in stabilized gold and prevents hydrophobic aggregation. Reducing the citrate concentration allows the hydrophobic interactions to predominate and the gold precipitates, just as increasing the ionic strength of the solution causes the double layer to collapse, also resulting in precipitation. Between these two extremes, the strength of the double layer and therefore the stability of the protein–gold complex depends critically upon solution conditions. With increasing ionic strength the instability of the complex

with respect to protein exchange is readily apparent, as the resultant non-specific binding of gold spheres to membranes cannot be inhibited by antibody. Highly charged structures (e.g. chromatin and histones) also tend to destabilize the antibody–gold complex (V. Foe, personal communication). The importance of control experiments in this system can hardly be overestimated since even in its destabilized state the antibody–gold complex does not bind to carbon films. Only membranes are tagged, giving the appearance of specificity.

Under properly stabilized conditions however, the gold sphere–antibody technique is highly specific and reproducible. This technique is of advantage in that it produces no mass confusion over the specimen, (except in the region immediately around the spheres). This could be of advantage in high resolution low dose imaging, where the gold spheres provide both a means of rapidly identifying an unstained specimen of little intrinsic contrast, and a means of rapid focusing on a region of the specimen, obviating the necessity for the evaporated gold islands used by Unwin & Henderson (1975) in their studies of purple membrane from *Halobacterium halobium*.

The experiments reported here show that the rosette-filled membranes contain densely packed acetylcholine receptor molecules and can be saturated with antibody-label. Whether these membranes contain *only* AcChRm remains an open question. In the electron microscope essentially all the rosette-filled membranes contain no other visible structures. Since AcChRm extends 55 Å above the membrane surface, it has a characteristic appearance clearly different from other types of structures. However, the preparations do contain both non-membranous material and non-receptor membranes. These impurities lower the specific (abutx binding) activity of the membrane fractions, which are rarely above 50% of that for AcChRp. Denaturing gels of the membrane fractions show similar patterns to those seen for AcChRp (Raftery *et al.*, 1975), but contain a number of added bands, at lower intensity. These facts are consistent with the idea that AcChRm may be the only protein in rosette-filled membranes. Alternatively, reports that 99% of the membranes in fractions containing about 60% of the specific activity of AcChRp (Sobel *et al.*, 1977) are filled with receptor rosettes suggest that some impurities or proteins not co-purified with AcChRp may well exist within the receptor membranes, perhaps even as part of the rosettes. The inability, despite repeated attempts, to purify receptor membranes to greater than 60% of the specific activity of AcChRp supports this view. If such proteins were directly associated with AcChRm one might expect to see a structure of larger volume than that observed for AcChRp. That this is not the case suggests that impurities are contained elsewhere.

The results of toxin-binding experiments on intact and Triton-solubilized membranes (Duguid & Raftery, 1973) and our own osmotic activity measurements, and agonist response measurements (Kasai & Changeux, 1971; Sugiyama *et al.*, 1976; Popot *et al.*, 1976; Hess & Andrews, 1977) confirm that the vesicles are right side out, as does the binding of anti-toxin antibodies to toxin-saturated membranes. Thus the rosette structures seen in negatively stained membranes represent the outside surface, of one side of a vesicle. The inside surface of receptor vesicles (or the outer surface of vesicles which are inside out) may look entirely different in negative stained images.

The inherent asymmetry of the molecule makes the extracellular side simple to identify. But, whether antibody is raised to both sides of the receptor membrane, and thus whether or not AcChRp represents the entire receptor–ionophore complex, still

remains unanswered. Recent studies have disagreed (Karlin *et al.*, 1978; Tarrab-Hazdai *et al.*, 1978) on whether the anti-AcChRp antibody recognizes the intracellular surface of receptor membranes. The observation that different anti-AcChRp preparations do not completely block the binding of others offers a partial explanation based on antibody heterogeneity of the different results.

(b) *The electron density profile*

The electron density profiles for AcChR membranes obtained by Ross *et al.* (1977), were previously scaled according to an assumed maximum density for phospholipid head groups and protein for the highest peak in the profile. The known density of solvent provides a constant fiducial point in the scale. The current scaling of the profile is based on experimental observation. The highest peak in the higher resolution profile (Fig. 5(c)) is 0·39 e/Å^3 (close to that in myelin membranes; Caspar & Kirschner, 1971) where it was previously assumed to be 0·43 e/Å^3. The maximum electron density for phospholipid head groups is about 0·45 e/Å^3 for lecithin bilayers (Engelman, 1971), but is only 0·39 to 0·40 e/Å^3 in myelin (Caspar & Kirschner, 1971). Presence of cholesterol or other neutral lipids thus alters the peak densities in the head group region. Analysis of the lipids in AcChR membranes has shown them to contain: 25% (by weight) neutral lipid (Michaelson & Raftery, 1974; or 20% cholesterol, 70% phospholipid (Schiebler & Hucho, 1978). In myelin the cholesterol content is 18% (by weight) of total lipid (Antilio *et al.*, 1966; O'Brian *et al.*, 1967; MacBrinn & O'Brian, 1969) though protein content is much lower (about 10% by vol.) than in AcChR membranes. Thus, the obtained density in the highest peak (0·39 e/Å^3) is entirely consistent with the known chemical composition. The lower density of 0·37 e/Å^3 for head groups on the other side of the membrane is presumably due to asymmetry of protein and lipid in the membranes. The profile in Figure 5(c) was from X-ray data to a minimum interplanar spacing of 13 Å. By the Rayleigh criterion the resolution is nominally 6·5 Å for a one-dimensional structure profile. This should be enough to resolve asymmetry in the bilayer itself, though the extremities of the profile are most subject to resolution limitation effects which may produce some artifactual diminution of the cytoplasmic peak.

The fact that AcChRm projects little beyond the cytoplasmic side of the bilayer implies that, even in the case of a membrane stained on both sides, 80 to 90% of the contrast in negative stain in-plane images is generated on the synaptic face. Thus, the dimensions subsequently used in scaling the electron density profile on the protein-rich side of the membranes are based on electron microscopy of the same surface. Errors in parameters used for scaling the profile are reflected in a final error of $\pm 10\%$ in molecular weight of AcChRm.

(c) *Molecular dimensions of AcChRm*

The molecular weight of the receptor–ionophore complex (AcChRm) limits the possible arrangements of constituent subunits. The values derived here are also quite close to the current values for AcChRp derived by osmometry (270,000, Martinez-Carrion *et al.*, 1975), chemical crosslinking and SDS/polyacrylamide gel electrophoresis (260,000, Bieseker, 1973; 270,000, Hucho *et al.*, 1978), and deuterium oxide density matching sucrose velocity sedimentation (250,000 Reynolds & Karlin, 1978).

The similarity between membrane-bound receptor and the detergent-solubilized receptor molecular weights makes it seem unlikely that a radical rearrangement

occurs upon solubilization. Fortuitously aggregated polypeptides should result in larger molecular weights for detergent-solubilized material. Alternatively, the impurities which may exist with the receptor in the membrane may adhere to the receptor complex upon solubilization, although this would leave the question as to why the specific activities for membrane-bound receptor are lower than for AcChRp unanswered. The question as to what, in fact, constitutes the functional receptor molecule awaits the demonstration of the minimal system of component subunits which will fully parallel *in situ* receptor response. Hazelbauer & Changeux (1974) and Schiebler & Hucho (1978) have reported the reconstitution of functional receptor from detergent-solubilized material. In the latter case, the receptor is a complex oligomer of 270,000 molecular weight with four distinct subunits. However, a minimal function system has yet to be determined.

Considering both molecular volumes and reconstitution experiments the receptor molecule as detergent-solubilized, traverses the membrane and includes both the receptor and the ionophore. Even if these two functionalities can be separated, a combined molecular weight for them both of about 280,000 is indicated. The molecular symmetry within AcChRm is limited by this value. The lattices of particles seen in preparations of AcChR membranes often appear to have approximately 60° angles, suggestive of 3-fold or 6-fold symmetry to the lattice. Since the lattice contains only one particle per unit cell (Cartaud *et al.*, 1973; Ross *et al.*, 1977) the lattice symmetry *must* arise from and can be no higher than the symmetry within the AcChRm particle. The 280,000 molecular weight and the fact that the smallest subunit of AcChR is ~40,000 implies that the receptor cannot have an hexagonal lattice, or 6-fold internal symmetry unless this is the only subunit type present in AcChRm. Presence of two and only two types of subunits in AcChRm would imply no more than 3-fold symmetry to the particle. However, even this seems unlikely. The immunospecific antibodies used here were made against AcChRp, which contains at least four subunit types. We observed no evidence for immuno labeling of any other particles than the regular rosettes of AcChRm. If all four subunits are part of the functional AcChRm, then the AcChRm particle can have no true internal symmetry. Correspondingly, image reconstructions of the in-plane lattices of AcChRm do not indicate internal symmetry (Ross *et al.*, 1977), and assumption of any lattice symmetry averaging procedures would lend bias away from the truth, rather than towards it.

This work was carried out with the support of the National Institutes of Health grant number GM 24485 and the National Science Foundation grant number PCM77-25407. One of the authors (M. W. K.) is a California Foundation for Biochemical Research Fellow and the other (R. M. S.) is a Sloan Foundation Fellow. We are grateful to Drs S. Froehner, M. A. Raftery, T. Claudio, A. Gordon, I. Diamond, Z. Hall, G. Reiness, J. Sanes, R. Kelly, J. Deutsch, V. Foe, E. Linney and D. McKay for materials and valuable discussion and advice. (M. W. K.) is a pre-doctoral student at the California Institute of Technology.

REFERENCES

Anderson, C. R. & Steven, C. F. (1973). *J. Physiol.* **235**, 655–692.
Antilio, L. A., Norton, W. T. & Terry, R. D. (1966). *J. Neurochem.* **13**, 213–222.
Bangham, A. D., Degier, J. & Grevelle, G. D. (1967). *Chem. Phys. Lipids*, **1**, 225–246.
Bieseker, G. (1973). *Biochemistry*, **12**, 4403–4409.
Carlson, S. S., Wagner, J. A. & Kelly, R. B. (1978). *Biochemistry*, **17**, 1188–1199.
Cartaud, J., Benedetti, E. L., Cohen, J. B., Meunier, J. C. & Changeux, J.-P. (1973). *FEBS Letters*, **33**, 109–113.

Cartaud, J., Benedetti, E. L., Sobel, A. & Changeux, J.-P. (1978). *J. Cell. Sci.* **29**, 313–337.
Caspar, D. L. D. & Kirschner, D. A. (1971). *Nature New Biol.* **231**, 46–52.
Changeux, J.-P., Benedetti, E. L., Bourgeouis, J.-P., Brisson, A., Cartaud, J., Devaux, P., Grunhagen, H., Moreau, M., Popot, J.-C., Sobel, A. & Weber, M. (1975). *Cold Spring Harbor Symp. Quant. Biol.* **40**, 211–230.
Clark, D. G., MacMurchie, D. D., Elliot, E., Wolcott, R. G., Landel, A. M. & Raftery, M. A. (1972). *Biochemistry*, **11**, 1663–1668.
Claudio, T. & Raftery, M. A. (1977). *Anal. Biochem.* **181**, 484–489.
Duguid, J. R. & Raftery, M. A. (1973). *Biochemistry*, **12**, 3593–3597.
Dupont, Y., Cohen, J. B. & Changeux, J.-P. (1974). *FEBS Letters*, **40**, 130–133.
Ellman, G. L., Courtney, K. D., Andres, V. Jr & Featherstone (1961). *Biochem. Pharmacol.* **7**, 88–95.
Engleman, D. M. (1971). *J. Mol. Biol.* **58**, 153–165.
Enüstün, B. V. & Turkevich, J. (1963). *J. Amer. Chem. Soc.* **85**, 3317–3328.
Faulk, W. P. & Taylor, G. M. (1971). *Immunochemistry.* **8**, 1081–1083.
Fertuck, H. C. & Salpeter, M. M. (1976). *J. Cell. Biol.* **69**, 114–155.
Furukawa, T. & Furukawa, A. (1959). *Japan. J. Physiol.* **9**, 130–142.
Gordon, A. S., Davis, C. G. & Diamond, I. (1977). *Proc. Nat. Acad. Sci., U.S.A.* **74**, 262–267.
Haschmeyer, R. H. & Meyers, R. J. (1972). In *Principles and Techniques of Electron Microscopy* (Hayat, M. A., ed.), vol. 2, van Nostrand Reinhold, New York.
Hazelbauer, G. L. & Changeux, J.-P. (1974). *Proc. Nat. Acad. Sci., U.S.A.* **71**, 482–486.
Hess, G. P. & Andrews, J. P. (1977). *Proc. Nat. Acad. Sci., U.S.A.* **74**, 482–486.
Heidmann, T. & Changeux, J.-P. (1978). *Annu. Rev. Biochem.* **47**, 317–357.
Horisberger, M., Rosset, J. & Baurer, H. (1975). *Experientia*, **31**, 1147–1149.
Hucho, F., Bandidi, G. & Suarez-Isla, B. A. (1978). *Eur. J. Biochem.* **83**, 335–340.
Karlin, A., Weill, C. L., McNamee, M. G. & Valderrama, R. (1975). *Cold Spring Harbor Symp. Quant. Biol.* **40**, 203–209.
Karlin, A., Holtzman, E., Valderrama, R., Damle, V., Hsu, K. & Reyes, F. (1978). *J. Cell. Biol.* **76**, 577–592.
Kasai, M. & Changeux, J.-P. (1971). *J. Membr. Biol.* **6**, 1–23.
Katz, B. & Miledi, R. (1972). *J. Physiol.* **224**, 665–699.
Laemmli, U. K. (1971). *Nature (London)*, **227**, 680–685.
Lowry, O. H., Rosebrough, N. J., Farr, A. L. & Randall, R. J. (1951). *J. Biol. Chem.* **193**, 265–275.
MacBrinn, M. C. & O'Brien, J. S. (1969). *J. Neurochem.* **15**, 7–12.
Marchalonis, J. J. (1969). *Biochemistry*, **113**, 299–305.
Markwell, M. A., Hass, S. M., Bieber, L. L. & Tolbert, N. E. (1978). *Anal. Biochem.* **87**, 206–210.
Martinez-Carrion, M., Sator, V. & Raftery, M. A. (1975). *Biochem. Biophys. Res. Commun.* **65**, 129–137.
Matthews, B. W. (1968). *J. Mol. Biol.* **33**, 491–497.
Meunier, J.-C., Sealock, R., Olsen, R. & Changeux, J.-P. (1974). *Eur. J. Biochem.* **45**, 371–394.
Michaelson, D. M. & Raftery, M. A. (1974). *Proc. Nat. Acad. Sci., U.S.A.* **71**, 4768–4772.
Nickel, E. & Potter, L. T. (1973). *Brain Res.* **57**, 508–517.
O'Brian, J. S., Sampson, E. L. & Stern, M. B. (1967). *J. Neurochem.* **14**, 357–365.
Peper, K., Dreyer, F. & Muller, K. D. (1975). *Cold Spring Harbor Symp. Quant. Biol.* **40**, 187–193.
Popot, J. L., Sugiyama, H. & Changeux, J.-P. (1976). *J. Mol. Biol.* **106**, 469–483.
Potter, L. T. & Smith, D. S. (1977). *Tiss. Cell.* **9**, 585–594.
Raftery, M. A., Bode, J., Vandlen, R., Michaelson, D., Deutsch, J., Moody, T., Ross, M. J. & Stroud, R. M. (1974). In *Protein–Ligand Interactions*, Konstanz, Germany.
Raftery, M. A., Vandlen, R. L., Reed, K. L. & Lee, T. (1975). *Cold Spring Harbor Symp. Quant. Biol.* **40**, 193–202.
Reed, K., Vandlen, R., Bode, J., Duguid, J. & Raftery, M. A. (1975). *Arch. Biochem. Biophys.* **167**, 138–144.
Reynolds, J. A. & Karlin, A. (1978). *Biochemistry*, **17**, 2035–2038.

Rosenbluth, J. (1975). *J. Neurocytol.* **4**, 697–712.
Ross, M. J., Klymkowsky, M. W., Agard, D. A. & Stroud, R. M. (1977). *J. Mol. Biol.* **116**, 635–659.
Salpeter, M. M. & Eldefrawi, M. E. (1973). *J. Histochem. Cytochem.* **21**, 769–778.
Sarma, V. R., Davies, D. R., Labaw, L. W., Silverton, E. W. & Terry, W. D. (1971). *Cold Spring Harbor Symp. Quant. Biol.* **36**, 413–419.
Schiebler, W. & Hucho, F. (1978). *Eur. J. Biochem.* **85**, 55–63.
Schmidt, J. & Raftery, M. A. (1973). *Anal. Biochem.* **52**, 349–354.
Sobel, A., Weber, M. & Changeux, J.-P. (1977). *Eur. J. Biochem.* **80**, 215–224.
Spencer, S. A. (1977). Ph.D. Thesis, California Institute of Technology.
Stroud, R. M. & Agard, D. A. (1979). *Biophys. J.* **25** in the press.
Sugiyama, H., Popot, J. L. & Changeux, J.-P. (1976). *J. Mol. Biol.* **106**, 485–496.
Tarrab-Hazdai, R., Geiger, B., Fuchs, S. & Amsterdam, A. (1978). *Proc. Nat. Acad. Sci., U.S.A.* **75**, 2497–2501.
Turkevich, J., Stevenson, P. C. & Hillier, J. (1953). *J. Phys. Chem.* **57**, 670–673.
Unwin, P. T. N. & Henderson, R. (1975). *J. Mol. Biol.* **94**, 425–440.
Witzemann, V. & Raftery, M. A. (1977). *Biochemistry*, **16**, 5862–5868.

CHAPTER FOUR

PROTEASES AS PROBES OF RECEPTOR AND MEMBRANE STRUCTURE

Compression cannot break, A center so congealed;
The tool can chip no flake: The core lies sealed.

-from The Adamant
by Theodore Roethke

INTRODUCTION

Protease digestion has long been a useful probe of the structure of membrane proteins. In the Fall of 1978 I began a series of experiments to examine the effects of various proteases on the acetylcholine receptor. This work is described in Part I of this chapter. The novel morphological changes in receptor vesicles brought on by proteolysis were hard to understand using only negative-stain techniques, but by collaborating with Dr. John E. Heuser (Physiology Dept., UCSF) in using his rapid-freeze, deep-etch, rotary shadowing techniques (2,3), we were able to clarify the process of the change. (These images are presented as stereo pairs and should be viewed using a pocket stereo viewer.)

A month after our manuscript (Part I) had been sent off for publication, a paper by Bartfeld and Fuchs (1) appeared which described the effects of trypsin digestion of detergent solubilized and affinity purified receptor. While largely complementary, some discrepancies (namely the nature of the limit digest polypeptides) did exist between the two. To resolve these possible conflicts, a series of experiments were carried out to define the effects of detergent solubilization on the trypsin digestion patterns. This work is presented as Part II of this chapter.

References:

1. Bartfeld, D. & S. Fuchs (1979). Biochem. Biophys. Res. Comm. 89, 512-519.

2. Heuser, J.E., T.S. Reese, M.J. Dennis, L.Y. Jan, Y.N. Jan, & L. Evans (1979). J. Cell Biol. 81, 275-300.

3. Heuser, J.E. & S.R. Salpeter (1979). J. Cell Biol. 82, 150-173.

PART I - PREPRINT

PROTEASE EFFECTS ON THE STRUCTURE OF ACETYLCHOLINE RECEPTOR MEMBRANES FROM TORPEDO CALIFORNICA ELECTROPLAQUES

Michael Wm. Klymkowsky*

John E. Heuser**

Robert M. Stroud***

*Division of Biology
California Institute of Technology
Pasadena, California 91125, USA

**Department of Physiology

***Department of Biochemistry & Biophysics
University of California, at San Francisco
San Francisco, California 94143, USA

ABSTRACT:

Protease digestion of acetylcholine receptor-rich membranes derived from Torpedo californica electroplaques by homogenization and isopycnic centrifugation results in dramatic changes in the morphology of the normally 0.5-2 micron diameter spherical vesicles when observed by either negative-stain or freeze fracture electron microscopy. Removal of peripheral, apparently non-receptor polypeptides by alkali stripping (Neubig, et. al. (1979) PNAS 76, 690-694), increased sensitivity of the acetylcholine receptor membranes to the protease trypsin as indicated by SDS-gel electrophoretic patterns and the extent of morphologic change observed in vesicle structure. Trypsin digestion of alkali-stripped receptor membranes results in complete degradation of all four receptor subunits without appreciably changing either the appearance of the receptor particles in negative-stain electron micrographs or affecting their ability to bind α-bungarotoxin specifically. Trypsin digestion does not substantially alter the sedimentation value of detergent solubilized receptor. The protease induced morphological transformation of receptor membranes is unaffected by whether the receptor exists as a monomer or as a disulfide bridged dimer.

INTRODUCTION:

Acetylcholine receptor membranes, isolated from the electrogenic tissue of Torpedo and Narcine, are unique systems ideally suited for the study of the structural organization of nicotinic, neuromuscular-type synapses, since the entire innervated surface of their electrocytes are densely packed with acetylcholine receptors. They offer a more readily accessible system than the limited synaptic endplate regions of muscle for the isolation of specialized post-synaptic membrane. Biochemical analysis and electron microscopy have shown that the post-synaptic membranes can be separated from the basal lamina, and much of the underlying cytoskeleton, uninnervated electrocyte and other cellular membranes by homogenization and isopycnic centrifugation, and that these membranes respond to agonist much like the in vivo post-synaptic membrane (9, 14).

Conventionally prepared receptor-enriched membrane fractions have receptor specific activities (nanomoles α-bungarotoxin (αbutx) bound per milligram protein) of at most one-half that of the solubilized, affinity purified receptor, and a more complex sodium dodecyl sulfate-polyacrylamide gel electrophoretic (SDS-PAGE) banding pattern. The complexity of these SDS-PAGE patterns can be greatly reduced by alkali-treatment (27, 10, this work) of the receptor membranes which removes a number of peripheral proteins, yet leaves the receptor functional. Such alkali-treated preparations contain less than 10% non-receptor protein by gel electrophoresis (27, 10, this work).

The work of Heuser & Salpeter (16) on gently sheared membranes in which synaptic morphology is largely preserved reveals a highly structured organization of the Torpedo neuro-electrocyte synapse, which

includes the receptor molecules within the post-synaptic membrane. Basal lamina and cytoskeletal attachment sites on the post-synaptic membranes are evident. Remnants of the post-synaptic membrane organization are visible in freeze-etch micrographs of non-alkali treated receptor-rich membranes (4) and may reflect the presence of structural proteins other than receptor.

Receptor-enriched membranes have been characterized structurally by both x-ray diffraction and electron microscopic analysis (9, Chapter Two, Chapter Three, 3, 4, 28, 30, 32). Through immunological labeling the membrane-bound receptor has been identified as a rivet-like molecule of length 11 nm with a maximum in-plane diameter 8.5 nm, which extends above the post-synaptic membrane into the synaptic cleft by approximately 5 nm and corresponds to the 9 S, 260,000 molecular weight monomer (Chapter Three).

We report here that proteolytic digestion induces a radical structural transformation in acetylcholine receptor membranes. The degree of susceptibility of the membrane proteins to protease digestion is variable between preparations, but parallels the degree of structural transformation. Even when proteolytically degraded, such that few polypeptides of molecular weight greater than 30,000 remain, the receptor molecule continues to bind α-bungarotoxin specifically and remains a high molecular weight (9 S) aggregate.

MATERIALS & METHODS:

Membrane Preparation and Characterization.

Membranes enriched in acetylcholine receptor were prepared from freshly killed and dissected Torpedo californica electroplaques (Pacific BioMarine) which had been cut into small (10 g) pieces after dissection, immediately frozen in liquid nitrogen, and stored at 90°C until use. Receptor-rich membranes were prepared by a modification of the procedure of Reed, et al. (31). Membranes were prepared by homogenization in argon-saturated 1 M NaCl, 50 mM Tris, 10 mM (ethylenedinitro)-tetra-acetic acid (EDTA), 10 mM ethyleneglycol-bis-(β-amino-ethyl ether)N,N'-tetraacetic acid (EGTA), and 0.1 mM phenylmethyl sulphonyl fluoride (PMSF) pH 7.4 (H buffer). Receptor was prepared in dimeric form by the addition of 10 mM N-ethyl maleimide (NEM) to the homogenization buffer (5), and in monomeric form by its omission. Dimeric receptor was converted to monomeric in certain experiments by reduction with 5 mM dithiotheritol (5 h, 4°C) followed by 10 mM NEM. Monomers formed in either way have identical properties.

After a low speed centrifugation to remove debris (10 minutes, 5000 g) the membranes were pelleted (60 minutes, 100,000 g). The membranes were then resuspended by dounce homogenization into 1 mM EDTA 0.1 mM PMSF, (pH 8.0) the remaining cellular debris spun out as above, and the membranes repelleted. At this point, the membranes were either resuspended in 28% w/w sucrose and run on a 38% → 29% w/w sucrose gradient in 10 mM Na phosphate, 1 mM EDTA, 1 mM EGTA pH 7.4 (gradient buffer) to provide conventional membranes or alternatively, the membranes were base-treated

(27) by being resuspended in distilled water and brought to pH 11 with 0.5% NaOH. After 1 hour at room temperature, the membranes were collected by centrifugation, then resuspended in 28% sucrose in gradient buffer and run on a 36% → 29% w/w sucrose gradient.

Membranes were characterized by assaying for protein, αbutx binding, and esterase activity as described previously (Chapter Three). d-Tubocurarine was from CalBiochem, all other reagents were of the highest purity commercially available.

Membranes were kept at 4°C or on ice at all times and used for experiments within one week. Membranes were stored in 10 mM Na phosphate, 1 mM EDTA, 0.02% NaN_3, pH 7.4. Even though the membranes had been washed extensively, and commonly contain greater than 90% receptor by gel electrophoretic analysis, the continued presence of endogenous proteases is revealed in the appearance of new polypeptides over time (Appendix II).

Conventionally prepared membranes were alkali-stripped by either first collecting them by centrifugation and resuspending them in doubly distilled water at 4°C or by dilution directly out of the gradient buffer into about 9 volumes of distilled water, and brought at once to pH 11-11.2 with 0.5% NaOH in a stirred cell. Membranes were either pelleted immediately by centrifugation for 30 min at 100,000 g at 4°C, or incubated at room temperature for 1 hour before centrifugation and

neutralization. Polypeptides released by alkali-stripping were recovered from the supernatant by trichloroacetic acid precipitation or by vacuum dialysis using colloidion bags (Schleicher & Schuell) with a 25,000 dalton pore retention size.

Linear SDS-PAGE (10%) was performed as described by Laemmli (22) in either a standard slab gel apparatus or a mini-gel apparatus (24), stained with Coomassie Brilliant Blue R, photographed on Kodak Plus-X Pan Type 4187 film, and scanned on a Syntex AD1 autodensitometer. Samples were dissolved in 125 mM Tris pH 6.8, 5% SDS, 10% glycerol and 0.01% bromophenol blue. For standard sized gels 30 µg total protein was loaded per lane, 1-3 µg per lane for mini-gels. During characterization of the gel system all gels were run using bovine serum albumin (66,000 daltons), catalase (57,000 daltons), aldolase (40,000) and lactate dehydrogenase (35,000). Later the positions of the receptor subunits were used to calibrate the gels. Gel scans were processed using computer programs written by M.J. Ross and D.A. Agard.

Glycerol gradients (80%→40% w/w) were formed in eleven equal steps, and linear sucrose gradients were formed using a gradient maker. Equilibrium centrifugations were run at 10^5 x g for greater than eight hours. Velocity sedimentation of I^{125} toxin-receptor and protease digested I^{125} toxin-receptor complexes was run on 5% to 20% w/w sucrose gradients, in 0.2% Triton X-100, 0.1 M NaCl, 10 mM Na phosphate and 1 mM $CaCl_2$ in an SW.50.1 rotor at 50,000 rpm for 5 hours at 4°C, using β-galactosidase and catalase (Sigma) as sedimentation markers. Glycerol and

sucrose concentrations were determined using a Zeiss refractometer.

Electron Microscopy.

Negative stain electron microscopy was carried out as described previously (Chapter Three) using either 2% sodium phosphotungstate, pH 7.4or 1% uranyl oxylate pH 6.0 negative stain. Both stains were effective in visualizing the membranes, but phosphotungstate provided better high resolution images.

Membrane pellets prepared by centrifugation were quick-frozen by slamming them against a block of copper cooled to 4°K. The design and operation of the apparatus used for freezing have been described previously (15). Frozen samples were stored in liquid nitrogen until transfer into a Balzers freeze-fracture machine (Balzers Corp., Nashua, N.H.). They were then fractured by gently scraping the surface with a new ultra-sharp razor blade mounted in the freezing microtome. Specimen was fractured at a vacuum of lower than 2.10^{-6} torr and a tissue temperature of -120°C. Samples were etched for 3 min at 100°C and rotary-replicated (23) with platinum-carbon using a Balzers rotary-stage attachment. The electron beam gun, mounted at a 16-24° angle relative to the tissue surface, was operated at 2,050 V and 70 μA for 6 S, during which time the tissue rotated through 360° six times. Replicas were backed with carbon deposited by 5-7 s of thermionic evaporation from pointed carbon rods. Replicas were removed from the Balzers to a plastic scintillation bottle of frozen methanol and allowed to thaw. Tissues

were rinsed once in water and submerged in standard household bleach (sodium hypochlorite). Replicas floated off in a few seconds, and were then broken into grid-sized pieces which were individually transferred through two rinses of water and picked up on 75-mesh carbon-coated Formvar grids.

The replicas were photographed at x 50,000 in a JEM 100C electron microscope operated at 80 kV with a 50 μM objective aperture. Stereo microscopy was performed with the high-resolution top-entry goniometer by tilting the grid ± 6°. Electron microscope negatives were routinely contact-reversed. Negative images in which platinum looks white and the shadows are black have been used throughout this paper. Particle sizes were measured from 5 x enlarged photographic prints.

Protease Digestion

Protease digestions with Staphylcoccus griseis protease (Sigma type V1 lot #57C-0152), papain (Sigma, Lot #58C-8005) and α-trypsin (chromatographically purified by L.M. Kay) were carried out at 4°C using final enzyme concentrations of 1 to 10 μM and membrane protein concentrations of 0.5 to 1 mg/ml. Some membrane fractions were subjected to three successive freeze-thaw cycles from dry ice/ethanol to a 37°C water bath in the presence of trypsin in order to allow the protease access to vesicle interiors. Limit digestion with trypsin was carried out until no further change was apparent in the SDS-PAGE pattern either by making the solution 1 μM in trypsin every 24 hours for 72 hours, for a final con-

centration of 3 μM trypsin, or by making the solution 5 μM in trypsin, and then adding a second aliquot after 6 hours for a final concentration of 10 μM. Standard trypsin digestion was carried out using a single addition of 10 μM trypsin (final concentration) to the receptor membranes (.5-1 mg/ml) and incubated overnight at 4°C. Protease activity was determined using the casein-agar clearing assay of Bjerrum et. al. (1) (BioRad Protease Detection Kit).

Most experiments were carried out using the purified α-trypsin in order to reduce the possibility of contamination by other proteases or lipases. Similarly prepared trypsin was used in the x-ray crystal structure determination of trypsin (35). In order to control for the possibility of contaminating lipases, the trypsin was inhibited either by a five to ten-fold molar excess of soybean trypsin inhibitor (STI) (CalBiochem Lot 300798 B grade - 7200 BAEE inhibitor units/mg), or by a greater than 100-fold molar excess of either PMSF (Sigma) or benzamidine HCl (Aldrich) or a combination of the two. PMSF was diluted from a stock solution in 100% ethanol such that the final ethanol concentration in the membranes was less than 10%, since concentrations of ethanol greater than 10% cause the fragmentation of receptor membranes (Appendix I).

The commercial STI contained a number of polypeptides of molecular weight greater than that of STI which were removed by column chromatography on Sephadex G-75-120 (Pharmacia) with 1 in 10 diluted H buffer. Failure to remove thesehigh molecular weight contaminants resulted in effects on membrane morphology caused by the crude STI alone. Trypsin

and inhibitor were premixed and allowed to incubate for from 15 to 30 minutes at room temperature before being added to the membranes. Leaving trypsin at room temperature (23°C) for this length of time had no effect on the result of subsequent digestion. Trypsin activity was measured by the rate of N-carbobenzoxyl-L-lysine-p-nitrophenyl ester (ZLONpH) hydrolysis as described in Koeppe, et al. (21).

RESULTS:

Acetylcholine receptor membranes prepared by homogenization and isopycnic centrifugation (31, 34) are between 0.5-2 μM in diameter (see fig. 1a). The receptor particles in negatively stained membranes have been identified as receptor by both their similarities in appearance to detergent solubilized receptor (25) and by direct and indirect immunospecific labeling (Chapter Three). Commonly over 90 to 99 percent (34) of the membrane vesicles are packed with receptor molecules. Under negative-stain conditions the membranes collapse and dry down onto the carbon support film with some distortion in membrane shape (see Appendix III). When the receptor membranes are examined by rapid-freezing, deep-etch, and rotary shadowing techniques (17, 18) (Figure 1b) they appear spherical and exhibit a distinct clustering of particles which is only rarely observed in negative-stain preparations (Compare Fig. 1a and b and ref. 4, Fig. 8 & 10). That these frozen and shadowed membranes correspond to the receptor-packed membranes viewed under negative stain conditions has been demonstrated by their decoration

with anti-receptor antibodies (J.E. Heuser & M.W. Klymkowsky, unpublished observations).

Conventionally prepared receptor-enriched membrane fractions contain a limited number of polypeptides (Fig. 2) and their specific αbutx binding activity of 2-4 nmol/mg protein indicates that approximately 20-50% of the protein present is receptor. The relative proportions of the polypeptides present vary from preparation to preparation, due perhaps to loss of loosely bound components, fortuitous accretion of other components with the membranes, and proteolysis by endogenous proteases during preparation.

The crude homogenate does not clear casein-agar protease detection plates, thus endogenous proteolytic activity must be fairly specific. Froehner & Rafto (10) have noted a proteolytic activity, inhibited by NEM which preferentially attacks the γ-subunit of receptor. Gel electrophoretic patterns of membrane fractions after sucrose density centrifugation are relatively stable, but do decay slowly over a period of one to two weeks, especially if the membranes are left at room temperature (Appendix II). The effects of this endogenous proteolytic activity are minimized by keeping the sample at all times at 4°C.

When receptor membranes are subjected to proteolytic degradation by either papain, Staph. griseis proteases or trypsin, a radical transformation occurs in vesicle morphology (Figs. 3, 4). Deep-etch images indicate that receptor molecules first aggregate into patches leaving particle free areas behind (see Fig. 5). In negative-stain images this

initial aggregation is often not apparent though the vesicles develop gently scalloped edges (see Fig. 3 arrow). The difference between the two may arise from the same causes that disrupt the clustering observed in deep-etch images. Even at the early stage of cluster formation (Fig. 5b) the patches have a positive curvature. These budding processes grow (see Fig. 5c), form a neck and constrict again, such that blebbed mini-vesicles of relatively constant size were formed (see Figs. 3, 5c, 6). The transformation occurs uniformly within any one vesicle (see Fig. 3-6). The end result of the process is the pinching off of the blebs into about 100 nm diameter mini-vesicles (see Fig. 5c).

Although the trypsin used throughout these experiments had been much further purified than that used by others to clip off extended parts of integral membranes (see for example 29) the novelty of the observed morphological changes led us to examine the possibility of lipase contamination of the added trypsin. When trypsin was first inhibited by a 10-fold excess of purified soybean trypsin inhibitor, the morphological transformation and receptor degradation was blocked. STI alone was without effect on vesicle morphology. The chemical inhibitors PMSF and benzamidine proved much less useful because even after pre-incubation of trypsin with a 500-fold molar excess of PMSF at room temperature for 12 hours followed by the addition of a 500-fold molar excess of benzamidine, the trypsin was still active as judged by receptor subunit degradation. Nevertheless, the extent of trypsin activity as judged by both SDS-PAGE and ZLONpH hydrolysis parallel the

extent of vesicle transformation. In trypsin inhibition experiments where degradation was not completely inhibited but had not reached the predominantly 27000 polypeptide stage (figure 7) most receptor vesicles failed to reach the final transformed morphology and many appeared unaltered (figure 8).

About 10-20% of conventionally-prepared receptor containing vesicles were transformed after 72 hours of trypsin treatment (1 μM trypsin added at 24 hour intervals) as determined by negative-stain electron microscopy. Freeze-thawing cycles in the presence of protease, aimed at breaking open the vesicles so as to allow increased protease accessibility to the intracellular surface had no appreciable effect on the extent of transformation. After 72 hours of trypsin digestion, the SDS-PAGE banding patterns were often relatively unchanged from the predigest pattern (figure 9a) with only 10-20% of the material appearing as new, lower molecular weight bands.

Neubig et al. (27) first reported that alkali treatment removes non-receptor, peripheral membrane proteins from acetylcholine receptor membrane fractions and leaves the receptor membranes intact and functional. Using their stripping techniques a number of major polypeptides were solubilized (Fig. 2b). Most notably, a doublet corresponding to the 43,000 dalton polypeptide proposed by Changeux and colleagues to be the receptor ionophore (16) and a second doublet of about 55,000 daltons were removed and released into the supernatant. The relative proportions on the receptor subunits sometimes changes upon alkali treatment for

reasons that are unclear but none of the subunits is preferentially released into the supernatant (fig. 2b). That the α, β, γ and δ polypeptides are receptor subunits is supported by both immunological (6) and photoaffinity experiments (26).

Alkali-stripped membranes have higher specific activities than unstripped membranes, simpler SDS-PAGE patterns (Fig. 2c), and appear quite similar to the unstripped membranes in negative-stain electron micrographs. The stripped membranes have significantly lower densities by isopycnic centrifugation in either sucrose (1.14 g/cm^3) or glycerol (1.16 g/cm^3)(Fig. 10) than conventionally prepared membranes (1.15 & 1.17 g/cm^3 respectively). These observations indicate that some of the solubilizable peripheral proteins are normally contained within the receptor membranes.

The extent to which these polypeptides are removed during purification and alkali treatment appears to greatly affect the sensitivity of the receptor molecule itself to proteolytic degradation (see Fig. 9). The extent of receptor degradation assayed by SDS-PAGE parallels the extent of the morphological transformation of the vesicles. After alkali stripping, membranes can be degraded by trypsin so that no distinguishable receptor subunits remain (Fig. 9). Detergent solubilization also results in much more complete digestion of the receptor (Chapter Four, Part II).

The stripped and digested receptor membranes contain particles which appear identical to normal receptor particles (Fig. 6, 11) and the

membranes retain full specific activity. d-Tubocurarine is fully competitive with αbutx binding (see Fig. 12) indicating that the αbutx binding is still specific. Isokinetic sedimentation analysis of Triton-solubilized receptor with catalase (S= 11.3) and β-D-galactosidase (S=16) as standards show that the toxin-binding component has an apparent S value of about 9, (Fig. 13) the same as that for undigested receptor.

Membranes prepared by us using the procedure of Chang & Bock (5) contain more than 80% of their receptor population in a form which sediments at 13 S, and have been shown to be a dimeric form, linked by a disulphide bond between δ (65,000 daltons) subunits (5, 13, 14, 19, 36, 37). Such membranes respond to trypsin digestion in the same way as does the monomeric receptor (see figure 7, tracks a & b compared with figure 9, and Chapter Four, part II, figures 1 & 2). The trypsin digested form of the dimeric molecule sediments at 9 S. The decreased S value indicates that the disulphide bridged δ subunits have been cleaved.

DISCUSSION:

Since approximately 95% of the receptor-containing vesicles are oriented with their original extracellular surfaces out (8, 15, Chapter Three) and because the receptor molecule projects by about 5 nm above the membrane surface (Chapter Three)(figs. 6, 9b), it seemed reasonable that protease digestion would either release a soluble, toxin-binding fragment, or result in a preferential digestion of specific subunits giving an indication of their location with respect to the membrane. Kalderon & Silman (20) had reported that autolysis and trypsin digestion would solubilize a toxin-binding receptor fragment without the use of detergents.

After extensive digestion with trypsin that leaves none of the receptor subunits as intact polypeptides on SDS-PAGE (figure 9b), triton-solubilized monomer and dimer receptor remain as tightly associated aggregates which sediment as single 9S components (figure 13). In the absence of detergents the receptor remained membrane-bound (figure 6). Trypsin digested receptor still binds αbutx and the binding can be competed with the unrelated antagonist dtubocurarine (figure 12), demonstrating that the active site for agonist/antagonist binding is preserved. The receptor particles appear unchanged in negative-stain electron microscopy after trypsin-digestion (figures 6 & 11) in keeping with the observations of Carroll, et al. (2) that the receptor resists denaturation by 6 M guanidinium salts. Shamoo and Eldefrawi (33) in fact reported that a trypsin-digested acetylcholine receptor would, upon

reconstitution, respond consistently to acetylcholine and carbamylcholine, producing a monovalent cation flux.

The time-course of trypsin-digestion at room temperature (using alkali-treated membranes) indicated a fairly uniform rate of degradation of all the protein components of the membranes, including the receptor subunits (Chapter Four, Part II) and so failed to provide any direct evidence as to which subunits are most exposed within the membrane.

However, even though the gross physical characteristics of the receptor molecule were relatively unchanged by trypsin digestion, striking changes did occur in receptor vesicle morphology (figures 3-6). Electron microscopy of vesicles in various stages of morphological transformation suggest that the process begins with a critical proteolytic clip in an unidentified 'structural' membrane component which causes the receptor molecules to aggregate (figure 5b) leaving apparently empty, phospholipid bilayer alongside the receptor aggregates (figure 5c). The scalloped appearance of the membranes in negative stain (figures 3 & 6) was due to the inherent curvature of the receptor aggregates (figure 5b). The continuation of this process results first in dome formation and then the budding out and beading up of the receptor-rich mini-vesicles (figure 5c).

One possible mechanism for the observed protease induced morphological effect would be a specific aggregation of receptor molecules such that the axes of adjacent molecules perpendicular to the membrane bilayer are no longer nearly parallel as they would be in the membrane

of a large vesicle but in the final budded vesicle form an angle of about 10°. This would result in the surprisingly uniform curvature of the mini-vesicles observed. This also would explain how the strings of mini-vesicles are formed, the juncture between blebs being weak points where the membranes might split off (figure 3).

The development of the blebbed vesicle morphology occurs much slower than the initial trypsin cleavages (hours vs. minutes) and seems to correlate more with the completion of trypsin digestion rather than its onset. Such a conclusion is supported by the results of inhibition experiments where inhibition was incomplete. In such cases where a limit digest pattern was not attained (figure 7), most of the vesicles were of normal or only slightly altered morphology when examined by negative-stain electron microscopy (figure 8).

Coakely, et al (7) noted a roughly similar blebbing effect on heat-denatured and sheared erythrocytes. In our case, however, where there is no shear stress, or obvious lipid effects, and alternative explanation is that the blebbing is due to the aggregation of the receptor particles within the plane of the membrane and to the geometry of that aggregation (figure 5). We have also noted a receptor membrane blebbing effect distinctly different than that produced by proteases caused by ethanol at concentrations greater than ten percent (Appendix I). In addition, as receptor vesicle preparations aged (greater than 10-14 days) some of the vesicles tend to assume shapes similar to those observed upon proteolysis. While the activity of endogenous protease

declines with receptor membrane purity, proteolytic activity was detected even in highly purified preparations (greater than 90% receptor by SDS-PAGE) (Appendix II). How these different effects are related, if they are, is unclear.

The protease susceptible component(s) which cause or allow receptor to aggregate in the membrane may be either a part of the receptor itself, one of the recognizable non-receptor polypeptides present in the membranes or a component present as a minor, as yet unrecognized constituent. This question is somewhat simplified since removal of the peripheral proteins (figure 2b) leaves membrane shape unchanged and yet enhances susceptability to the protease induced effects.

That some of the peripheral proteins are located in receptor-containing vesicles is demonstrated by the decrease in receptor membrane density after their removal by high pH, .008 g/cm^3 in sucrose and .014 g/cm^3 in glycerol as measured by isopycnic centrifugation (figure 10). The receptor molecules in the alkali-treated membranes appear equally densely packed (if not more so, see figure 11a,b), and very little receptor (figure 2) is solubilized implying that the decrease in membrane density is a direct result of the removal of peripheral proteins.

Since alkali-treated membranes contain almost pure receptor (figure 2c), and since as visualized by electron microscopy (figure 5) the morphological effects appear to be caused by a specific aggregation of receptor molecules, we concluded that the most likely candidate for the target protein is the receptor itself.

The possibility that the vesicle structure change is caused not by the protease itself, but rather by another contaminating enzyme, such as a lipase is excluded since specific inhibition of trypsin by purified soybean trypsin inhibitor completely blockes both subunit degradation (as judged by SDS-PAGE) and the morphological changes in the membranes as visualized by electron microscopy.

The results reported here indicate the complexity of the receptor-rich membranes isolated from Torpedo californica electroplaques and illustrate the insensitivity of ligand binding to proteolytic degradation of the receptor, and raise the possibility that integral membrane proteins such as the acetylcholine receptor may have structural roles in determining membrane morphology as well as their more obvious functional ones.

ACKNOWLEDGEMENTS:

This work was supported by grants from the National Institutes of Health, number GM 24485 and the National Science Foundation PCM77-25407 to Dr. Stroud, and United States Public Health Service Grant number NS-11979 and by a Muscular Dystrophy Association grant to Dr. Heuser.

We would like to thank Dr. Zach Hall for the gift of d-tubocurarine, his encouragement, and along with Drs. J.B. Miller, N. Nathanson and G. Miljanick for their valuable discussions. MWK is a doctoral student at the California Institute of Technology and RMS is a Sloan Foundation Fellow.

REFERENCES:

1. Bjerrum, O.J., Ramlan, J., Clemmesen, I., Ingeld, A, and Bøg-Hansen, T.C. (1975). An Artefact in Quantitative Immunoelectrophoresis of Spectrin Caused by Proteolytic Activity in Antibody Preparations. Scand. J. Immunology Sys. 2, (N.H. Axelsen, ed.) Aus & Wahl, Oslo, Norway, pp. 81-88.

2. Carroll, R.C., Eldefrawi, M.E., and Edelstein, S.J. (1973) Studies on the Structure of the Acetylcholine Receptor from Torpedo marmorata. BBRC 55, 864-872.

3. Cartaud, J., Benedetti, E.L., Cohen, J.B., Meunier, J.E., and Changeux, J-P. (1973). Presence of a Lattice Structure in Membrane Fragments Rich in Nicotinic Receptor Protein from the Electric Organ of Torpedo marmorata. FEBS Lett. 33, 109-113.

4. Cartaud, J., Benedetti, E.L., Sobel, A., and Changeux, J-P. (1978). A Morphological Study of the Cholinergic Receptor Protein from Torpedo marmorata in its Membrane Environment and in its Detergent Extracted Purified Form. J. Cell. Sci. 29, 313-337.

5. Chang, H.W. and Bock, E. (1977). Molecular Forms of Acetylcholine Receptor. Effects of Calcium Ions and a Sulfhydryl Reagent on the Occurrence of Oligomers. Biochem. 16, 4513-4520.

6. Claudio, T. and Raftery, M.A. (1977). Immunological Comparison of Acetylcholine Receptor and Their Subunits from Species of Electric Ray. Arch. Biochem. & Biophys. 181 , 484-489.

7. Coakley, W.T., Bater, A.J. and Delley, J.O.T. (1978) Vesicle Production on Heated and Stressed Erythrocytes. Biochim. Biophys. Acta. 512, 318-330.

8. Duguid, J.R., and Raftery, M.A. (1973). Fractionation and Partial Characterization of Membrane Particles from Torpedo californica Electroplax. Biochem. 12, 3593-3597.

9. Dupont, Y., Cohen, J.B. and Changeux, J-P. (1974) X-ray Diffraction Study of Membrane Fragments Rich in Acetylcholine Receptor Protein Prepared from the Electric Organ of Torpedo marmorata. FEBS Lett. 40, 130-133.

10. Elliott, J., S.M.J. Dunn, S.G. Blanchard & M.A. Raftery (1979). Specific Binding of Perhydrohistrionicotoxin to Torpedo acetylcholine Receptor. PNAS (USA) 76, 2576-2579.

11. Fambrough, D.M. (1979) Control of Acetylcholine Receptors in Skeletal Muscle. Physiol. Rev. 59, 165-227.

12. Froehner, S.C. and Rafto, S. (1979). Comparison of the Subunits of Torpedo californica Acetylcholine Receptor by Peptide Mapping. Biochem. 18, 301-307.

13. Hamilton, S.L., McLaughlin, M. & Karlin, A. (1977). Disulfide Bond Cross-Linked Dimer in Acetylcholine Receptor from Torpedo californica. Biochem. Biophys. Res. Comm. 79, 692-699.

14. Hamilton, S.L. McLaughlin, M. and Karlin, A. (1979) Formation of Disulfides linked Oligomers of Acetylcholine Receptor in Membrane from Torpedo Electric Tissue. Biochem. 18, 155-163.

15. Hartig, P.R. and Raftery, M.A. (1979) Preparation of Right Side-Out, Acetylcholine Receptor Enriched Intact Vesicles from Torpedo californica Electroplaque Membranes. Biochem. 18, 1146-1150.

16. Heidmann, T. and Changeux, J-P. (1978) Structure and Functional Properties of the Acetylcholine Receptor Protein in its Purified and Membrane-Bound States. Ann. Rev. Biochem. 47, 317-357.

17. Heuser, J.E., Reese, T.S., Dennis, M.J., Jan, Y., Jan, L. and Evans, L. (1979) Synaptic Vesicles Exocytosis Captured by Quick Freezing and Correlated with Quantal Transmitter Release. J. Cell Biol. 81, 275-300.

18. Heuser, J.E., and Salpeter, S.R. (1979). Organization of Acetylcholine Receptors in Quick-Frozen, Deep-Etched and Rotary Replicated Torpedo Postsynaptic Membrane. J. Cell Biol. 82, 150-173.

19. Hucho, F., Bandini, G. and Swarez-Isla, B.A. (1978) The Acetylcholine Receptor as Part of a Protein Complex in Receptor-Enriched Membrane Fragments from Torpedo californica Electric Tissue. Eur. J. Biochem. 83, 335-340.

20. Kalderon, N. and Silman, I. (1977) Water-Soluble Acetylcholine Receptor from Torpedo californica: Solubilization, Purification and Characterization. Biochem. Biophys. Acta 465, 331-340.

21. Koeppe, R.E., M. Krieger & R.M. Stroud (1977). The Effect of Pre-Incubation on Trypsin Kinetics at Low pH. Biochim. Biophys. Acta 481, 617-621.

22. Laemmli, U.K. (1970) Cleavage of Structure Proteins during the Assembly of the Head of Bacteriophage T4. Nature (London) 227, 680-685.

23. Margaritis, L.A., Elgasaeter, H.A., & Branton, D. (1977) Rotary Replication for Freeze-Etching. J. Cell Biol. 72, 47-56.

24. Matsudaira, P.T. & D.R. Burgess (1978). SDS-Microslab Linear Gradient Poly Acrylamide Gel Electrophoresis. Anal. Biochem. 87, 386-396.

25. Meunier, J.-C., R. Sealock, R. Olsen & J-P. Changeux (1974). Purification and Properties of the Cholinergic Receptor Protein from Electrophorus electricus Electric Tissue. Eur. J. Biochem. 45, 371-394.

26. Nathanson, N. and Z.W. Hall (1979). In Situ Labeling of Torpedo and Rat Muscle Acetylcholine Receptor by a Photoaffinity Derivative of α-Bungarotoxin. Biochem . in press.

27. Neubig, R.R., Krodel, E.K., Boyd, N.D., and Cohen, J.B. (1979) Acetylcholine and Local Anaesthetic Binding to Torpedo nicotinic Post-synaptic Membranes after Removal of Nonreceptor Peptides. PNAS 76, 690-694.

28. Nickel, E., and Potter, L.T. (1973) Ultrastructure of Isolated Membranes of Torpedo electric tissue. Brain Res. 57, 508-517.

29. Nishi, Y., and Takesue, Y. (1978) Localization and Intestinal Sucrose-Isomaltase Complex on the Microvillous Membrane by Electron Microscopy Using Non-labelled Antibodies. J. Cell Biol. 79, 516-525.

30. Potter, L.T. & Smith, D.S. (1977) Post-synaptic Membranes in the Electric Tissue of Narcine: I. Organization and Innervation of Electric Cells. Fine Structure of Nicotinic Receptor-Channel Molecules Revealed by Transmission Microscopy. Tissue Cell 9, 585-694.

31. Reed, K., Vandlen, R., Bode, J, Duguid, J. and raftery, M.A. (1975) Characterization of AcChR-rich and AcChE-rich Membrane Particles from Torpedo californica Electroplaques. Arch. Biochem. Biophys. 167, 138144.

32. Schiebler, W., & Hucho, F. (1978) Membranes Rich in Acetylcholine Receptor: Characterization and Reconstitution to Excitable Membranes from Exogenous Lipids. Eur. J. Biochem. 85, 55-63.

33. Shamoo, A.E. and Eldefrawi, M.E. (1975) Carbamylcholine and Acetylcholine Sensitive Cation-Selective Ionophore as Part of the Purified Acetylcholine Receptor. J. Membrane Biol. 25, 47-63.

34. Sobel, A. Weber, M. and Changeux, J.-P. (1977) Large-Scale Purification of the Acetylcholine-Receptor Protein in its Membrane-Bound and Detergent-Extracted Forms from Torpedo marmorata Electroplaques. Eur. J. Biochem. 80, 215-224.

35. Stroud, R.M., L. Kay, R.E. Dickerson (1974). The Structure of Bovine Trypsin: Electron Density Maps of the Inhibited Enzyme at 5 Å and at 2.7 Å Resolution. J. Mol. Biol. 83, 185-208.

36. Suarez-Ilsa, B.A. & Hucho, F. (1977) Acetylcholine Receptor: -SH Group Reactivity as Indicator of Conformational Changes and Functional States. FEBS. Lett. 75, 65-69.

37. Witzemann, V., & Raftery, M.A. (1978). Specific Molecular Aggregates of Torpedo californica Acetylcholine Receptor. Biochem. Biophys. Res. Comm. 81, 1025-1031.

FIGURE CAPTIONS:

Figure 1.

A. Receptor containing membranes (marked by (r)) show the distorted vesicle shape and homogeneous particle distribution common in negative stained images. Magnification is 88,000 X with the bar marking 0.1 micrometers.

B. Spherical receptor-filled vesicles are seen in quick-freeze, deep-etch & rotary-shadowed images.

Figure 2.

Receptor-enriched membrane fractions (a) contain only a few polypeptides other than the receptor subunits (labeled $\alpha,\beta,\gamma,\delta$) when visualized by SDS-PAGE. Of these nonreceptor polypeptides, a number can be solubilized by alkali-treatment (b).Track on left side is molecular weight standards. Track (c) is a mini-gel pattern of alkali-treated receptor membranes under non-reducing conditions.

Figure 3.

After protease digestion receptor membranes take on a distinctive overall membrane shape. Single arrow marks vesicle at an early stage of the transformation, characterized by a gently scalloped edge structure. At later stages (double arrows) the process has

continued. Minivesicles packed with receptor molecules are connected to the parent vesicle. The center areas of these digested vesicles are free of receptor particles, and vesicles that are entirely free of receptor particles (marked by '1') may represent the end result of the protease transformation process. Magnification is 56,000 X and the bar marks 0.2 micrometers.

Figure 4.

A low magnification stereo pair of rapidly frozen, deep etched and rotary shadowed proteolytically digested receptor membranes. Many of the membranes exhibit the blebbing characteristic of the proteolyzed membranes but without the distortions that arise in the negative stain procedure the vesicles remain as spheres. Some of the vesicles have been fractured. Image should be viewed with a pocket stereo viewer to have the correct sense of depth. Magnification is 14,000 X and bar marks 0.5 micrometers.

Figure 5.

At higher magnification the spherical nature of the receptor membranes and the tendency of receptor particles to cluster in the plane of the membrane are apparent (part a). The effects of trypsin at an early stage can be seen in part (b). Particles in the membrane have clustered into small patches leaving behind cleared areas. The inherent curvature of these clusters is apparent around the vesicle periphery, even in this early stage. Part (c) shows a

vesicle at a late stage. The entire surface of the residual large vesicle has been cleared of particles and the aggregated receptors are now budding out of the membrane. Arrow points to what appears to be released minivesicles. Magnifications are 100,000 X and the bar marks 50 nanometers for all three parts.

Figure 6.

A digested receptor vesicle which clearly shows the ring of receptors and the particle free central area of the membrane. The 5 nm high receptor head can clearly be seen all along the membrane edge (arrow). Magnification is 215,000 X and the bar marks 50 nanometers.

Figure 7.

Track (a) shows the SDS-PAGE pattern for undigested dimeric receptor. Digestion of the dimer receptor membranes (track b) results in the same pattern as does the digestion of monomeric receptor (see fig. 9). If trypsin is partially inhibited by incubation with either PMSF (track c) or benzamidine (d)(at 100-fold molar excess) trypsin digestion of receptor membranes is incomplete and does not reach the "limiting" 27,000 dalton stage indicated by closed arrows, and seen in track b. Tracks e and f are for incubation with inhibitor alone (no trypsin) (e PMSF f benzamidine). 't' marks the position of trypsin.

Figure 8.

Membranes taken from (a) the uninhibited trypsin digestion (figure 4, track b) and (b) the PMSF-inhibited trypsin digest (fig-

ure 4, track c) as visualized by negative stain (PTA) microscopy. Bar marks 100 nm. Altered vesicles in part (b) are marked by 'a's.

Figure 9.

The effects of trypsin digestion on the subunit pattern of both conventionally prepared and alkali-stripped receptor-rich membranes are shown in these densitometer tracings of SDS-PAGE patterns. The top pair of before (solid line) and after (dashed line) limit trypsin digestion reveals that in these conventional membranes little of the receptor subunits are degraded. In alkali-treated membranes however all of the receptor subunits have been digested.

Figure 10.

Gradient profiles in sucrose (A & B) and glycerol (C & D) of I^{125}-αbutx-receptor membrane complexes show the difference in density between normal (A & C) and alkali stripped membranes. The membranes were stripped in base as described in the text before having been run on the sucrose gradient, and then peak fractions were run on glycerol gradient. I^{125}-αbutx-receptor is plotted (□), in all parts. Protein concentration (+) and acetylcholine esterase (o) activity are plotted in parts A & B. Esterase activity is totally abolished by the base treatment.

Figure 11.

Receptor molecules in (a) conventionally prepared, (b) alkali-stripped and (c) alkali-stripped, trypsin digested membranes appear quite similar in negative-stain. Arrows in parts (a) & (b) point out edge structure arising from receptor heads. The edge effect is more prominent in the ordered receptor in part (b). All three parts are at a magnification of 358,000 X with the bar marking 50 nanometers.

Figure 12.

Incubation of either normal (solid circle) or digested (open circle) receptor membranes with I^{125}-αbutx and varying amounts of d-tubocurarine (final concentrations ranging from 3 mM to 0.3 μM) results in identical curves for the binding of the αbutx to the receptor.

Figure 13.

Both pre-digest and digested receptor membranes bind αbutx and form a complex which sediments with a value of 9S. Open and closed v's mark positions of β-galactosidase and catalase in each of the velocity gradients.

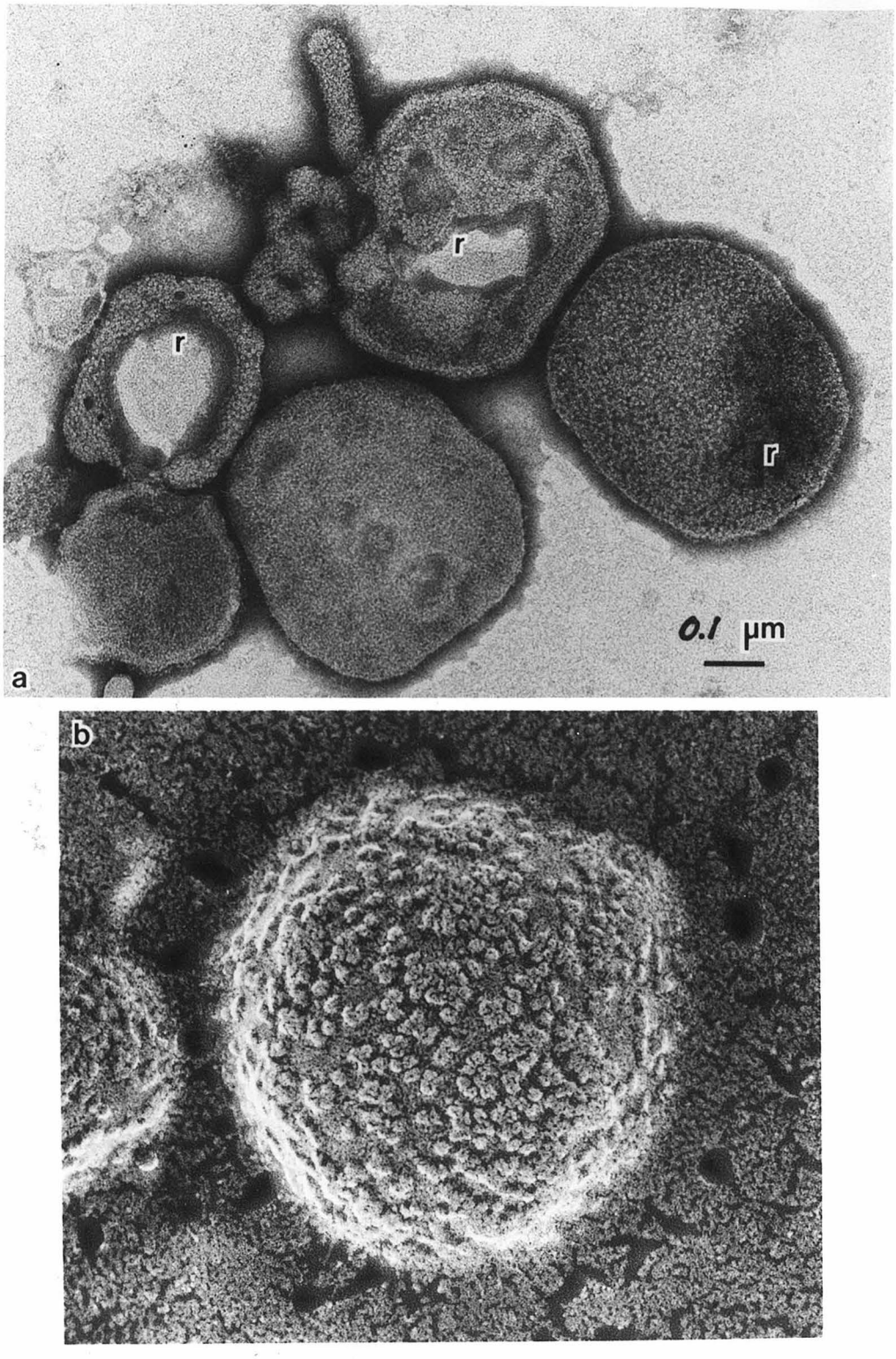


Figure 1

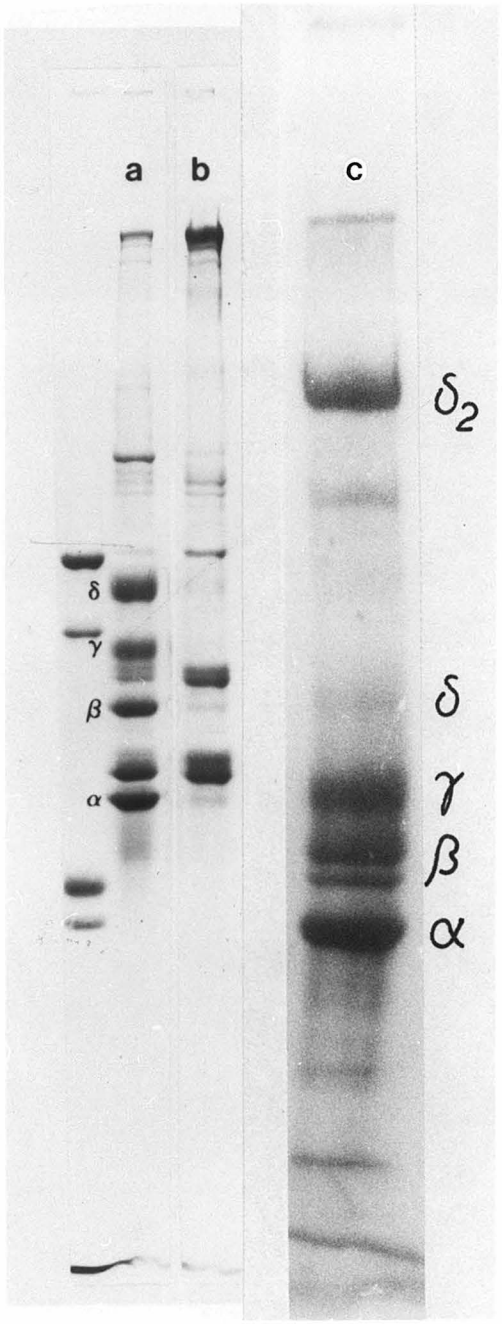


Figure 2

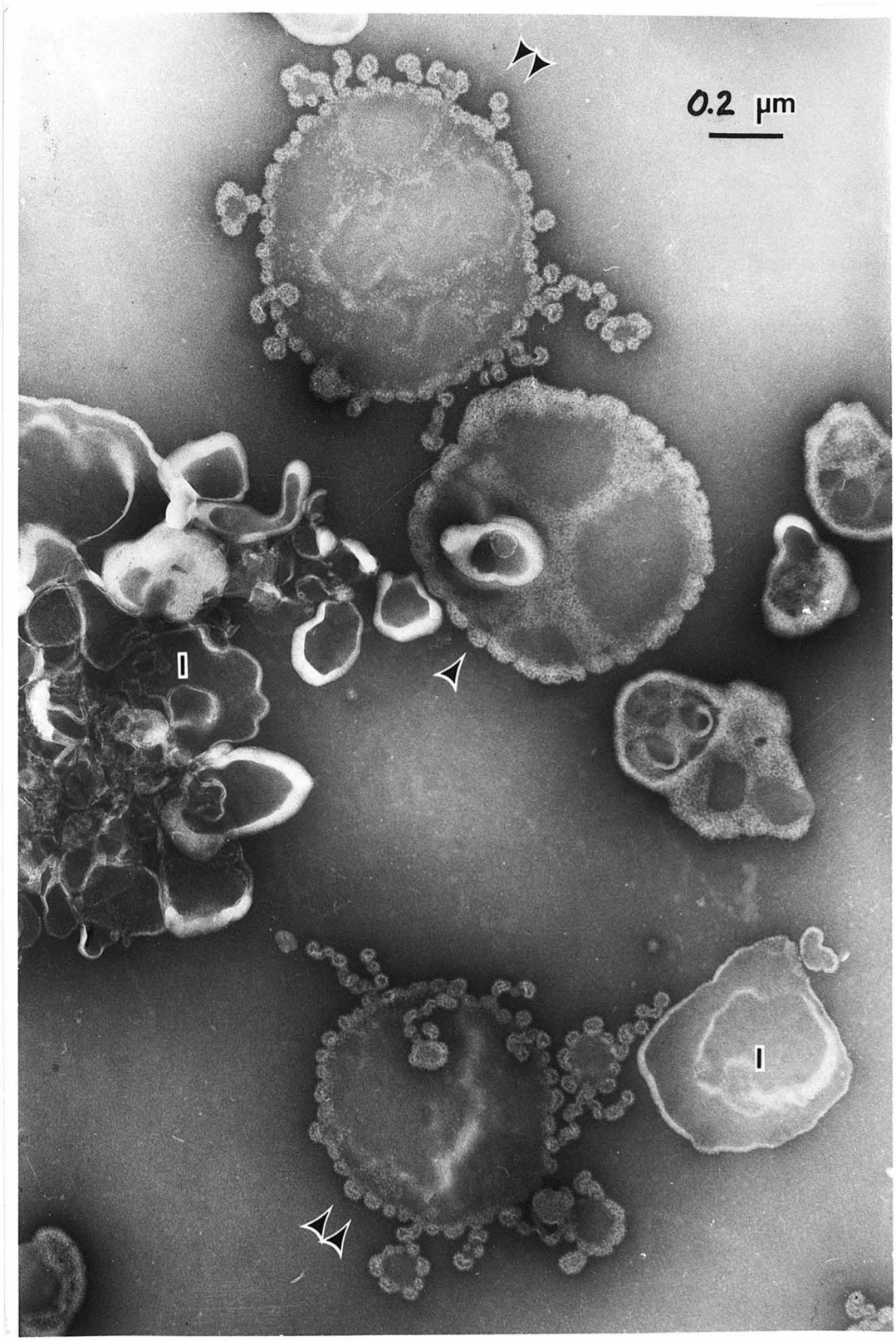


Figure 3

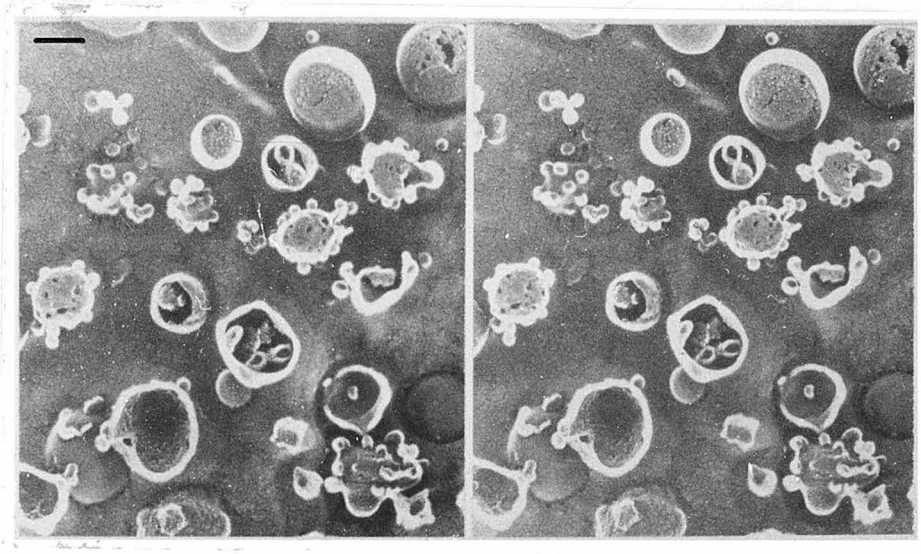


Figure 4

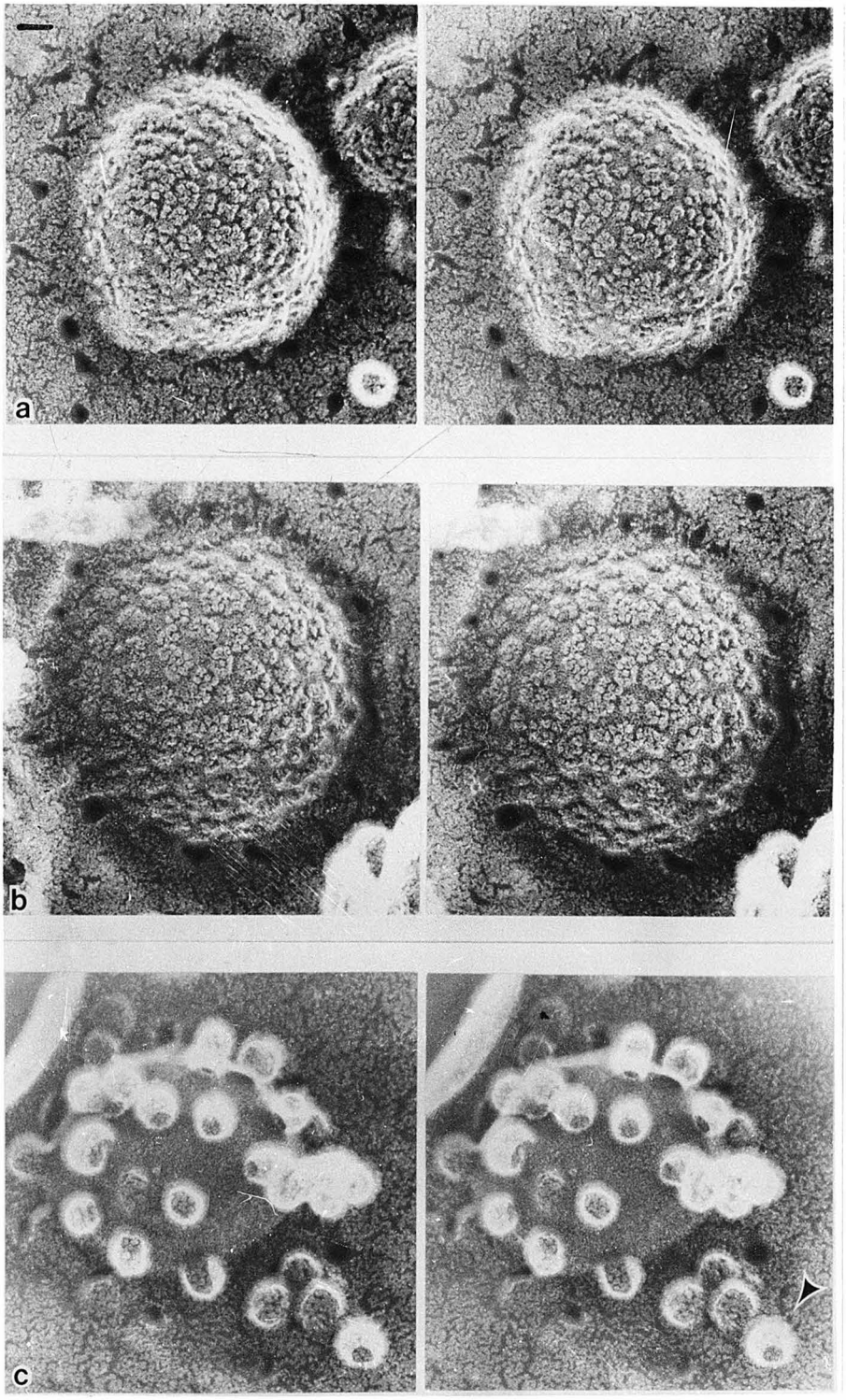


Figure 5

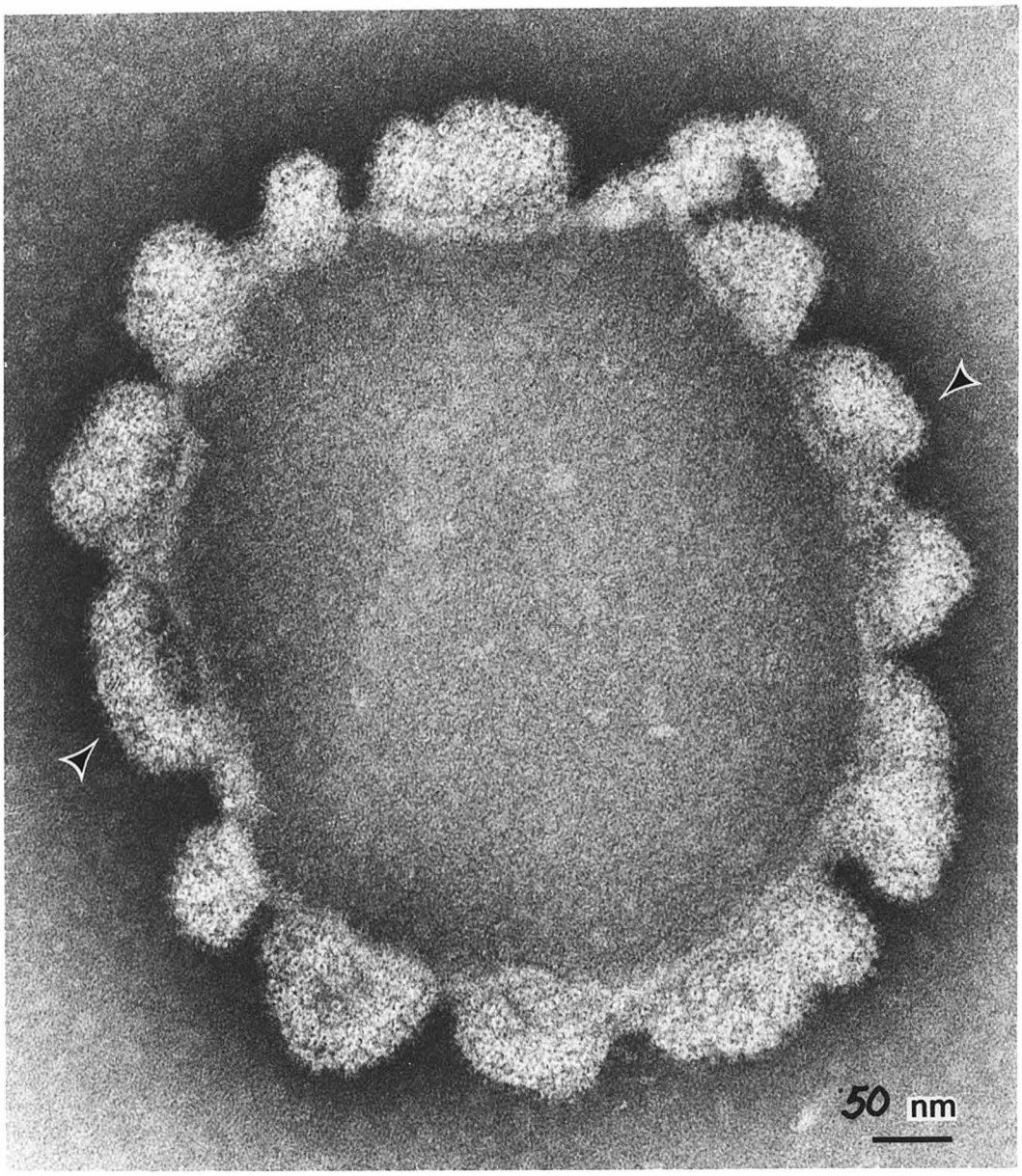


Figure 6

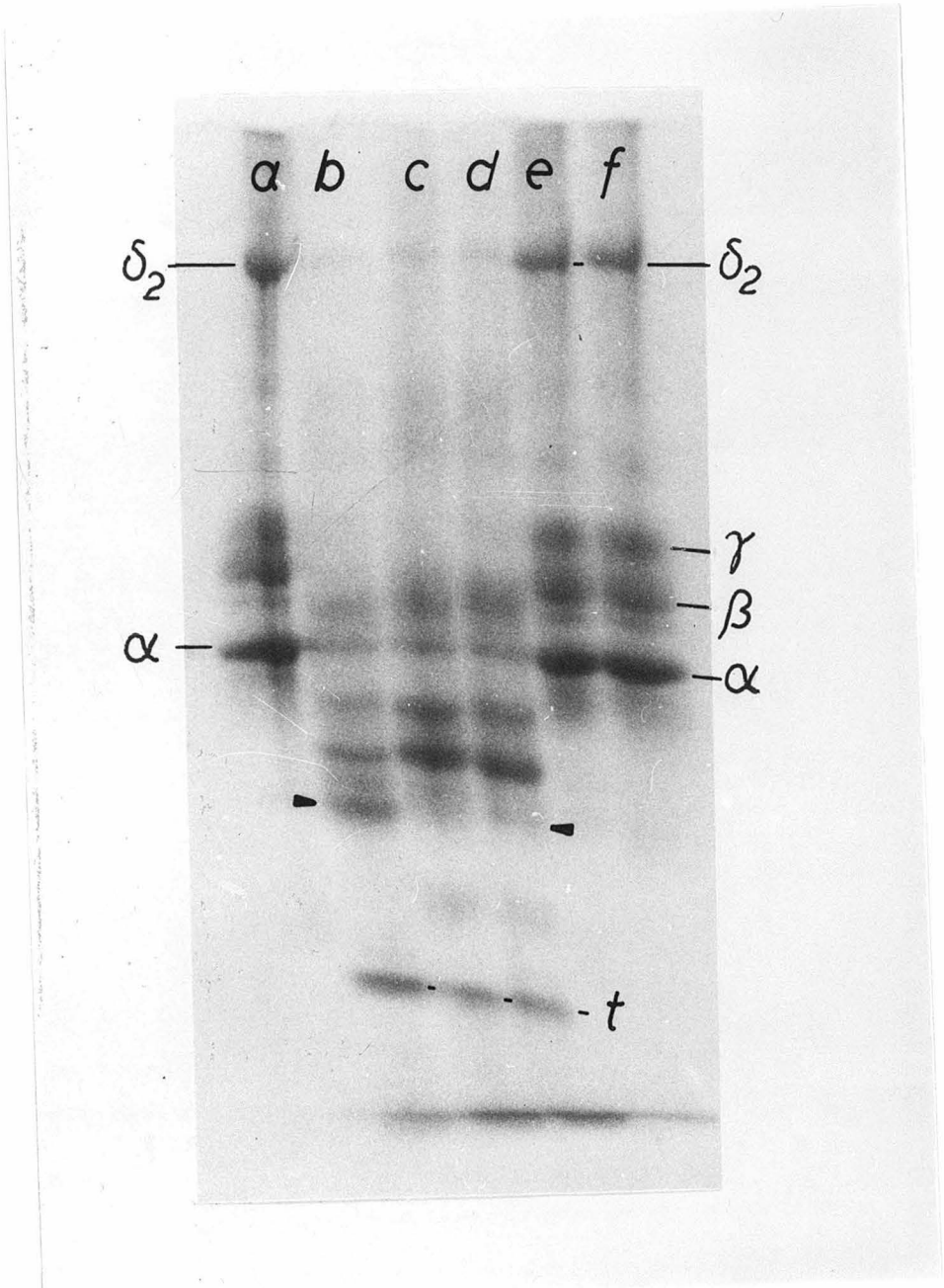


Figure 7

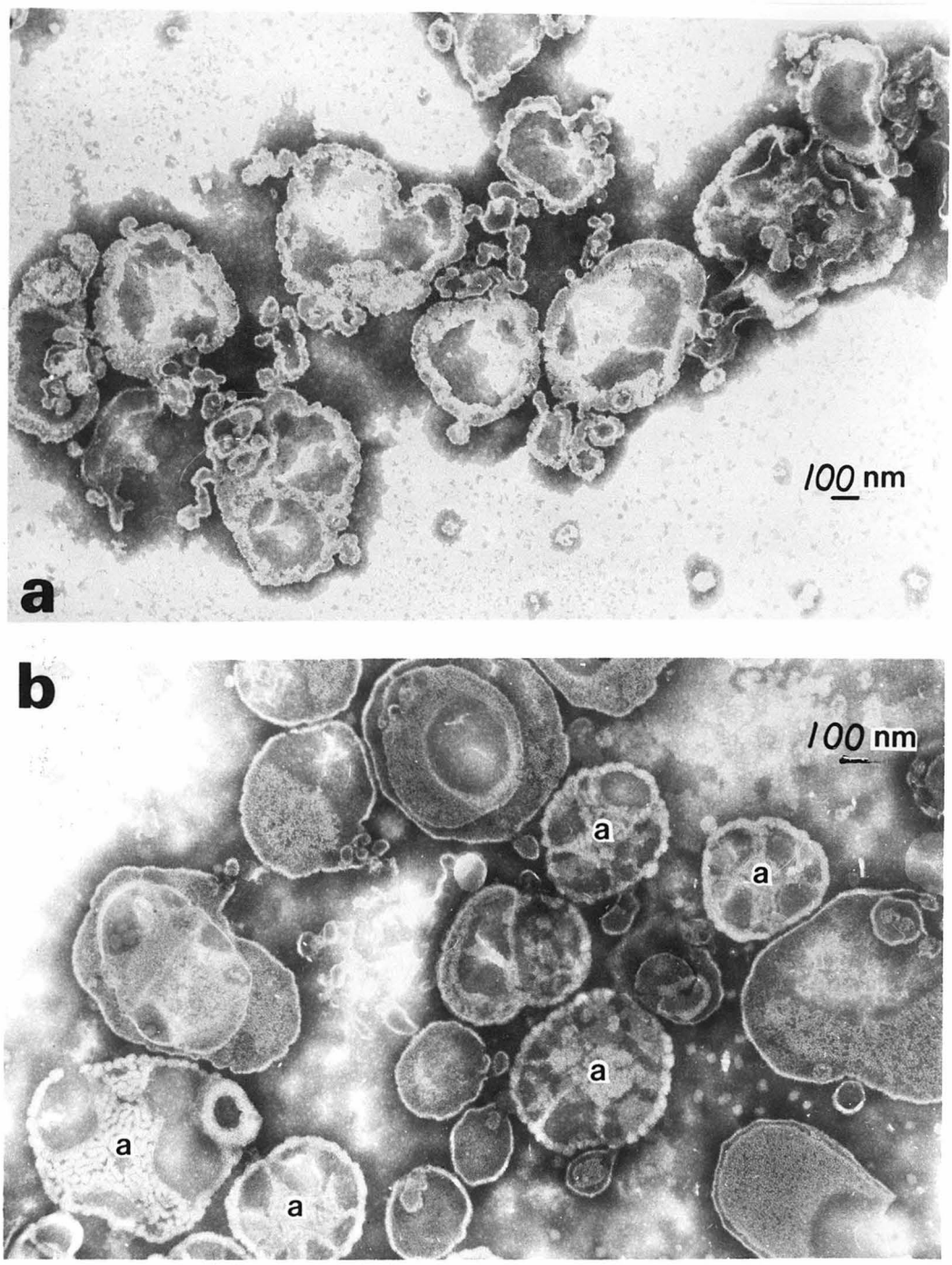


Figure 8

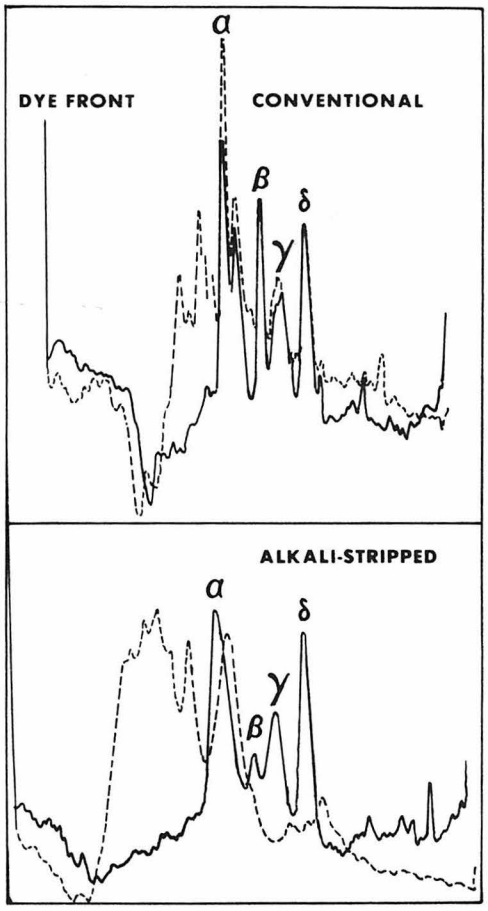


FIGURE 9

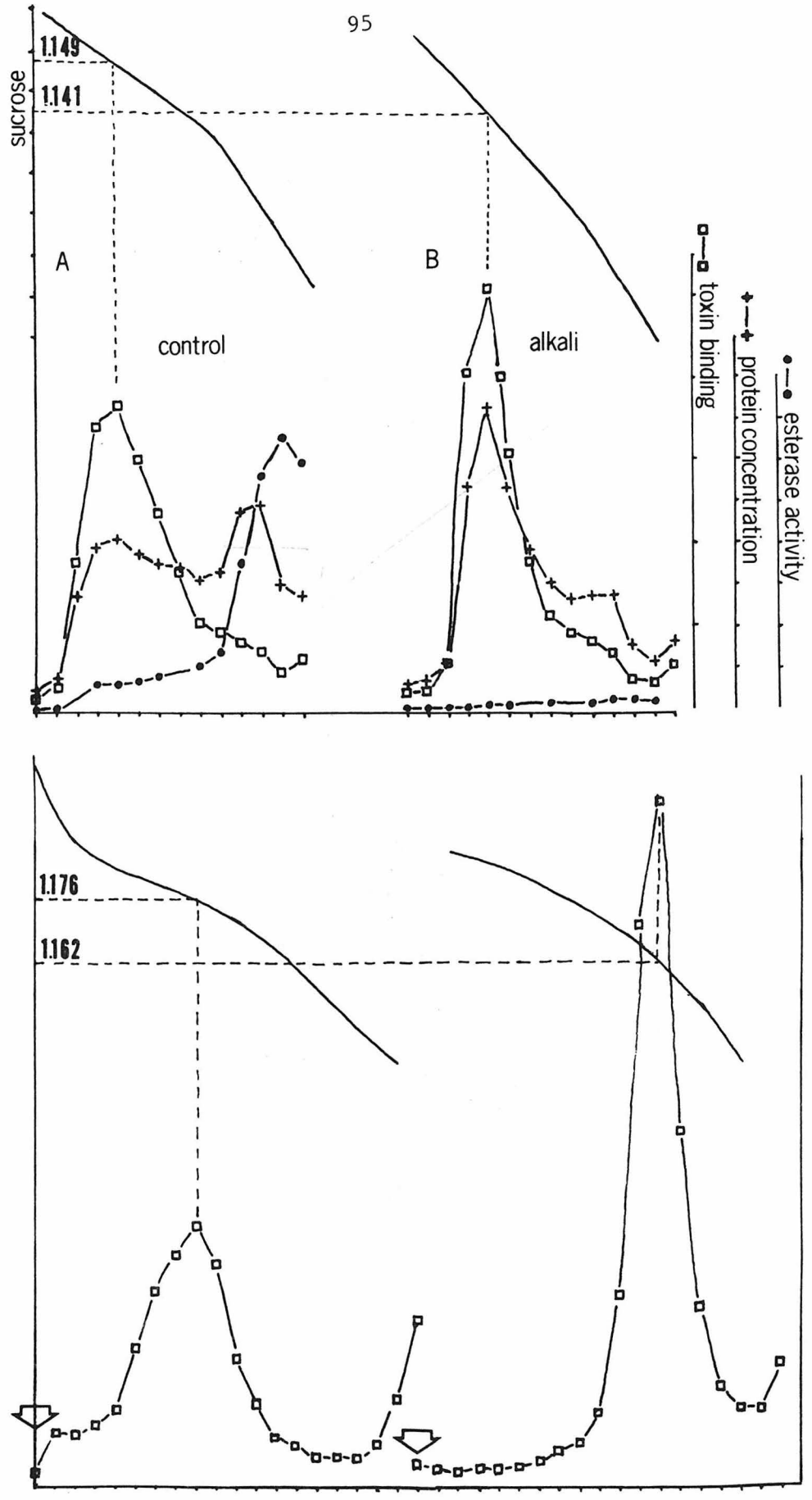

sucrose
1.149
1.141
A
control
B
alkali
toxin binding
protein concentration
esterase activity
1.176
1.162

FIGURE 10

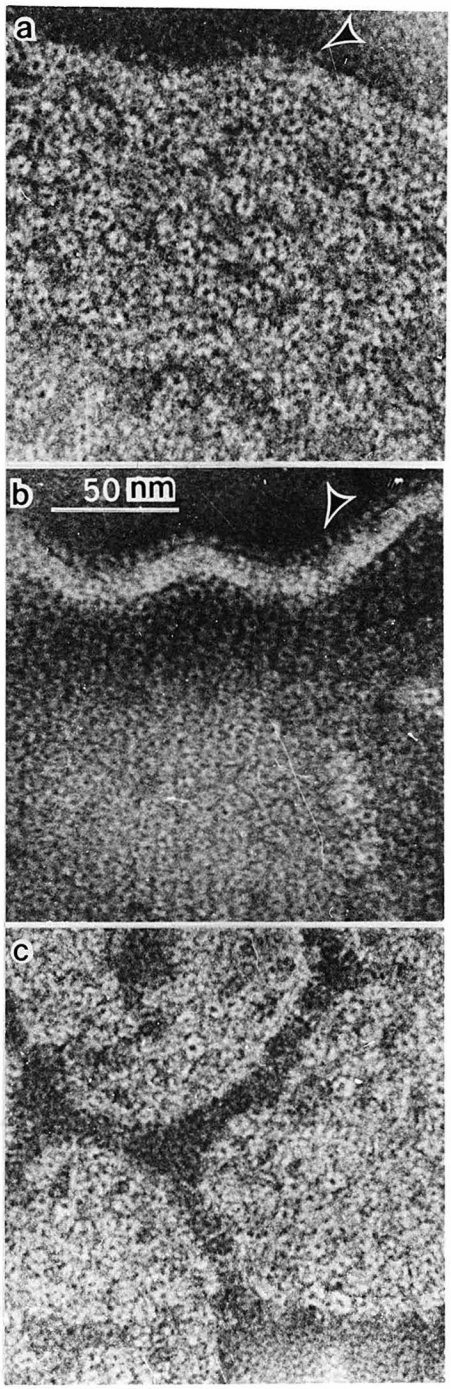


Figure 11

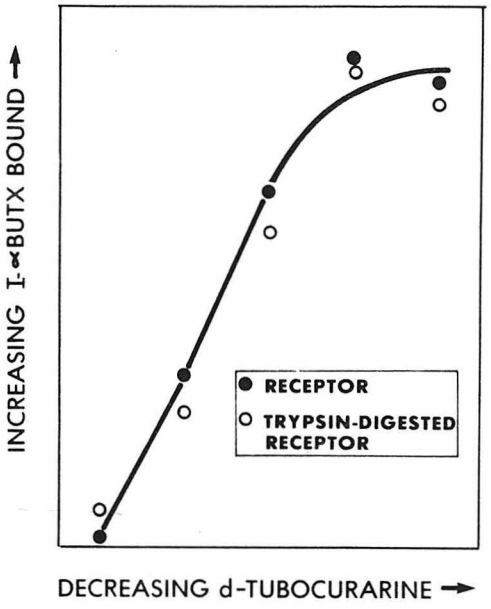


FIGURE 12

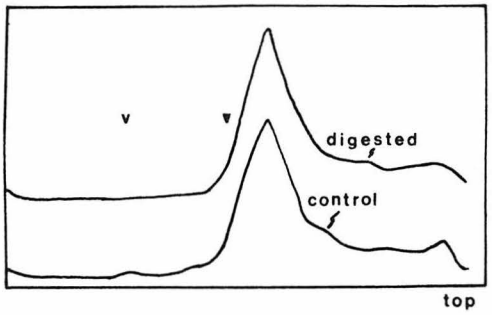


FIGURE 13

PART II

DETERGENT EFFECTS ON TRYPSIN DIGESTION OF THE TORPEDO ACETYLCHOLINE RECEPTOR.

The discrepancy between our work on protease digestion of the membrane-bound receptor (this Chapter, Part I) and the work of Bartfeld & Fuchs (1979) on detergent-solubilized and affinity-purified receptor is the limit digest pattern. They observed only a single band at 27000 daltons whereas we routinely observed a triplet after 72 hours of digestion (3 μM final trypsin concentration) of between 27000 and 33000 daltons. In order to clarify this difference in results we examined the effects of the detergents triton X-100, deoxycholate and digitonin (purchased from Sigma) on the trypsin-digest pattern of acetylcholine receptor.

Because of the observed differences in relative mobilities of the subunits of receptor in different gel systems, I have assumed the following molecular weights for the subunits alpha-40000, beta-50000, gamma-60000, delta-65000 and $delta_2$-185000 (Vandlen et al., 1979; Hamilton et al., 1979), in order to facilitate comparison.

Receptor-enriched membranes were prepared by alkali-treating crude membranes before sucrose gradient centrifugation (Part I) and were found to have specific activities of between 4 to 6 nanomoles αbutx bound per milligram protein as determined by DEAE-disk assay (Schmidt & Raftery, 1973) and greater than 80% receptor by SDS-PAGE.

Limit digestion (5 μM final trypsin concentration, trypsin added every 24 hours) of receptor membranes and triton-solubilized (figure 1b & d) reveals that both the membrane-bound and triton solubilized form the same initial (figure 1a & c) and limit polypeptides (figures 1b and d), but that the extent and rate of digestion is much greater in detergent. In both cases the major end-product is a band (possibly a doublet) of 27000 daltons. A broad band at about 45000 daltons also appears upon digestion but disappears again with time (figure 1).

A portion of the membrane-bound receptor resists degradation (figure 1b) in the limit digest case. Conventionally prepared membranes are often very resistant to trypsin digestion (Part I), and these membranes were rendered susceptible to trypsin digestion by alkali-removal of peripheral proteins. The effect of triton solubilization seems to be common to all detergents since deoxycholate and digitonin also enhance both the rate and extent of trypsin degradation (figure 2).

Since detergent disruption of the membrane enhances receptor digestion by trypsin but does not result in new trypsin-sensitive sites it appears that the detergent effect is primarily one of overcoming the steric hindrance inherent in the geometry of the membrane (figure 3), either through disrupting the lipid bilayer and the packing of receptor molecules (figure 3b) or by removing peripheral proteins from the neighborhood of the receptor molecules (figure 3c). Since a large proportion of the receptor molecules are degraded in the membranes it seems unlikely that the membrane geometry alone is responsible for the residual undigested receptor. It may be fortuitous, but the amount of

residual 43000 dalton peripheral protein at the start of the digestion (figure 1a) and the amount of undigested alpha at the limit seem roughly equivalent.

References:

Bartfeld, D., & S. Fuchs (1979). Biochem. Biophys. Res. Comm. 89, 512-519.

Hamilton, S.L., M. McLaughlin & A. Karlin (1979). Biochem. 18, 155-163.

Schmidt, J. & M.A. Raftery (1973) Anal. Biochem. 52, 349-354.

Vandlen, R.L., W.C.-S. Wu, J.C. Eisenach & M.A. Raftery (1979) Biochem. 18, 1845-1854.

FIGURE LEGENDS

Figure 1.

The onset of trypsin degradation is extremely rapid. Parts (a) and (c) show membrane-bound and triton solubilized receptor, respectively, at time zero and 1, 2, and 5 minutes after the addition of 10 μM trypsin (final concentration). Limit digestion of membranes (b) and triton-solubilized (d) receptor was accomplished by making the receptor 5 μM trypsin at time zero, 2, 3, 4, 5, and 5.5 days. Except for the last point which was incubated at room temperature, the digests were carried out at 4°C. Open arrow marks location of 45000 dalton band and solid arrow marks 27000 dalton digest product.

Figure 2.

Gel shows the effects of detergent (c-triton, d-deoxycholate, e-digitonin each at 0.1% final concentration) on trypsin digestion of the receptor. Track a is the pre-digest control and track b is the pattern obtained by digesting the receptor membranes. Digestion was overnight at 4°C with a trypsin concentration of 10 μM.

Figure 3.

The increase in both rate and the extent of trypsin digestion of detergent-solubilized receptor as compared with membrane-bound receptor may arise from the effect of detergent in breaking up (a) the steric constraints on trypsin accessibility inherent in the receptor packed membrane (b) and the removal of residual peripheral proteins (c) which may block trypsin access to the receptor. Trypsin molecule (oval shape) and receptor molecules are drawn to scale.

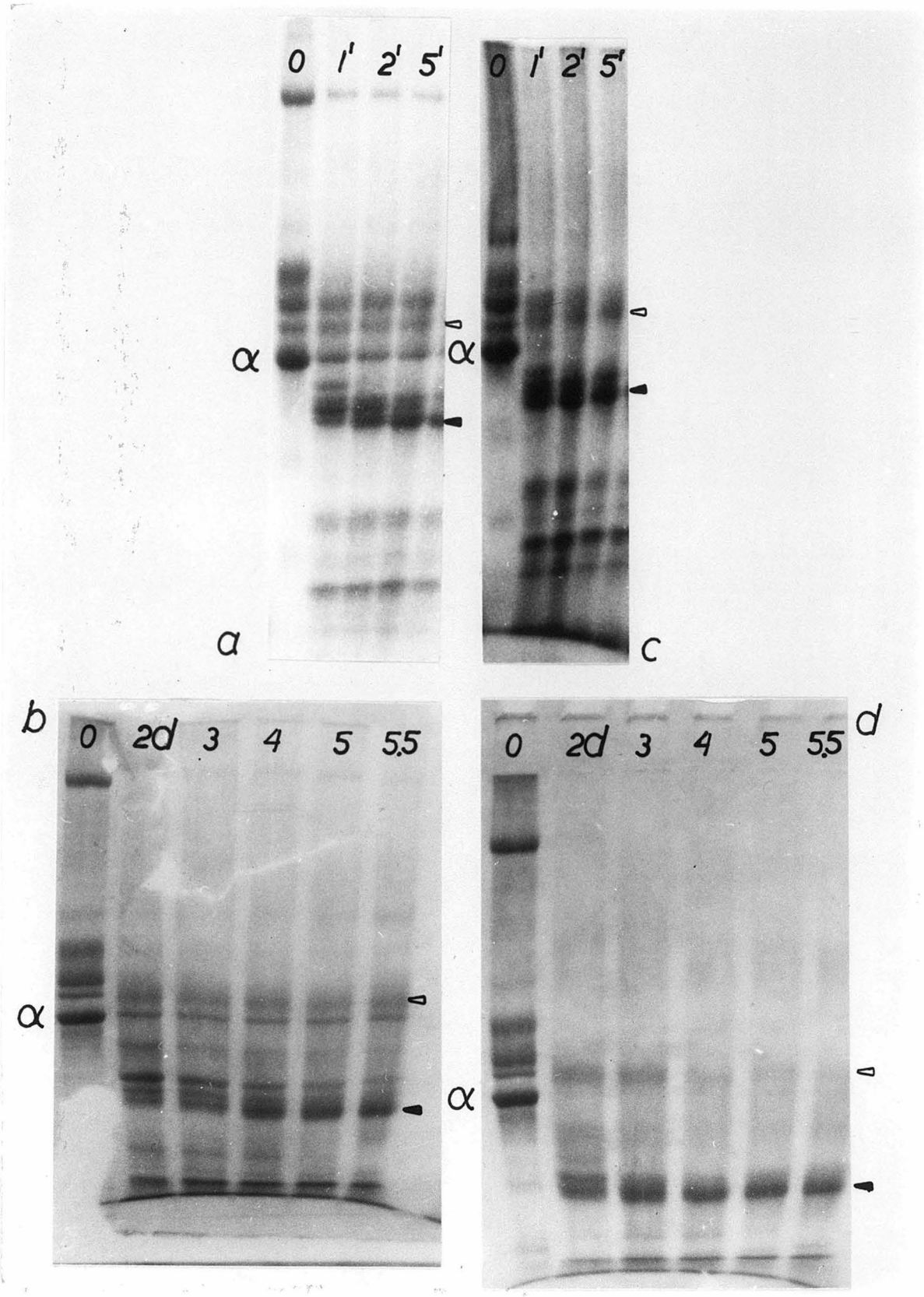


Figure 1

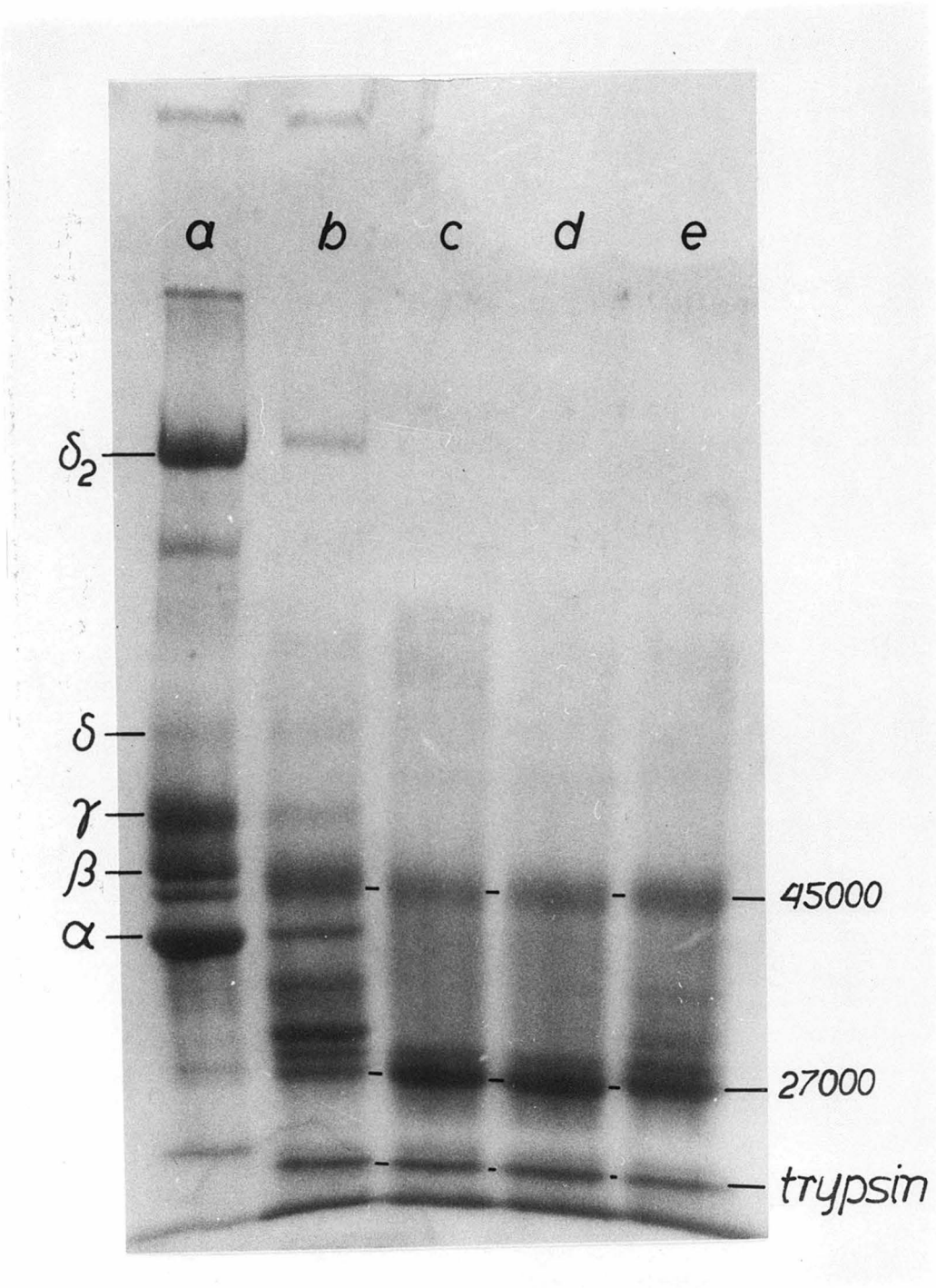


Figure 2

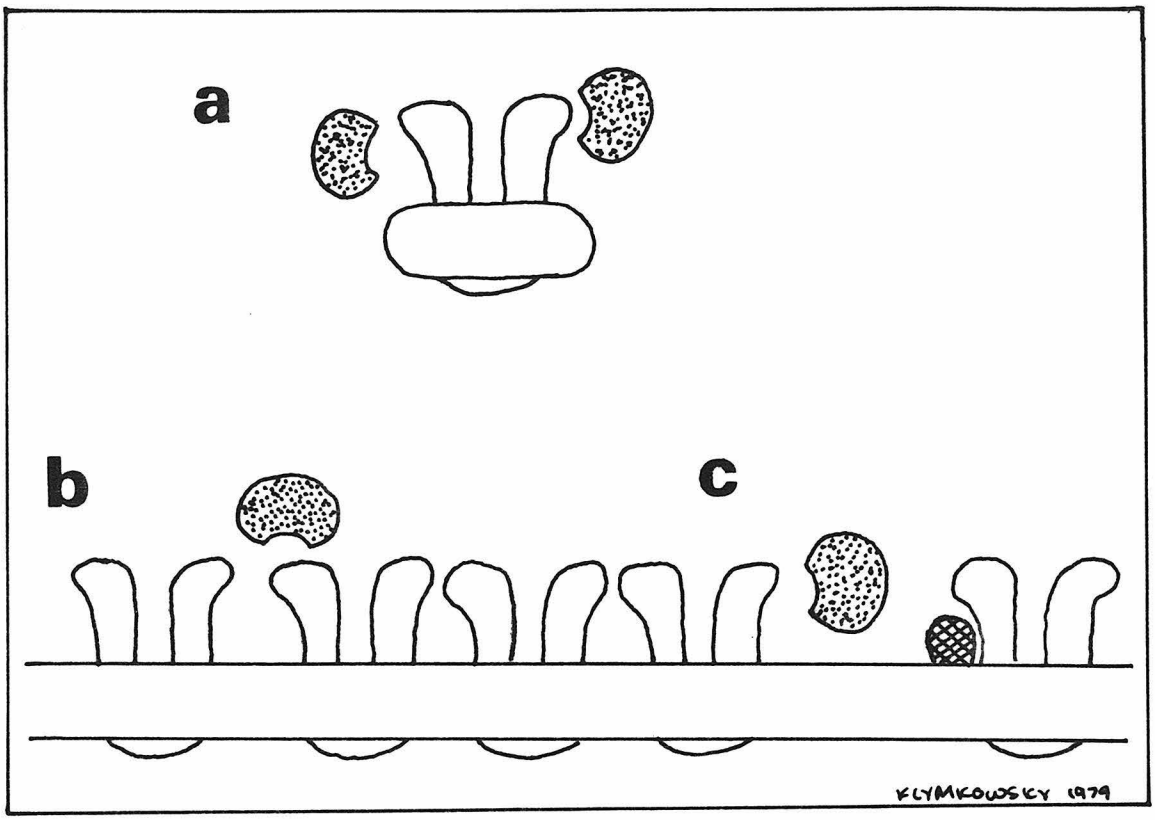


Figure 3

CHAPTER FIVE

LOW RESOLUTION STRUCTURE

Marco Polo describes a bridge, stone by stone,
"But which is the stone that supports the bridge"
Kublai Khan asks.

"The bridge is not supported by one stone or another,"
Marco answers,
"but by the line of the arch that they form."

Kublai remains silently reflecting. Then he adds:
"Why do you speak to me of the stones?
It is only the arch that matters to me."

Polo answers,
"without stones there is no arch."

from: Invisible Cities
by Italo Calvino

INTRODUCTION

This final chapter describes electron microscopic and Fourier image analysis of highly purified, membrane-bound acetylcholine receptor in both monomeric and dimeric forms. This work coupled with our previous x-ray (Chapter Two) and electron microscopic analysis (Chapter Three) resulted in a low resolution structure of the membrane-bound acetylcholine receptor (figure 10), one of the first eukaryotic plasma membrane proteins to be visualized in such detail.

Starting with this basic knowledge of the receptor's molecular shape, new experiments designed to further elucidate the receptor's structure can be devised and more readily interpreted.

ON THE LOW RESOLUTION STRUCTURE OF A MEMBRANE-BOUND ACETYLCHOLINE RECEPTOR

Michael W. Klymkowsky* & Robert M. Stroud**

*Division of Biology

California Institute of Technology

Pasadena, California 91125

**Department of Biochemistry & Biophysics

University of California at San Francisco

San Francisco, California 94143

ABSTRACT:

Electron microscopic analysis of acetylcholine receptor-rich membranes derived from Torpedo californica indicates that the receptor molecules extend less than 10 Å out from the intracellular surface and image reconstructions of small crystalline patches of negatively-stained dimeric receptor, in membranes stripped of peripheral proteins show asymmetry even at approximately 38 Å resolution. The molecule has a large central channel, accessible to both tungstate and uranyl ions, which descends down to the membrane surface. Receptor molecules in prepararations which preserve the disulfide cross-linked dimer show major repeats at low resolution corresponding to a unit cell of dimensions a=88 ± 5, b=88 ± 3 Å, γ= 118° ± 2°, essentially the same as found for monomer preparatons where the unit cell contains a single 260,000 dalton monomer. No indication of a super lattice was obtained in the dimer preparations and correspondingly, there is no evidence for two-fold symmetry axes between monomers in the dimeric species. The lattices contain approximately 22% lipid, 78% protein. The calculated radius of gyration of the experimentally determined structure is 41 to 42 Å for the monomer and about 60 to 61 Å for the membrane-bound dimer.

A second set of rarely occurring non-receptor crystalline membranes has been identified in receptor preparations which has a significantly larger unit cell: a=97 ± 4, b=95 ± 5 Å, γ= 121° ± 3°. The repeating unit in these areas has a featureless convex spherical profile in tungstate stain and has a shallow central well in uranyl stains. By

immunochemical, biochemical, and morphological criteria these areas have been demonstrated to be different from the receptor.

This work is a continuation of our low resolution x-ray diffraction and electron microscopic structural analysis of the acetylcholine receptor from Torpedo.

INTRODUCTION:

Membranes prepared from the electric organ of Torpedo and Electrophorus offer an accessible system for the study of a nicotinic acetylcholine receptor, particularly in Torpedo where the entire innervated surface of the electrocyte is densely packed with the receptor molecules. These postsynaptic membranes can be isolated by homogenization and isopycnic centrifugation (Duguid & Raftery, 1973; Cohen, et al., 1972) and have been studied biochemically (for a review of the extensive work in this area, see Fambrough, 1979) and structurally by x-ray diffraction (Dupont, et al., 1974; Raftery, et al., 1975; Chapter Two), circular dichroism (Moore, et al., 1974), neutron scattering (Wise, et al., 1978), and electron microscopy (Nickel & Potter, 1973; Cartaud, et al., 1973, 1978; Raftery, et al., 1974; Potter & Smith, 1977; Chapters Three & Four). Significant details of the shape, size, secondary structure and lipid environment have been determined (Chapters Two & Three).

The occurrence of ordered areas of receptor particles (Cartaud, et al., 1973, 1978) makes fourier image analysis possible, but the ordered areas are rare. Techniques which have been developed to preserve the native dimer (Chang & Bock, 1977; Hamilton, et al., 1977) and to remove many of the residual peripheral proteins associated with the receptor (Neubig, et al., 1979; Elliot, et al. 1979), make possible the preparation of essentially pure receptor membranes, which tend to show greater degrees of crystallographic ordering. Using such membranes we have applied electron-microscopic and image analysis techniques which extend our previous conclusions on receptor structure (Chapters Two &

Three) and permit a description of the overall structural features of the molecule.

MATERIALS & METHODS:

Conventional and alkali-treated receptor-enriched membrane fractions were prepared by homogenization and isopycnic centrifugation as described previously (Chapter Four, part I). The specific activity of the receptor membranes was typically in the range of 3-6 nmoles α-bungarotoxin (αbutx)/ mg protein as measured by the DEAE-disk assay of Schmidt & Raftery (1973). Peripheral proteins were removed from conventionally prepared membranes as described in Neubig, et al., 1979. Membranes prepared with 10 mM N-ethyl maleimide (NEM) preserved the native dimer (greater than 80%)(Chang & Bock, 1977). Monomers were formed either by omitting the NEM from the homogenization buffer or by treating dimeric receptor with 5 mM β-mercaptoethanol (βME) for 4 h at 4°C. The relative proportion of dimer to monomer was assayed by SDS-PAGE (Laemmli, 1977) without reduction of the sample prior to electrophoresis. Gels were photographed and scanned as described in Chapter Four, part I. The peaks corresponding to the δ and δ_2 subunits were cut out and weighted to quantitate the proportion of monomeric to dimeric receptor. Electron microscopy was as previously described (Chapter Three) using 2% Na phosphotungstate (PTA)(pH 7.4), 1% uranyl oxylate (pH 6) or 2% methylamine tungstate (MAT) (pH 7).

Densitometry was performed on a Syntex Analytical AD1 flat-bed scanner using a 32 μm spot size. Image analysis was carried out as described in Chapter Two using programs written in this laboratory for use on a Data General Nova 800 computer. Diffraction patterns were indexed

such that $F_{(10)} > F_{(01)} > F_{(1\bar{1})}$ and the angle between (1,0) and (0,1) reflections defined as acute. A figure of merit was calculated for each reflection according to

$$m(hk) = \frac{\Sigma_{ij} F_{ij}^2 \cos(\phi_{ij} - \bar{\phi})}{\Sigma_{ij} F_{ij}^2} \quad hk.$$

where i and j index the area averaged around each reflection (Chapter Two). The overall figure of merit for the lattice is defined as

$$M = \frac{\Sigma_{hk} F_{(hk)}^2 \, m_{(hk)}}{\Sigma_{hk} F_{(hk)}^2}$$

All image reconstructions presented are from masked phase-averaged, transforms where resultant $F_{(hk)}$ are placed on the lattice points. The advantages and disadvantages of phase averaging have been discussed previously (Chapter Two). In this case the sharpness of the reflections and the generally good phase coherence of the reflections (overall merit between .86 and .97) justifies the phase averaging procedure.

Lattices were grouped on the basis of morphology since the characteristic ∿85 Å rosette has previously been shown to correspond to the receptor, and can now be unambiguously identified in these membranes as a result (Chapter Three). The significance of the difference between the cell dimensions of the crystalline types was tested using the Welch

statistical test which is independent of population variance (see Mack, 1967).

To calculate the radius of gyration of the monomeric receptor, the model derived from x-ray diffraction and electron microscopic information (Figure 9) was digitized in sections of thickness Δ = 5 Å, and the inner (r_i) and outer (r_{oj}) radii were measured at the center of each section of height h_j. The molecular weight was calculated from the volume of the model, and using the value of .74 g/cm^3 for the partial specific volume, calculated from the receptor's amino acid composition (Changeux et al., 1975). The center of mass (h) was calculated using the formula

$$\frac{\Sigma_i \; V_i \; h_i}{V} = h$$

where V_i is the volume of the section at height (h_i) with the origin at the intracellular surface end of the molecule. $V = \Sigma_i \; V_i$ is the total molecular volume (335,000-347,000) corresponding to a molecular weight range of between 272,000 to 282,000. The radius of gyration (Rg) ($\Sigma mR^2/\Sigma m$ with respect to the center of mass) of a solid sphere is

$$Rg = \sqrt{\frac{3}{5}} \; R_s$$

where R_s is the radius of the sphere. The radius of gyration of the model structure was calculated assuming cylindrical symmetry and con-

stant density according to

$$Rg = \left[\frac{\Delta\Pi}{2V} \quad \Sigma_j (r_{oj}^4 - r_{ij}^4) + 2\Sigma (h_j - \bar{h})^2 (r_{oj}^2 - r_{ij})^2 \right]^{1/2} .$$

RESULTS:

Using an iterative method for phasing the continuous x-ray diffraction pattern of orientated membranes (Stroud & Agard, 1979, Chapter Two), an electron density profile, normal to the membrane plane was determined for the receptor-enriched membranes. We have previously shown (Chapter Three) by direct electron microscopic observation that the molecule does indeed protrude above the extracellular membrane surface by 55 Å as predicted. However, only the extracellular portion of the receptor is unambiguously recognizable and the distribution of protein on the intracellular membrane surface has to this point remained unobserved by electron microscopy.

As membranes dry down onto the carbon support film, folds are often formed. A small portion of these are sharp, and unambiguously show receptor molecules in the buckled membrane (see Figure 1a & b). The extracellular head of the receptor is clearly visible projecting on each side of the fold, as illustrated schematically in figure 1c. The maximum width of the folded doublemembranes is ∿200 Å. This corresponds well with the expected maximum 220 Å double membrane thickness based on

the 110 Å length of the receptor molecule as determined by x-ray diffraction analysis (Chapter Two). The central double bilayer thickness of ∿76 Å also agrees well with twice the 40 Å distance between phospholipid head groups for a single bilayer (Chapter Two) considering the shrinkage likely to occur with dehydration within the electron microscope. Since the doubled bilayer thickness is twice the observed bilayer width there must be little of the receptor protruding on the intracellular surface.

Rare areas of limited ordering of the receptor molecules were observed in membranes prepared without removal of peripheral proteins and in which the receptor existed predominantly (>80%) in the 9S, monomeric form (fig. 2a). The diffraction pattern of the area in figure 2a (figure 3a) can be masked and back-transformed (figure 4) to provide a low resolution image of the receptor. Removal of peripheral protein by alkali-treatment (Neubig, et al., 1979) and the preservation of the receptor in dimeric form results in more frequent and better ordered regions (figure 2b). Figure 3b shows the diffraction pattern of one of such areas. Contoured plots of reconstructed images (masked, phase-averaged and back-transformed) from four different ordered receptor areas are shown in figure 5. Of these, 5a, b & c were stained using PTA, and d was stained by uranyl oxylate. Parts b, c & d are unambiguously from membrane sheets which form by the apparent tearing open of receptor vesicle under negative stain conditions (see Appendix III).

The images in figure 5 are arranged so that the angle between the (1,0) & (0,1) reflections is acute, and the order of the first order reflections has a clockwise sense, so that the resultant images are all in the same orientation. The common features of all four areas are most likely to be representative of the actual structure of the receptor. The common asymmetric shape, most notably the shallow channel in the upper part of each particle, and the deep central hole which in all cases descends down to the surrounding level, are probably real features of the molecule.

The overall similarity between these receptor areas is striking considering that the areas differ in phase coherence (figure of merit from .86 to .97) and include only reflections out to the (2,0) shell (resolution 38 Å), which are the best determined in the transform. In every case, at most 1 or 2 more reflections are observed beyond this shell, which is surprising considering the sharpness of the first three sets of diffraction orders.

The receptors in the membranes from which the images shown in figure 5 where drawn were greater than 90% dimeric, as assayed by SDS-PAGE under non-reducing conditions. However, the location of the dimer disulfide linkage is not evident from the reconstructed images, the asymmetry in the structure and absence of any reflections in the image transform corresponding to a dimer repeat (≈180 Å)(Fig. 3b)(above the noise level or phase coherence criteria used previously, -see Chapter Two) does not permit an analysis of the dimeric association.

Homologous, or heterologous interactions of the type shown in figure 6 are possible. Orientation as in 6a should result in a two-fold symmetric image. The molecules may all be oriented similarly (6b) in which case the images (figure 5) reflect the actual structure of a single monomeric receptor, or the molecules can have different orientations (figure 6c) and the reconstructed images from dimeric species are a superposition of the two different orientations.

The similarity between monomeric (fig. 4) and dimeric receptor images (fig. 5) supports a scheme similar to fig. 6b, however the possibility exists that even in the absence of a disulfide bond between monomers, the molecules aggregate in the membrane in a manner analogous to the dimer form.

We have also observed a second, rarely occurring type of crystalline domain in the receptor-rich fractions. These membranes differ from the receptor membranes in their overall morphology which is either sheet-like (figure 7b & d) or is populated with sharply defined crystalline patches (figure 7a & c) in otherwise particle free membranes. Crystalline membranes of this type are made up of round particles when visualized in PTA or methylamine tungstate (see figure 7a, b & c) and have a shallow central well in uranyl stains (fig. 7d). These membranes are unlabeled by antireceptor antibodies attached to colloidal gold (Chapter Three) and do not undergo the protease-induced morphological transformation seen in receptor membranes (Chapter Four, part I).

The two lattice types (i.e., receptor and other) can be grouped

separately and their a and b cell edge lengths plotted (figure 8). The difference between receptor lattice dimensions (a=88 ± 5, b=88 ± 3 Å, γ= 118° ± 2° n=5) and this second type (a=97 ± 4, b=95 ± 5, γ= 121° ± 3°, n= 12) is evident and can be useful as a diagnostic for these species. The mean values of the two classes are significantly different to within a confidence level $p \geq .99$ as determined by the Welch statistical test.

We have observed equatorial x-ray diffraction reflections from oriented, highly purified dimeric and monomeric receptor membranes corresponding to reciprocal spacings of 76 and 42 Å (Fairclough, Klymkowsky & Stroud, manuscript in preparation) which are consistent with the first (1,0) and second (1,1) orders of a receptor lattice of a=b= 88 Å.

Electron microscopic analysis (Chapter Three) indicates that the in-plane cross section of the receptor molecule narrows from about 85 Å diameter to ∿60 Å at the membrane surface (figure 9). The unit cell area is 6700 ± 500 $Å^2$. The receptor membranes are 110 Å thick thus a "unit volume" of 737,000 $Å^3$ contains a single monomeric receptor molecule. The molecular weight of the monomeric receptor species derived by Reynolds & Karlin, 1978; Martinez-Carrion & Raftery, 1975; Hucho, et al., 1978, is about 260,000 daltons. The partial specific volume for the receptor protein is 0.74 cm^3/g (Changeux, et al., 1975), thus the monomer is expected to occupy a volume of 320,000 $Å^3$, quite close to the volume calculated from our model, 335000-347000 $Å^3$. If the molecular diameter is assumed to remain roughly constant at about 60 Å through the membrane

bilayer then ∿3900 $Å^2$ of the unit cell area would be occupied by lipid, with a volume for the 40 Å thick membrane of 156,000 $Å^3$. Together lipid and protein make up ∿65% of the "unit cell volume" which would then be 35% solvent. Assuming that each lipid molecule occupies a mean surface area of 62.7 $Å^2$ (Levine & Wilkins, 1971), and assuming a lipid molecular weight of 600 (based on the 1:1 molar ratio of phospholipid to cholesterol (Schielber & Hucho, 1978), then there would be about 74,600 daltons (or about 100 molecules) of lipid per unit cell bilayer volume. This results in a calculated lipid to protein ratio of 22%:78% for the close packed, latticed areas which is suprisingly close to the experimental value determined by Schielber & Hucho (1978) of 30%:70%. The difference arises mainly from the denser packing density of receptor molecules in the ordered regions compared to the membranes as a whole. The amount of receptor-free area in receptor-rich vesicles is well illustrated in freeze-etched membranes (Cartaud, et al., 1978; Chapter Four, part I).

Using neutron scattering and deuterium density matching of detergents, Wise et al (1979) measured the radius of gyration of the detergent-solubilized receptor monomer to be 46 ± 1 Å. While some structural rearrangements occur upon solubilization (Witzemann & Raftery, 1977) the overall shape of the molecule is undoubtably conserved. From the model of receptor monomer (figure 9) a radius of gyration for the membrane-bound molecule was calculated, which depending on whether the intracellular end was rounded or not had a Rg of between 41 and 42 Å, which is in rough agreement with the value obtained from neutron scattering.

The Rg of dimer receptor in the membrane is calculated to be about 60-61 Å.

DISCUSSION:

The combination of x-ray diffraction and electron microscopic analysis is a powerful one for studying macromolecules, especially integral membrane proteins such as the nicotinic acetylcholine receptor which have yet to be crystallized. High angle x-ray diffraction analysis on oriented samples (Chapter Two) showed the presence of 80 Å long α-helices oriented perpendicular to the membrane plane in the receptor molecule, demonstrated the fluid-nature of the membrane lipids at 4°C and indicated the presence of a small sub-population of solid phase lipids both at 4°C and at 20°C. Small angle x-ray diffraction analysis of the oriented, continuous diffraction pattern, phased by the constrained, iterative method of Stroud & Agard, 1979 gave the electron density distribution normal to the membrane plane (Chapter Two). Electron microscopic observation of first the extracellular portion (Chapter Three) and now indirectly the intracellular surface (figure 1) confirm and extend information derived from the x-ray profile.

The radius of gyration (Rg) calculated from the electron microscopic/ x-ray diffraction composite model (figure 9) was compared with that determined by neutron scattering (Wise, et al., 1979). The neutron scattering studies were carried out on detergent solubilized receptor, with detergent matched out by the appropriate D_2O/H_2O solvent ratio, and gave a value Rg = 46 ± 1 Å which compares favorably with the Rg = 41-

42 Å for our model. The agreement between the neutron result and our model further confirms our assumptions about those areas of the molecule buried in the bilayer, about which there is little direct information.

The calculated value of Rg for dimeric receptor in the membrane is 60-61 Å. This value is readily calculated from the closest approach of individual monomers within the dimer, and the Rg of the monomer. Thus it reflects both the orientation and intramonomer contacts seen in the membrane. The detergent solubilized dimeric species would have a value different from this if it had different associative orientation in detergent micelles.

The diffraction analysis of ordered areas of dimeric receptor reveals a strong lattice for $|h|+|k|< 3$; ($S^{-1} \simeq 38$ Å) whereupon the signal to noise ratio diminishes significantly. Even such limited resolution provides significant detail if many individual reconstructed areas are compared in the same apparent orientation (figure 5).

Since the reconstructed areas are quite similar (see figs. 4, 5) it is reasonable to assume that the common features, the deep stain-filled central hole and the shallow groove, reflect true features of the molecule. The central hole is also quite apparent in edge views of the molecule (Chapter Three). The presence of the shallow groove indicates a non-symmetric object. However, the roughly circular shape of the receptor molecule gives rise to reflection phases which, by necessity, are close to 0 or π in the lower orders due to the centrosymmetric component of the molecule. After refinement of the lattice origin to

minimize the differences between the low order phases and 0 or π, the resultant sets of phases for different lattices can be compared to give a quantitative estimate of confidence in the particle asymmetry (Table 1).

Perhaps the simplest analysis of asymmetry is provided by comparison of amplitudes, F_o and phase ϕ for first order (hk=(1,0),(0,1), $(\bar{1},1)$) second order (hk=(1,1),$(\bar{1},2)$, $(\bar{2},1)$) and third order (hk=(2,0), (0,2), $(\bar{2},2)$) reflections <u>within</u> single image reconstructions. If the particle were cylindrically symmetric each order would have the same amplitude and phase (0 or π only). If it were two-fold symmetric the phases would be equal within each order (0 or π only) and the amplitudes different. If asymmetric both amplitudes and phases would be different for each reflection.

The average value (four lattices) of $R_{sym} = \bar{\Sigma}|F_{hk}-\bar{F}|/\bar{\Sigma}|F_{hk}|$ for reflections (hk) within each order of one lattice are:

	R_{sym}:	$<\lvert\phi - \pi/(o)\rvert>$
1st order:	16.5%	2.5° ± 1.5°
2nd order:	7.6%	20.6° ± 11.0°
3rd order:	21.5%	23.7° ± 19.0°

At face value these intra-lattice statistics quantitate the degree of asymmetry. However, the three reflections within each order are contained in a high noise environment that itself could enhance the

apparent degree of asymmetry. A more objective test is comparison of inter-lattice equivalent reflections for which the values of $R_{comp} = \sum_{j=1-4} | F_{hk_j} - \bar{F}_{hk} | / \sum_j |F_{hk_j}|$ were:

	R_{comp}	$\sqrt{2}\ R_{sym}$
1st order:	6.8%	23.3%
2nd order:	4.7%	10.4%
3rd order:	7.1%	30.4%

The fact that R_{comp} values are consistently lower than values for R_{sym} show that consistency between the same reflections in different lattices is about 2.5 times better than the consistency between all reflections of the same order within one lattice. This is strong evidence for the degree of particle asymmetry, since a fully (six-fold) symmetric particle, where all differences were due to random noise, should have $R_{comp} \simeq \sqrt{2}\ R_{sym}$, whereas in this case, $R_{comp} \simeq 0.4\ R_{sym}$.

The crystalline receptor areas are most probably made up of dimeric receptor in which the packing types illustrated in either figure 6b or 6c could occur since packing of type 6a should result in a two-fold symmetric image. The lack of a superlattice dimer repeat on the order of 176 Å (figure 3b) indicates that the difference between inter- and intra-dimer repeats has not been observed; thus both monomeric halves (fig. 4) of the dimer are superimposed in the reconstructed images (figure 5), and at this resolution the two monomers look essentially the

same.

That reoxidation of receptor monomers form only dimers linked by δ subunits (Hamilton et al. 1979) suggests that dimer formation excludes the possibility of further inter-molecular disulfide formation. While the simplest explanation for this observation would be that the same sulfhydryl on each δ subunit was involved in dimer formation resulting in a homologous (2-fold) interaction (fig. 6a), there is as yet no evidence from image analysis (i.e., a two-fold axis) to support this contention and thus alternate, heterologous schemes must still be considered (figs. 6b, c).

In the case of 6b dimer formation must result in a conformational change which renders the second δ sulfhydryl non-reactive. In 6c the very geometry of the dimer would prohibit sterically the reactions of the second sulfhydryls. Only in the case of 6b would the image correspond to the image of a single monomeric molecule. The similarity of monomeric receptor (fig. 4) to the dimer (fig. 5) image indicates either that the monomeric receptor packs in a unit cell similarly to the dimer or that the dimer packing is as in figure 6b.

If the crystalline areas seen in dimer-rich membranes are composed of dimeric receptor (as opposed to being made up of monomeric receptor) in at least one direction the unit cell size should be twice the size of the monomer spacing. It seems unlikely that monomer would segregate from dimer and so the lack of a super-lattice implies that the monomer components of the dimer are not sufficiently different at

low resolution. Thus how the dimers are cross-linked remains unanswered.

That the dimer has a function is indicated by the indirect observation that histrionicatoxin (HTX) (a local anaesthetic type toxin) binds in a stoichiometry of 1 molecule per 4 α-bungarotoxin sites (Elliot & Raftery, 1977). Since there are 2 αbutx sites per monomer, the simplest explanation would involve binding of one HTX to the dimeric molecule.

During the course of our work on receptor membranes a second two-dimensionally crystalline species has been observed. These membranes are always sheets or distinct regions within otherwise empty vesicles (figure 7). They have a different unit cell than that of receptor (figure 8), cannot be labeled by antireceptor antibody, and do not undergo the protease-induced morphological change characteristic of receptor membranes ($data_a$ not shown). Unlike receptors, they also appear different in uranyl and phosphotungstate stains. We presume them to be gap or spot junctions derived from other cell types in the electroplaques, although they may well be something else.

We present here a low resolution model of the receptor (fig. 10) derived from both electron microscopic and x-ray diffraction analysis. Starting with this model, we can hope to map out specific sites such as the agonist and toxin binding sites.

TABLE I.

Average values of amplitude ($\bar{F}_{hk}$) and phase ($\bar{\phi}_{hk}$) for the four dimer lattices shown, to 38 Å resolution.

	hk ,	$\bar{F}_{hk} \pm \sigma_{hk}$	$\bar{\phi}_h$	$\pm \sigma_\phi$°
1st order $\phi \sim 0.0$	(10)	19.1 ± 2.0	0.0	± 1.5
	(01)	14.2 ± 0.6	0.0	± 1.5
	($\bar{1}$1)	12.6 ± 1.3	0.0	± 1.5
2nd order $\phi \sim \pi$	(11)	13.2 ± 0.7	160	± 18
	($\bar{1}$2)	11.4 ± 0.6	180	± 33
	($\bar{2}$1)	13.5 ± 1.0	169	± 20
3rd order $\phi \sim \pi$	(20)	12.3 ± 0.9	167	± 35
	(02)	7.6 ± 0.4	157	± 10
	($\bar{2}$2)	8.1 ± 1.1	176	± 34

REFERENCES

Cartaud, J., Benedetti, E.J., Cohen, J.B., Meunier, J.E. & Changeux, J.-P. (1973). FEBS Lett. 33, 109-113.

Cartaud, J., Benedetti, E.L., Sobel,A. & Changeux, J.-P. (1978) J. Cell Sci. 29, 313-337.

Chang, H.W. & Bock, E. (1977). Biochem. 16, 4513-4520.

Changeux, J.-P., Benedetti, E.L., Bourgeouis, J.-P., Brisson, A., Cartaud, J., Devaux, P., Grunhagen, H., Moreau, M., Popot, J.-C., Sobel, A. & Weber, M. (1975). Cold Spring Harbor Symp. Quant. Biol. 40, 211-230

Cohen, J.B., Weber, M., Huchet, M. & Changeux, J-P. (1972). FEBS Lett. 26, 43-47.

Duguid, J.R., and Raftery, M.A. (1973). Biochem. 12, 3593-3597.

Dupont, Y., Cohen, J.B. and Changeux, J-P. (1974). FEBS Lett. 40, 130-133.

Elliott, J. & Raftery, M.A. (1977). Biochem. Biophys. Res. Comm. 77, 1347-1353.

Elliott, J., S.M. Dunn, S.G. Blanchard, & M.A. Raftery (1979). PNAS 76, 2576-2579.

Fambrough, D.M. (1979). Physiol. Rev. 59, 165-227.

Hamilton, S.L., McLaughlin, M. & Karlin, A. (1977). Biochem. Biophys. Res. Comm. 79, 692-699.

Hamilton, S.L., McLaughlin, M. & Karlin, A. (1979). Biochem. 18, 155-163.

Hucho, F., Bandini, G. and Suarez-Isla, Eur. J. Biochem. 83, 335-340.

Laemmli, U.K. (1971) Nature (London) 227, 680-685.

Levine, Y.K. & Wilkins, M.H.F. (1971) Nature New Biol. 230, 69-72.

Mack, C. (1967) Essentials of Statistics for Scientific and Technologists, Plenum Publications, New York.

Martinez-Carrion, M., Sator, V. and Raftery, M.A. (1975). Biochem. Biophys. Res. Comm. 65, 129-137.

Moore, W.M., Holladay, L.A., Puett, D., Brady, R.N. (1974). FEBS Lett. 45, 145-149.

Neubig, R.R., Krodel, E.K., Boyd, N.D., and Cohen, J.B. (1979). PNAS 76, 690-694.

Nickel, E., and Potter, L.T. (1973). Brain Res. 57, 508-517.

Potter, L.T. & Smith, D.S. (1977). Tiss. Cell 9, 585-594.

Raftery, M.A., Bode, J., Vandlen, R., Michaelson, D., Deutsch, J., Moody, T., Ross, M.J. and Stroud, R.M. (1975). in Protein-Ligand Interactions, (H. Sund & G. Blaner, eds.) pp. 328-352, Walter de Gruyter & Co. Berlin.

Reynolds, J.A. and Karlin, A. (1978) Biochemistry 17, 2035-2038.

Schiebler, W. and Hucho, F. (1978) Eur. J. Biochem. 85, 55-63.

Schmidt, J. and Raftery, M.A. (1973) Anal. Biochem. 52, 349-354.

Stroud, R.M. and Agard, D.A. (1979) Biophys. J. 25, 495-512.

Suarez-Isla, B.A. & Hucho, F. (1977) FEBS Lett. 75, 65-69.

Vandlen, R.L., W.C.-S. Wu, J.C. Eisenach & M.A. Raftery (1979) Biochem. 18, 1845-1854.

Wise, D. & Karlin A. (1979) Biophys. J. -in the press.

Witzemann, V. & Raftery, M.A. (1977) Biochemistry 16, 5862-5868.

FIGURE LEGENDS

Figure 1

Negatively-stained receptor-filled vesicles show sharp membrane folds. Bar marks 100 nm in low power view and 10 nm in higher magnification in both parts A and B. Arrow heads mark regions of sharp bend as illustrated schematically in part C. Measurement across heads (o) and doubled bilayer (i) allows an estimate of the intracellular extent of the receptor molecule.

Figure 2

Conventionally prepared, predominantly monomeric (greater than 90%) receptor membrane sheet (A) with an ordered area (marked by 'a' and box) was used to produce the diffraction pattern and reconstructed image in figures 3a and 4. Membrane preparations in which peripheral proteins had been removed (B) and the native dimeric receptor (greater than 85%) preserved, result in a greater degree of ordering, although still of fairly limited extent. Bar marks 100 nm in both parts.

Figure 3

Computed diffraction pattern from (A) the ordered region in figure 2a, and (b) from a dimeric, alkali-stripped receptor membrane. Patterns are on different scales as a result of the scan step sizes used. Note the lack of superlattice in dimeric (B) transform.

Figure 4.

Phase averaged image reconstructed from monomeric receptor membrane in figure 2a.

Figure 5.

Four independent reconstructions of ordered alkali-stripped dimeric receptor regions. Parts A, B and C were stained by PTA; part D was stained by uranyl oxylate.

Figure 6.

Receptor dimers may pack in any of three ways (a,b & c), such that the same sulfhydryl on each monomer is involved in dimer formation (a) or different sulfhydryls are used (b,c).

Figure 7.

Lattices of non-receptor infrequently occur in receptor-rich membrane fractions. They exist within otherwise apparently empty vesicles (a & c marked by arrows and 'a' in part C or in sheets (b & d). In PTA or MAT stains they are featureless while in uranyl stain (d) they have a slight central hole. Bar mark 100 nm in all parts. Parts c & d are at the same final magnification.

Figure 8.

Scatter plot of the a (1,0) and b, (0,1) unit cell dimensions of

receptor (o) and non-receptor (•) lattice. Means and standard deviations are indicated.

Figure 9.

Schematic of receptor structure used in calculating the radius of gyration.

Figure 10.

Drawing of acetylcholine receptor membranes, sodium ions in channel are drawn to scale, alpha helices within molecule are also indicated.

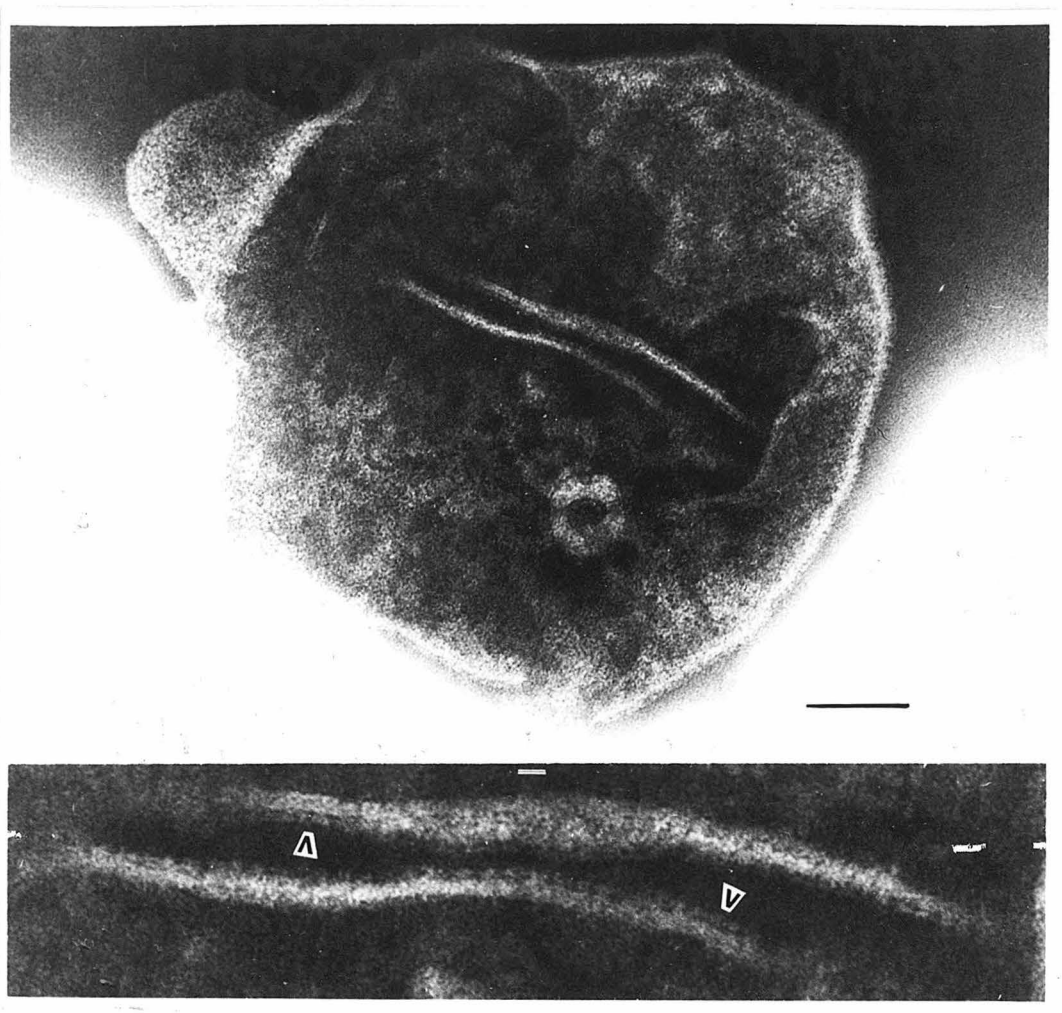


Figure 1a

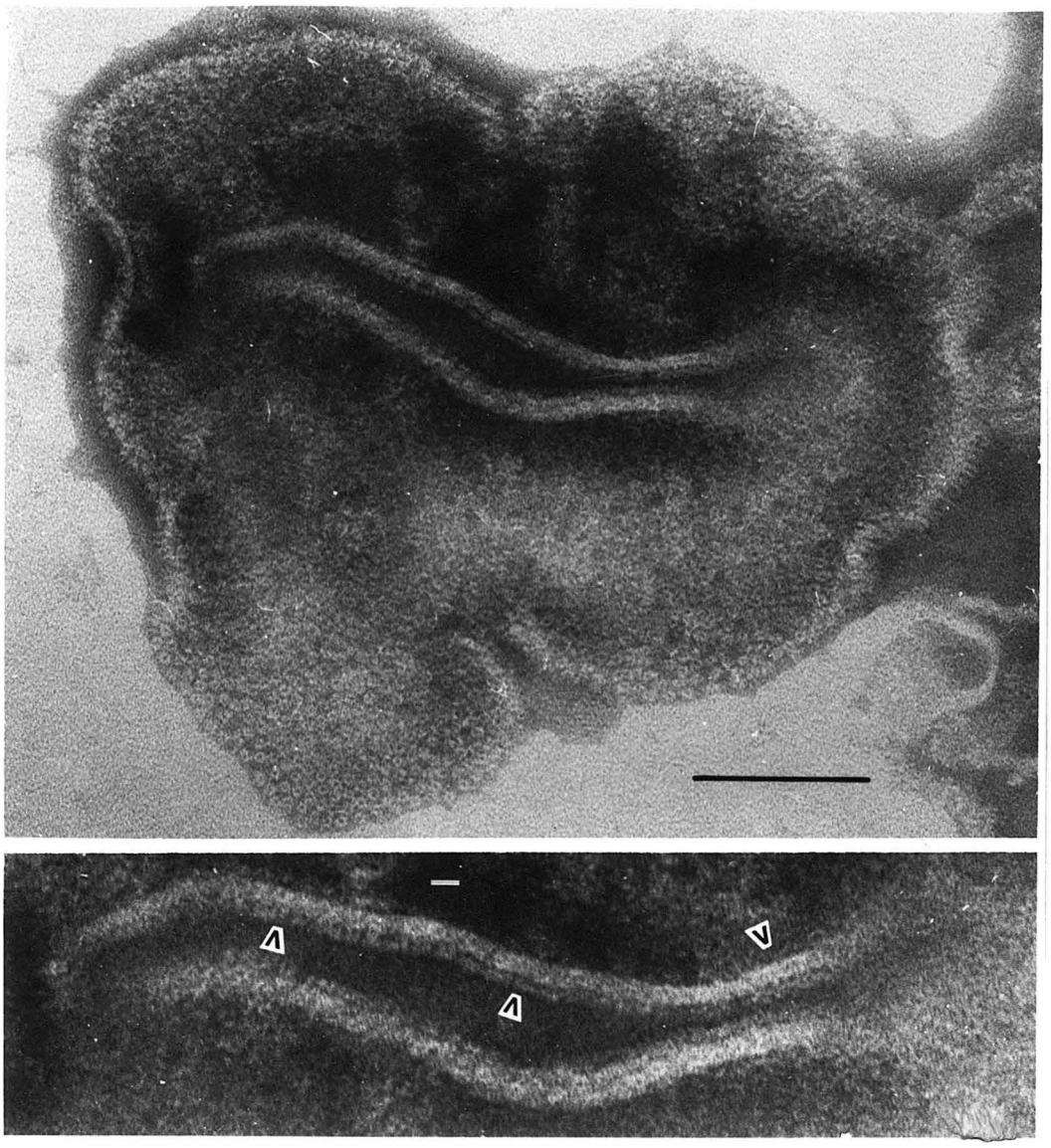


Figure 1b

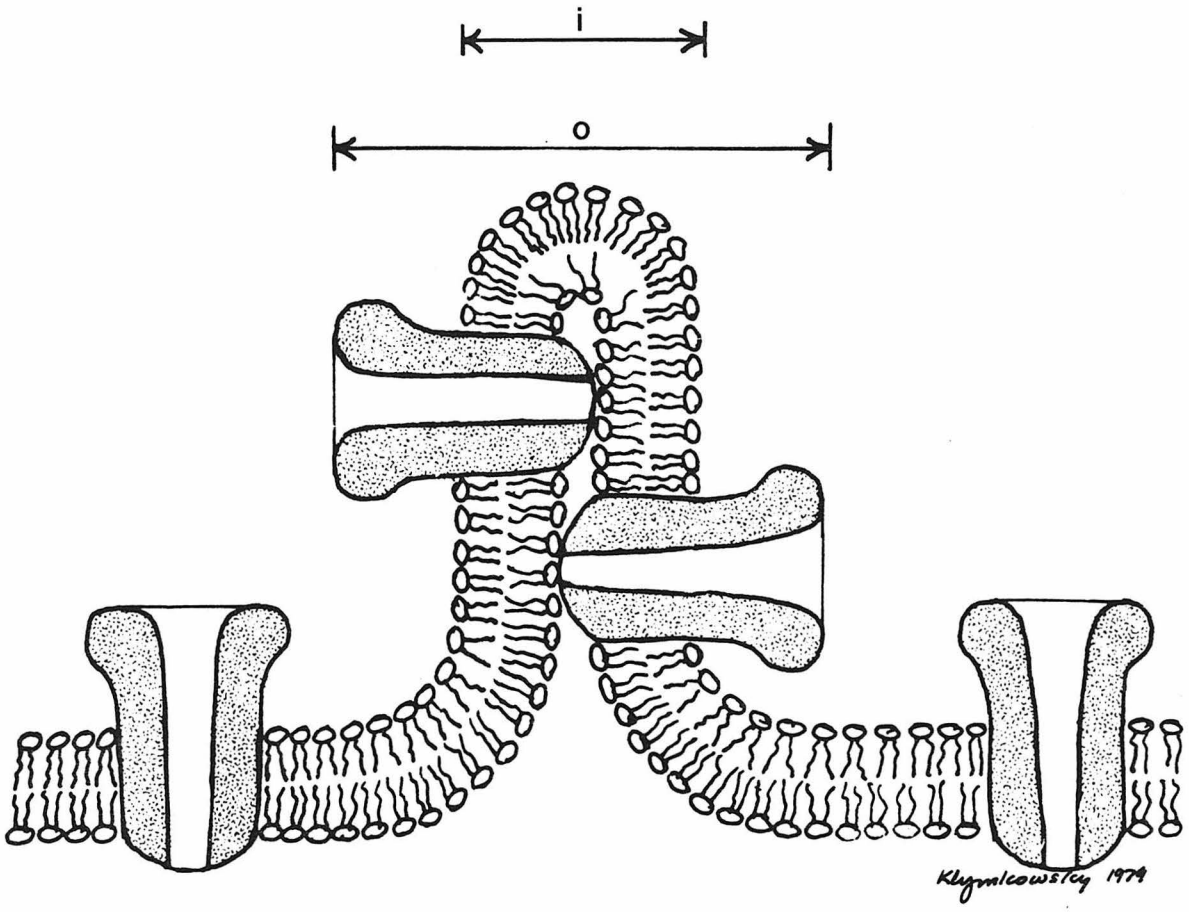


Figure 1c

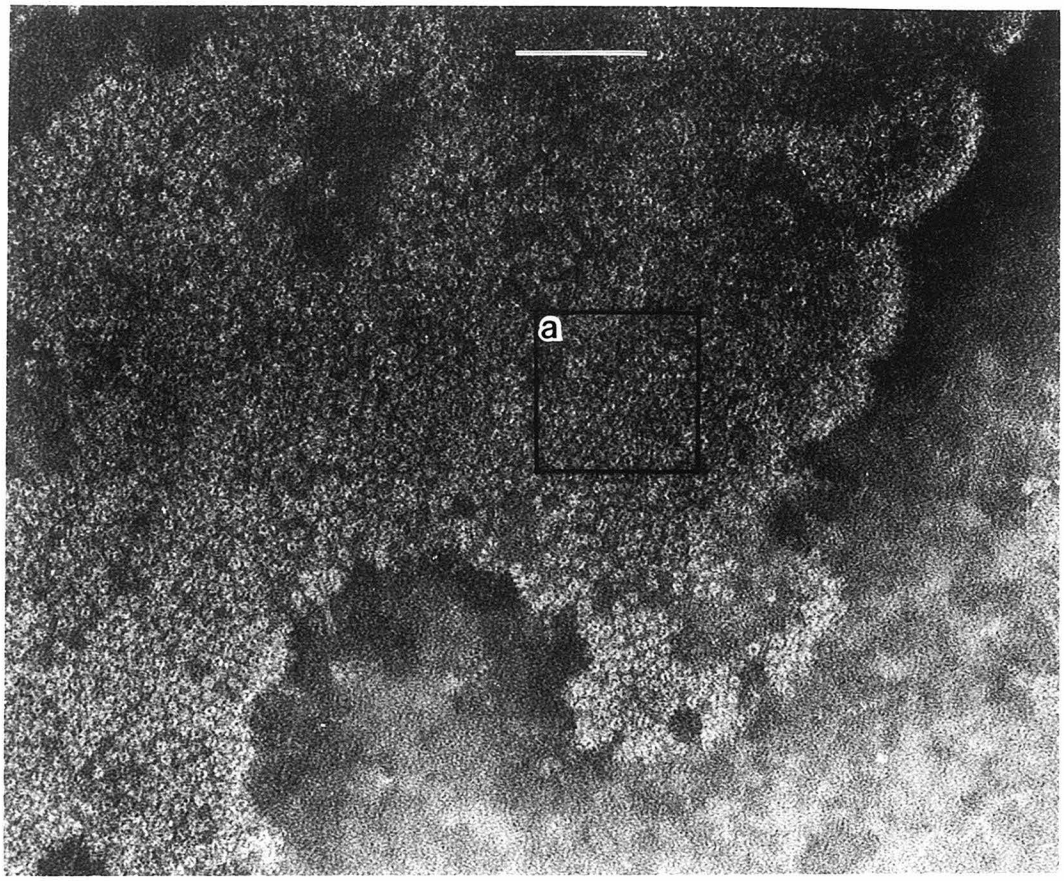


Figure 2a

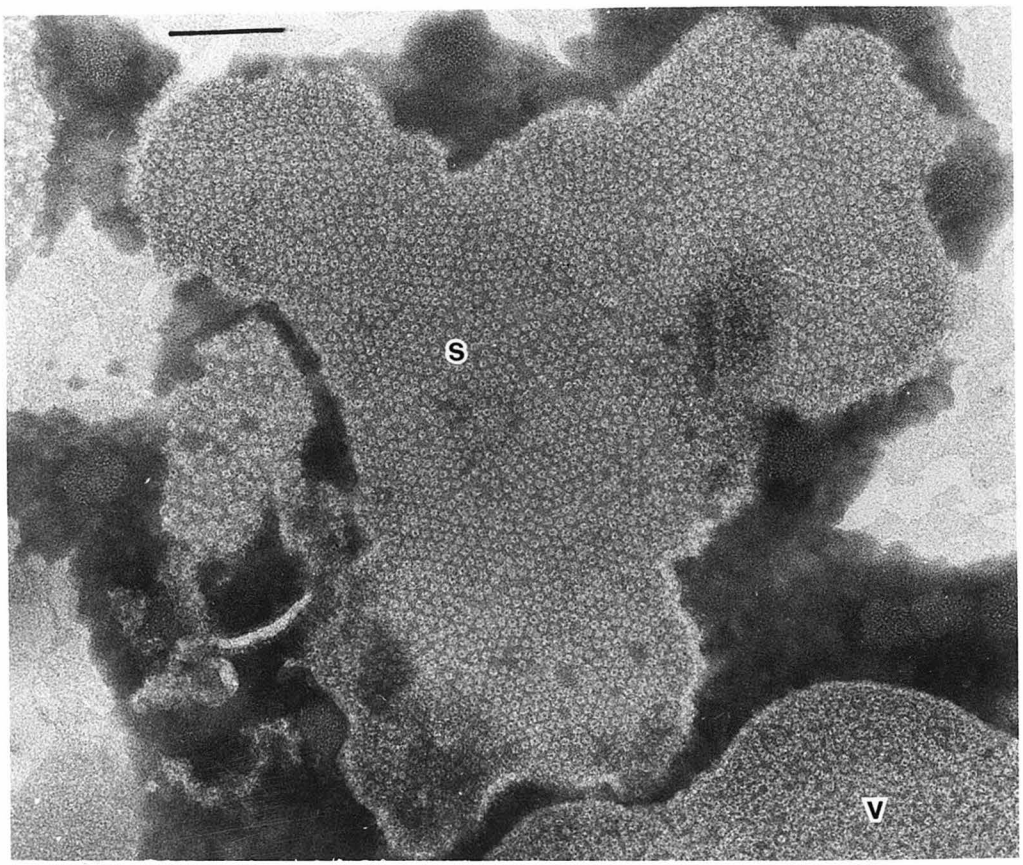


Figure 2b

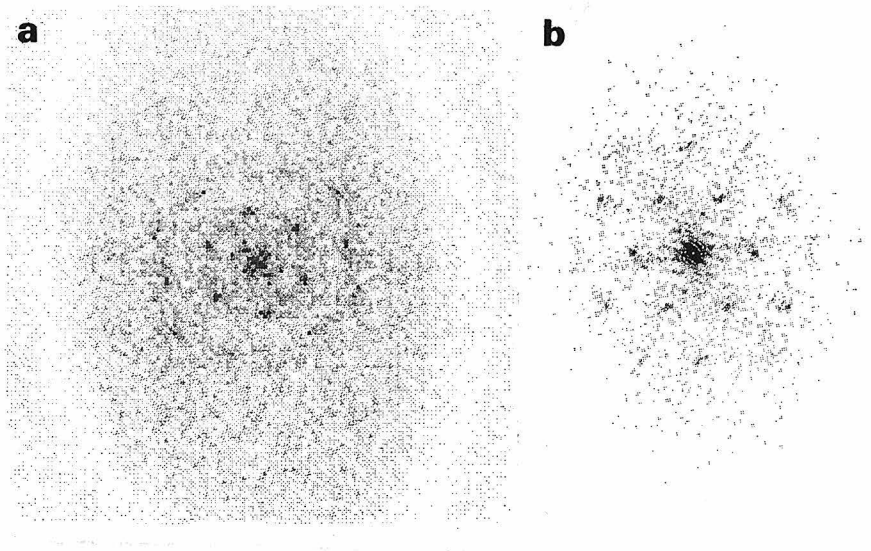


Figure 3

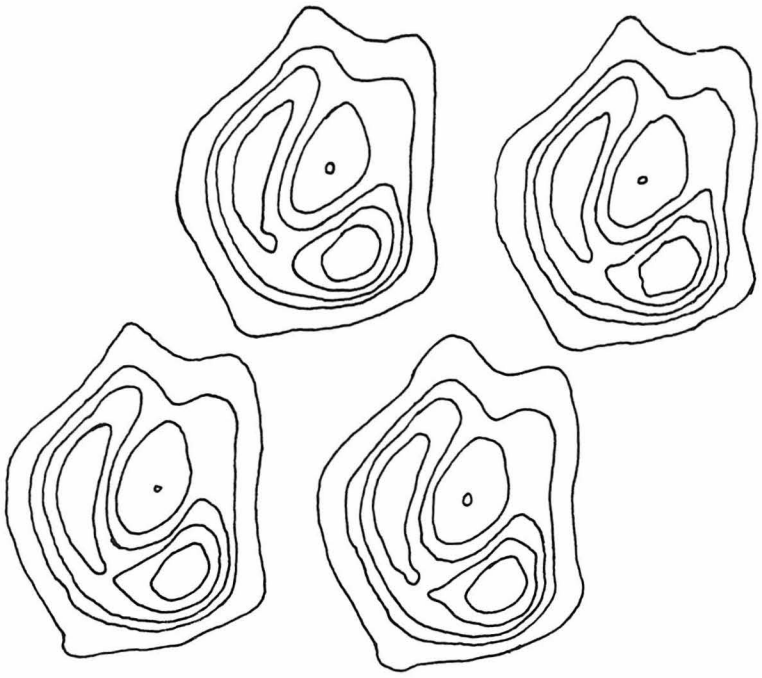


Figure 4

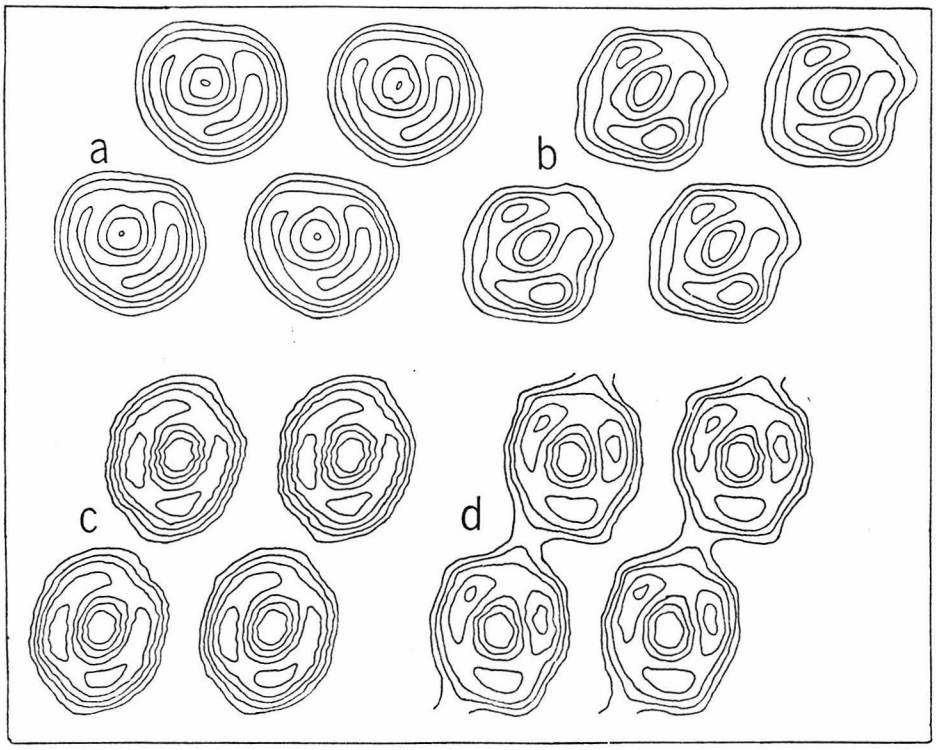


FIGURE 5

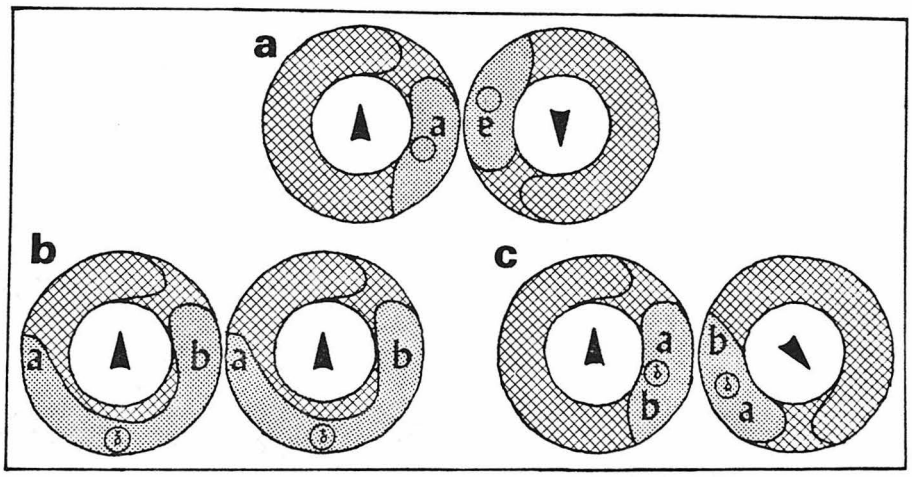


FIGURE 6

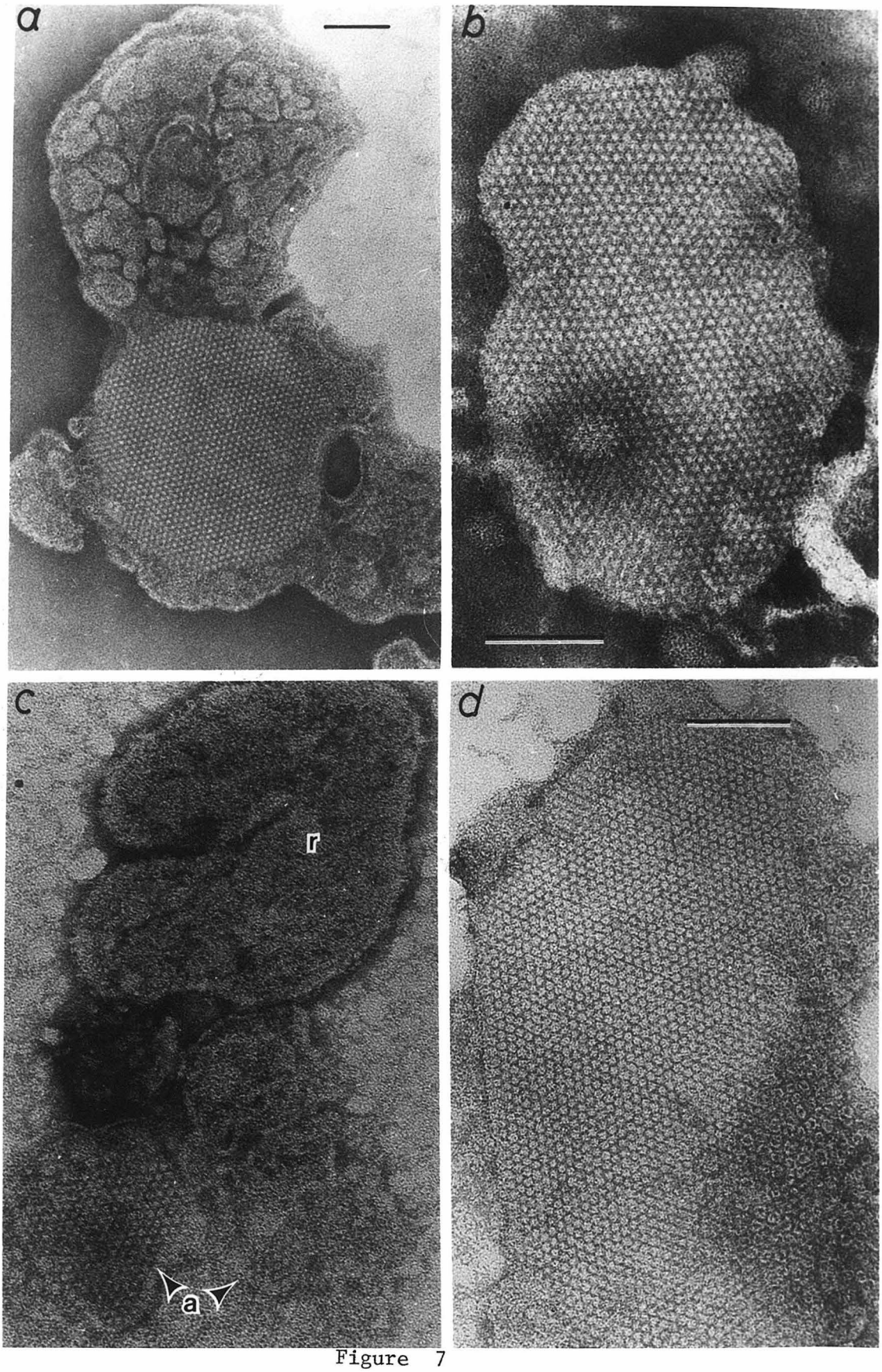


Figure 7

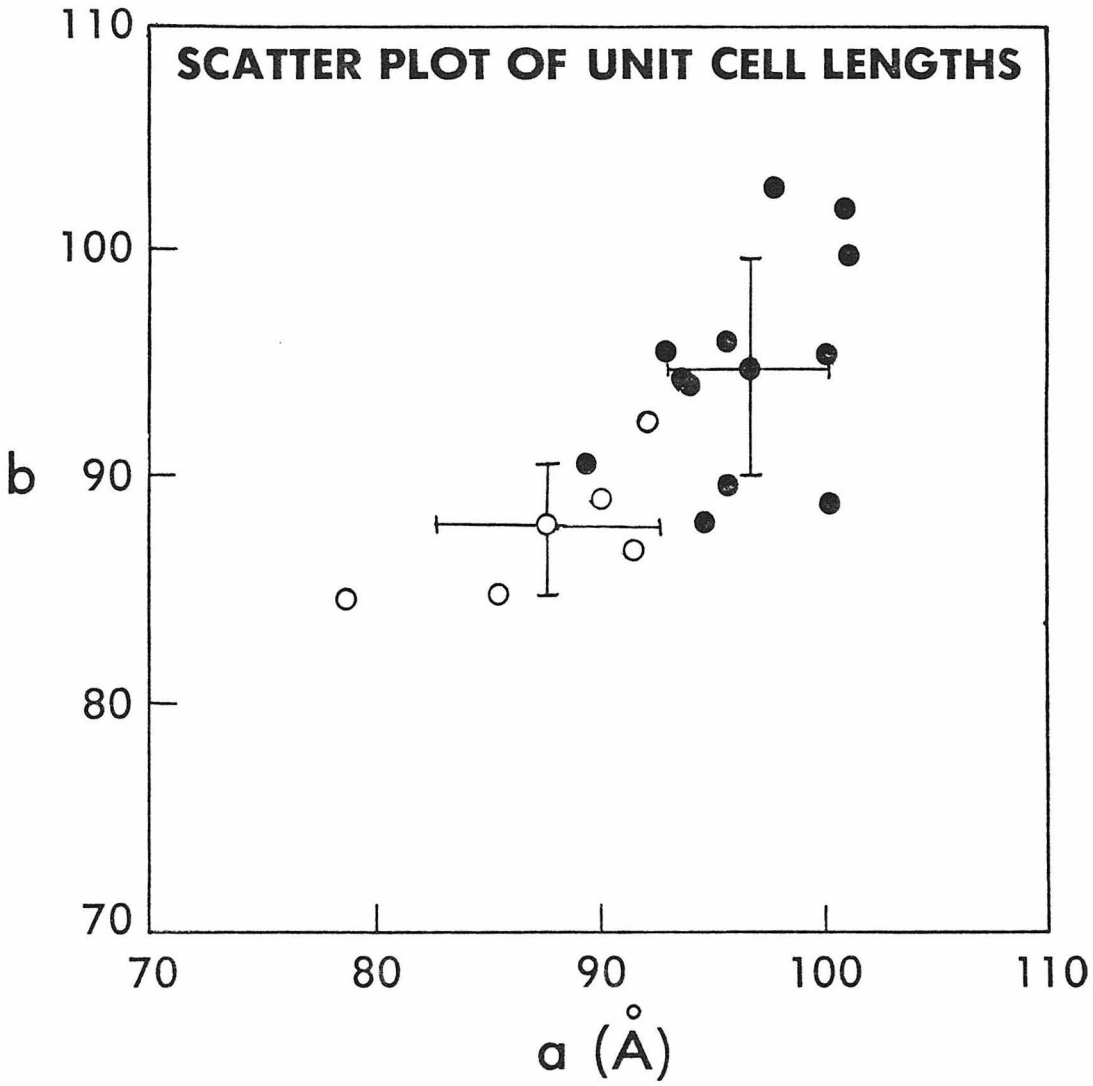

SCATTER PLOT OF UNIT CELL LENGTHS
110
100
90
80
70
b
70
80
90
100
110
a (Å)

FIGURE 8

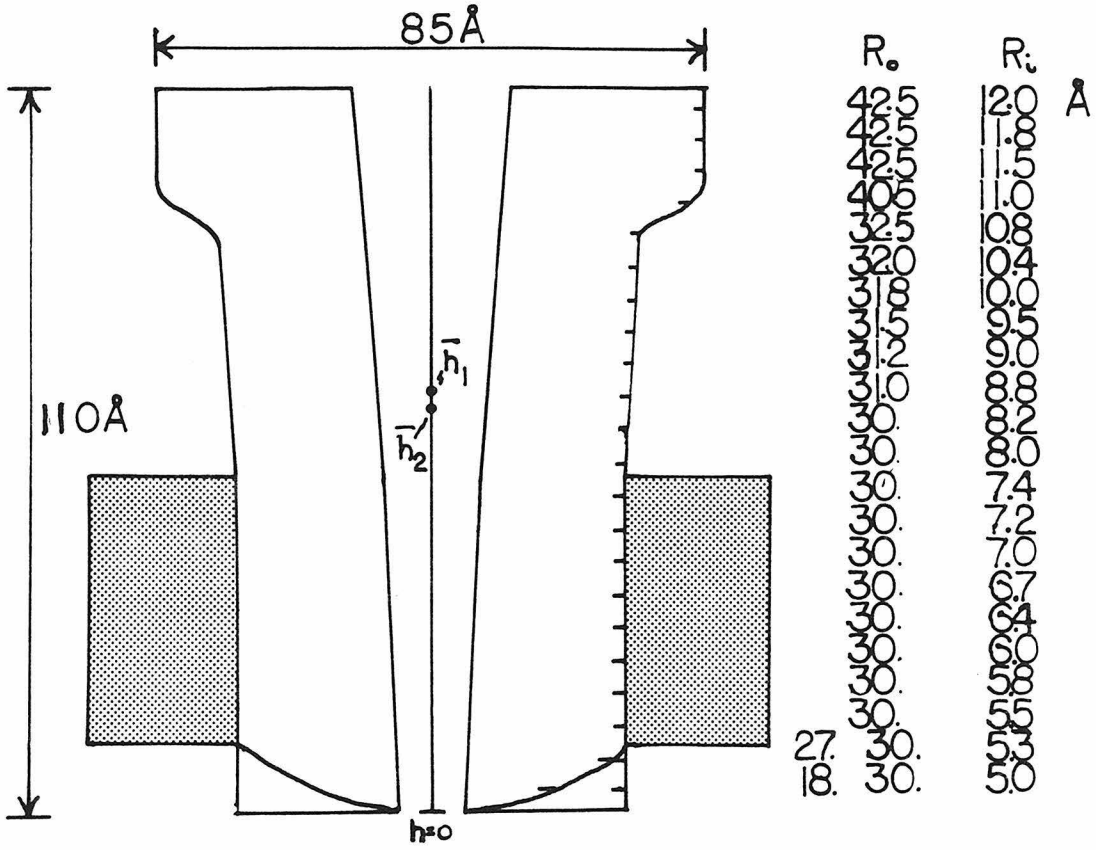


Figure 9

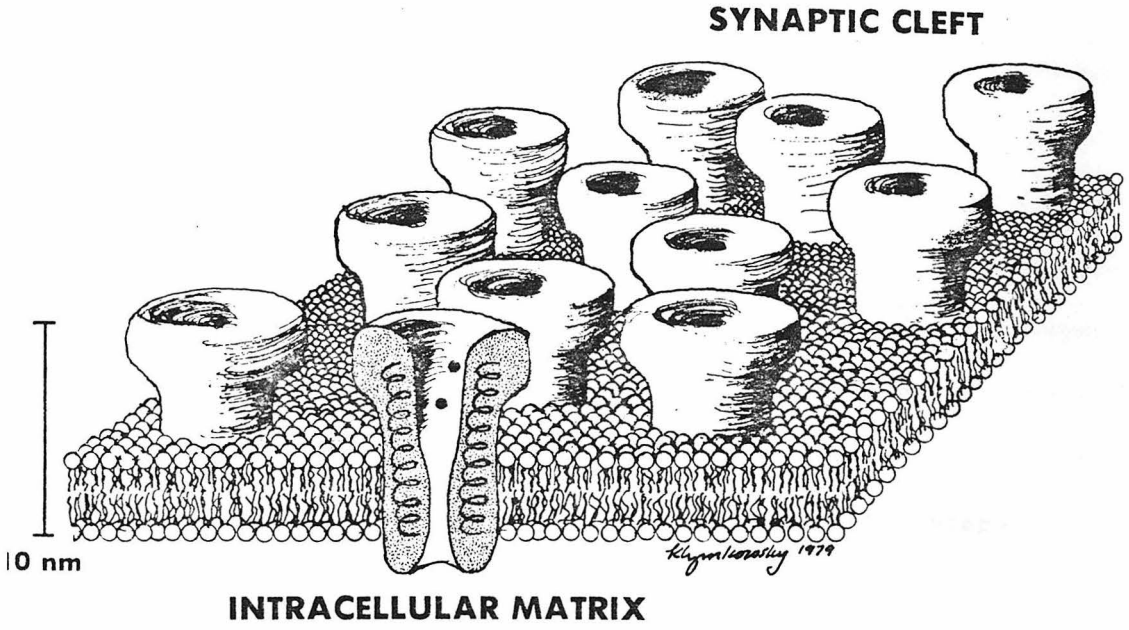


FIGURE 10

APPENDICES

Breaking the silence
Of an ancient pond
A frog jumped into water-

A deep resonance.

-Bashō

APPENDIX I - ETHANOL EFFECTS ON RECEPTOR MEMBRANE MORPHOLOGY AND MEMBRANE DELIPIDATION.

In the course of my work on the effects of proteases on the acetylcholine receptor (Chapter Four), I used the serine protease inhibitor phenylmethylsulfonyl fluoride (PMSF). Since PMSF has a limited solubility (100 μM) and hydrolyzes in aqueous solution, stock solutions (50 to 250 mM) were made up in 100% ethanol. Each inhibition experiment included the effect of the inhibitor alone on membrane morphology and in certain experiments the ethanol concentration was ten percent for 12 hours at 4°C.

Negative stain electron microscopy of these ten percent ethanol-treated membranes revealed that from 0.5 to 1 percent of the vesicles had become highly blebbed while the rest of the membranes remained quite normal in appearance (figure 1a). This blebbing of membranes appeared different under negative stain condition from the effects produced by protease digestion (compare figure 1 with figures 3 & 6 in Chapter Four, Part I).

In order to further examine the ethanol effect on membrane structure, ethanol concentrations (without PMSF) were varied from ten to fifty percent (3 hours at 4°C). At ten percent the effect of ethanol alone was the same as with ethanol/PMSF. All the vesicles were affected by 20% ethanol (figure 1b) and little additional change was obvious at 30%. Some small cylindrical, receptor-packed vesicles were produced (figure 1b insert). At 40% ethanol essentially all the vesicles had

blebbed into small vesicles (50 to 100 nm diameter)(Figure 2a), each of which were packed with receptor molecules (figure 2b). By 50%, membrane structure had completely broken down and receptor particles were no longer apparent. Finger-print patterns (figure 3) which are probably lipid structures were visualized.

The dense packing of receptor particles into ethanol induced mini-vesicles (figure 2b) led me to examine whether ethanol treatment might be useful in producing receptor membranes selectively enriched in receptor protein. Membranes were treated with 40% ethanol and then labelled with I^{125}-αbutx. These labelled membranes were then run on a 40% to 25% (w/w) sucrose gradient (14 hours, 200000 g, SW41 rotor). The treated membranes gave rise to a population of receptor vesicles banding at 36% sucrose, much heavier than the original membranes which banded at 33% sucrose. A light fraction (30% sucrose) was also seen (figure 4a), which may be unbound αbutx. The heavier peak was then collected by ultracentrifugation (4 hours at 200000 g) and over 80% of the counts were recovered. This material was then run on a 80% to 40% (w/w) glycerol gradient for 24 hours at 200000 g in glycerol, which permeates the membrane bilayer and reduces the effects of trapped solvent, the toxin-receptor complex pelleted through the gradient (figure 4b) indicating a density of greater than 1.2 g/cm^3. The difference between sucrose and glycerol gradient densities indicates that the new heavy vesicles were sealed and impermeant to sucrose and that their apparent density in sucrose is the result of trapped solvent.

In a second experiment to determine whether ethanol treatment would

selectively enrich for receptor with respect to other proteins present, 35% ethanol treated membranes were pelleted through 60% w/w glycerol and the pelleted membranes run on SDS-PAGE. No significant enrichment of receptor protein compared with the other proteins was observed.

The mechanism of the ethanol effect is unclear and the limited transformation of vesicles at 10% ethanol seems out of keeping with the presumably general nature of ethanol's interaction with membranes and indicates variability between the receptor-rich vesicles. Ethanol extraction of lipids resulting in the increased density of the receptor membranes may prove to be a useful method for the preparation of acetylcholine receptor in a lipid-depleted yet still membrane-bound form.

FIGURE LEGENDS

Figure 1

A. Of membranes treated with 10% ethanol only a few are morphologically altered (e) in phosphotungstate negative stain. Bar marks 100 nm.

B. By 20% ethanol most of the membrane vesicles have been affected. Insert shows small cylindrical vesicles, receptor heads are visible (arrow). Bar marks 0.5 μm and 10 nm in insert.

Figure 2.

40% ethanol treatment results in almost complete conversion of large receptor vesicles into mini-vesicles. Part B shows higher magnification of mini-vesicles packed with receptor molecules. Bar marks 100 nm in A.

Figure 3.

Treatment of membranes with 50% ethanol results in the total breakdown in vesicle structure and the appearance of patterns most likely resulting from lipids. Bar marks 100 nm.

Figure 4.

A. Membranes treated with 40% ethanol and labeled with I^{125}-αbutx were run on a 38% to 28% sucrose gradient. (+) marks sucrose

concentrations and (●) counts/minutes per fraction. Large arrow marks the position of untreated membranes.

B. When the heavy peak off the sucrose gradient is collected and run on an 80% to 40% glycerol gradient the toxin-receptor complexes pellet, indicating a density of greater than 1.2 g/cm^3.

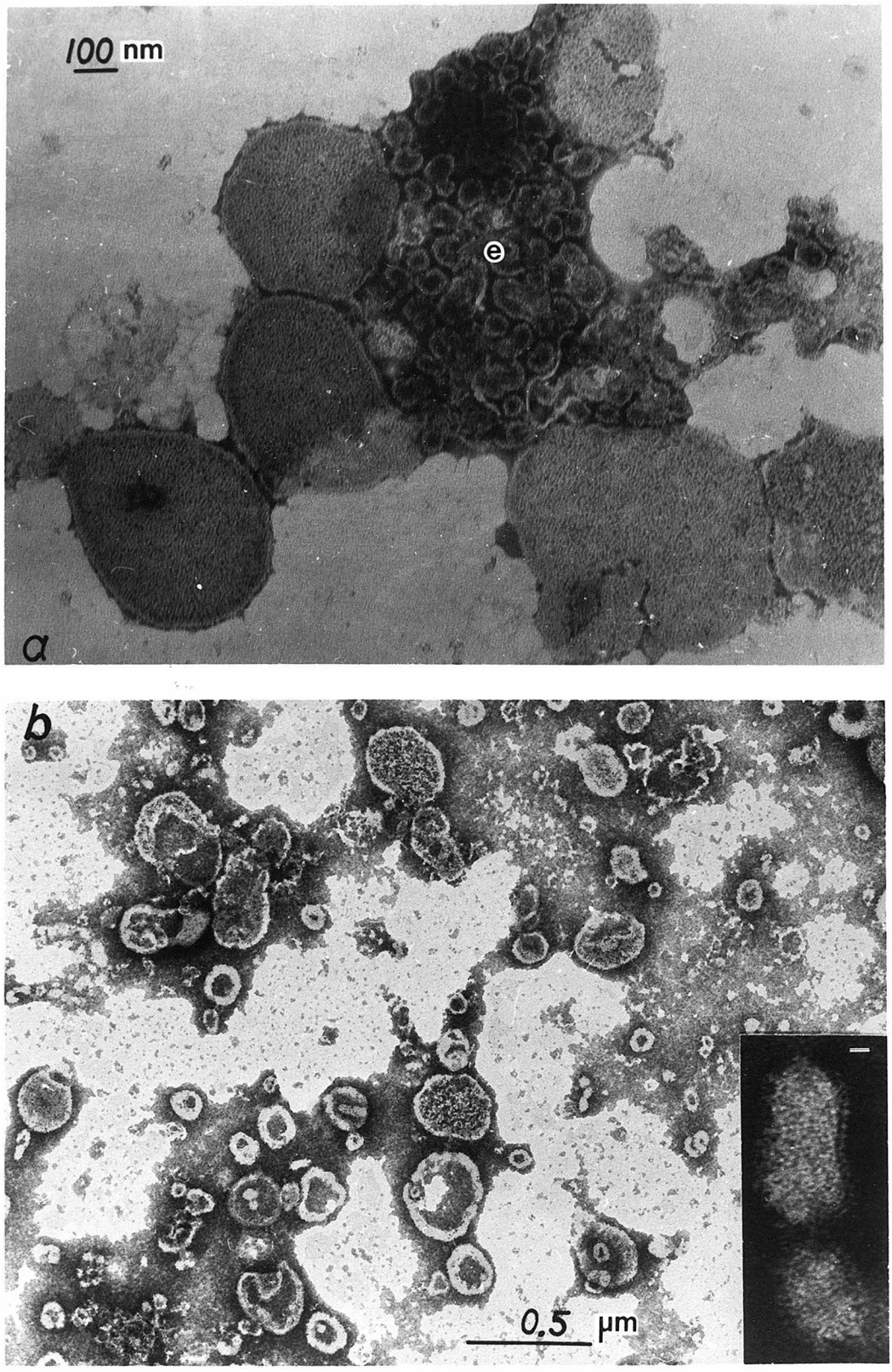
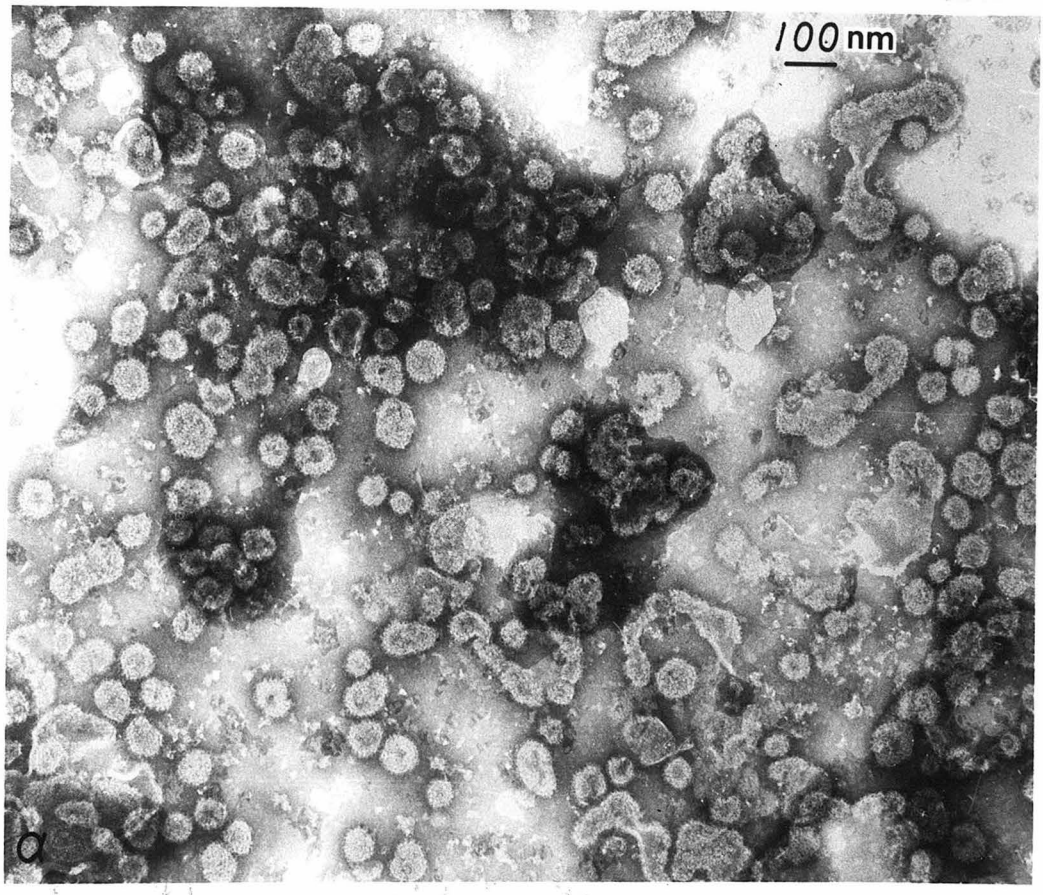


Figure 1



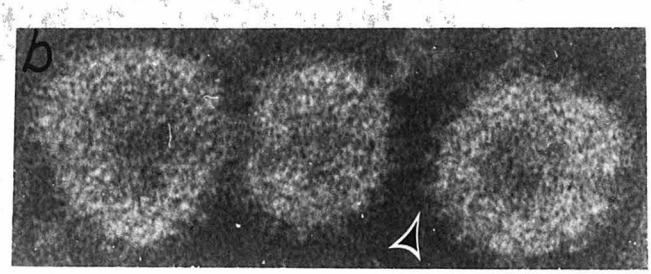


Figure 2

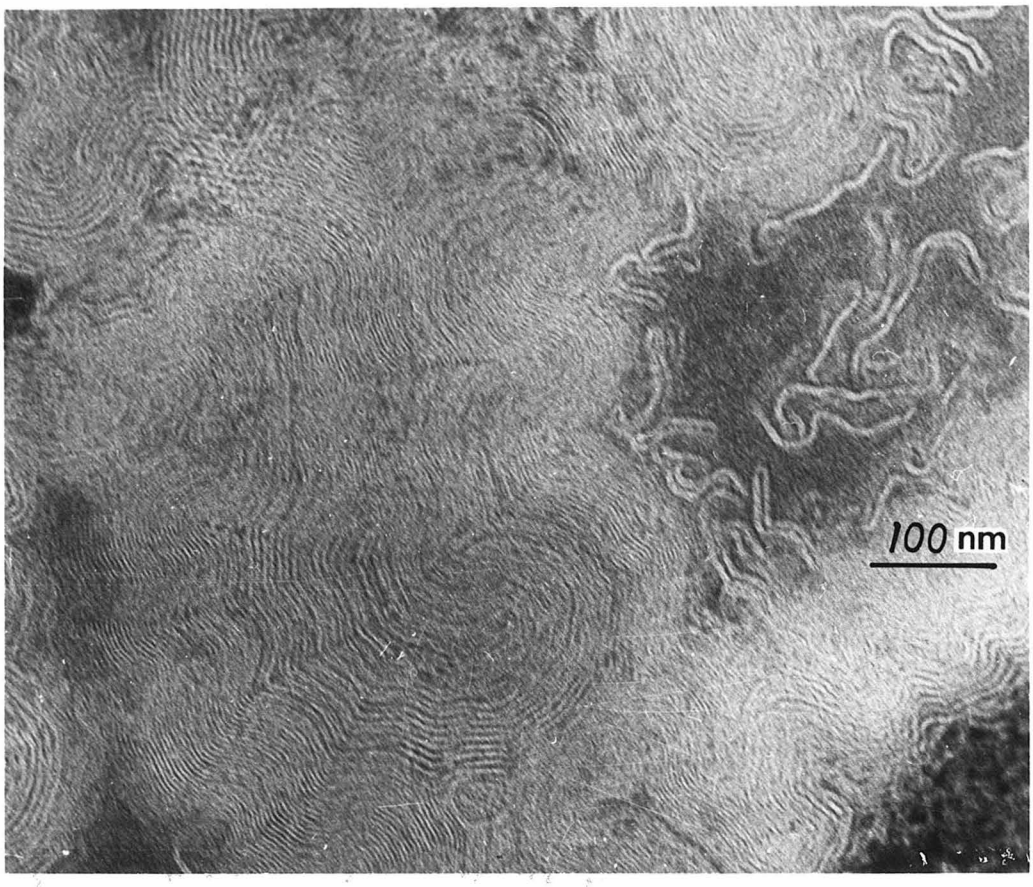


Figure 3

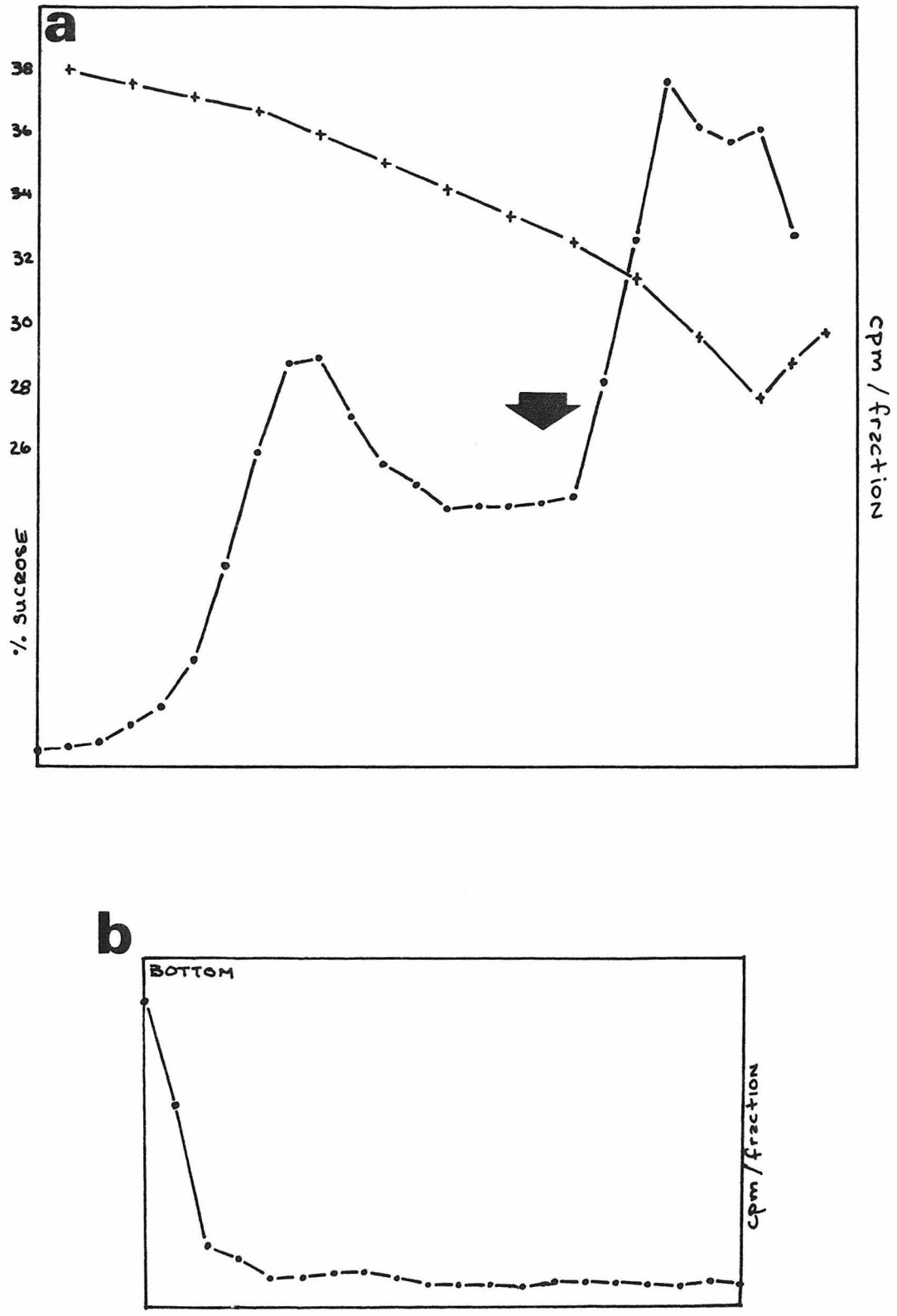

a
38
36
34
32
30
28
26
% SUCROSE
cpm / fraction
b
BOTTOM
cpm / fraction

Figure 4

APPENDIX II - ENDOGENOUS PROTEASES AND RECEPTOR MEMBRANE MORPHOLOGY

Receptor-rich membranes in which greater than 80 to 90% of the protein present, as estimated by coomassie brilliant blue staining of gel bands, is receptor (figure 1) contain an endogenous protease activity revealed by the appearance of new polypeptides with time (figure 1). Whether this protease activity is responsible for the morphological changes which sometimes occur in receptor vesicles with time (figure 2) is unclear, especially since proteolytic digestion (Chapter Four, Part I) is not the only factor which can cause changes in membrane morphology (Appendix I).

The changes observed are not limited to the kind of mini-vesicles formation brought on by protease digestion (Chapter Four, Part I) and ethanol treatment (Appendix I). Sometimes long receptor-packed membrane tubes are seen (figures 3, 4 & 5). These tubes can either be interrupted (figure 3) by particle free regions or uniform (Figure 4). They can also be relatively thick (figures 3 & 4) or thin (figure 5). Especially in thin tubes (figure 5b) the projecting receptor heads are particularly visible.

Since the actual subunit composition of the Torpedo receptor has been the center of some controversy (see Heidemann & Changeux, 1978; Fambrough, 1979 for latest references) the presence of uninhibited endogenous proteases is an important, possibly complicating factor.

REFERENCES

Heidemann, T & Changeux, J-P (1978) Ann. Rev. Biochem. 47, 317-357.

Fambrough, D. (1979) Physiol. Rev. 59, 165-227.

FIGURE LEGENDS

Figure 1.

SDS-gel of receptor rich membranes left at room temperature (22°C) for 1,4,7 and 10 days; open arrows point to new bands which arose during the time at room temperature and the closed arrows point to bands present at time zero (left most track) which appear to increase with time.

Figure 2.

Receptor-packed vesicle from aged membrane fraction shows some distortion (marked by open arrows), and a mini-vesicle (marked by 'm'). Receptor head projection is visible around the entire periphery of the vesicle. All images in this section are negatively stained by phosphotungstate pH 7.4.

Figure 3.

Some receptor vesicles take on strange tubular shapes. Filled arrows point to apparently receptor free regions of the tubes.

Figure 4.

An almost entirely tubular vesicle with fairly uniform tubes, one, small particle free stretch (marked by open arrows) is present.

Figure 5.

Receptor membrane tubes of a second, narrower type are also seen. Receptor head structures are visible along the entire tube (A). At higher magnification (B) the individual heads are clearly visible (arrow).

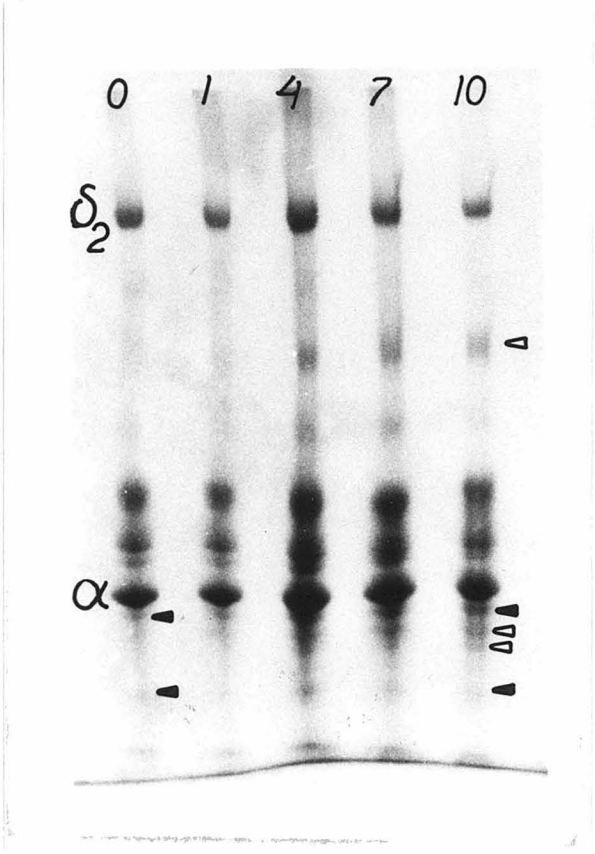


Figure 1

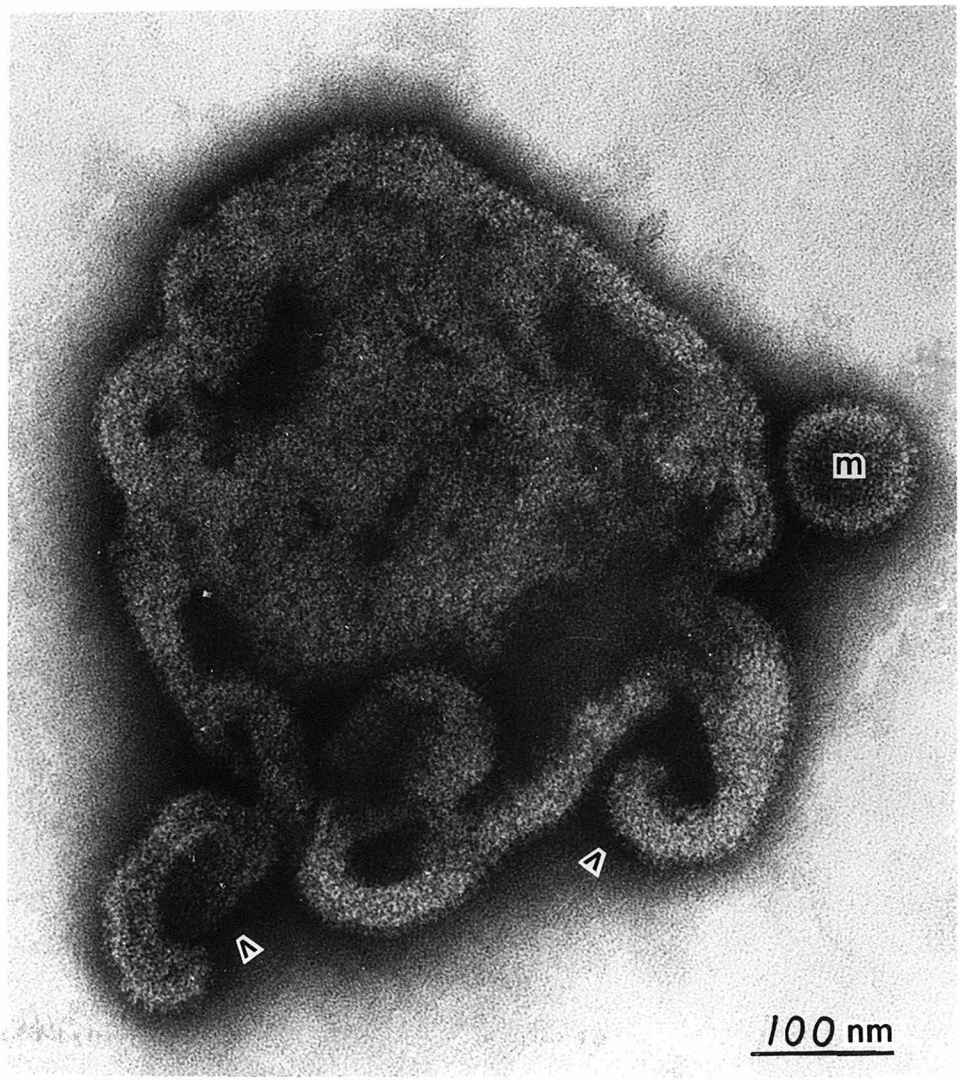


Figure 2

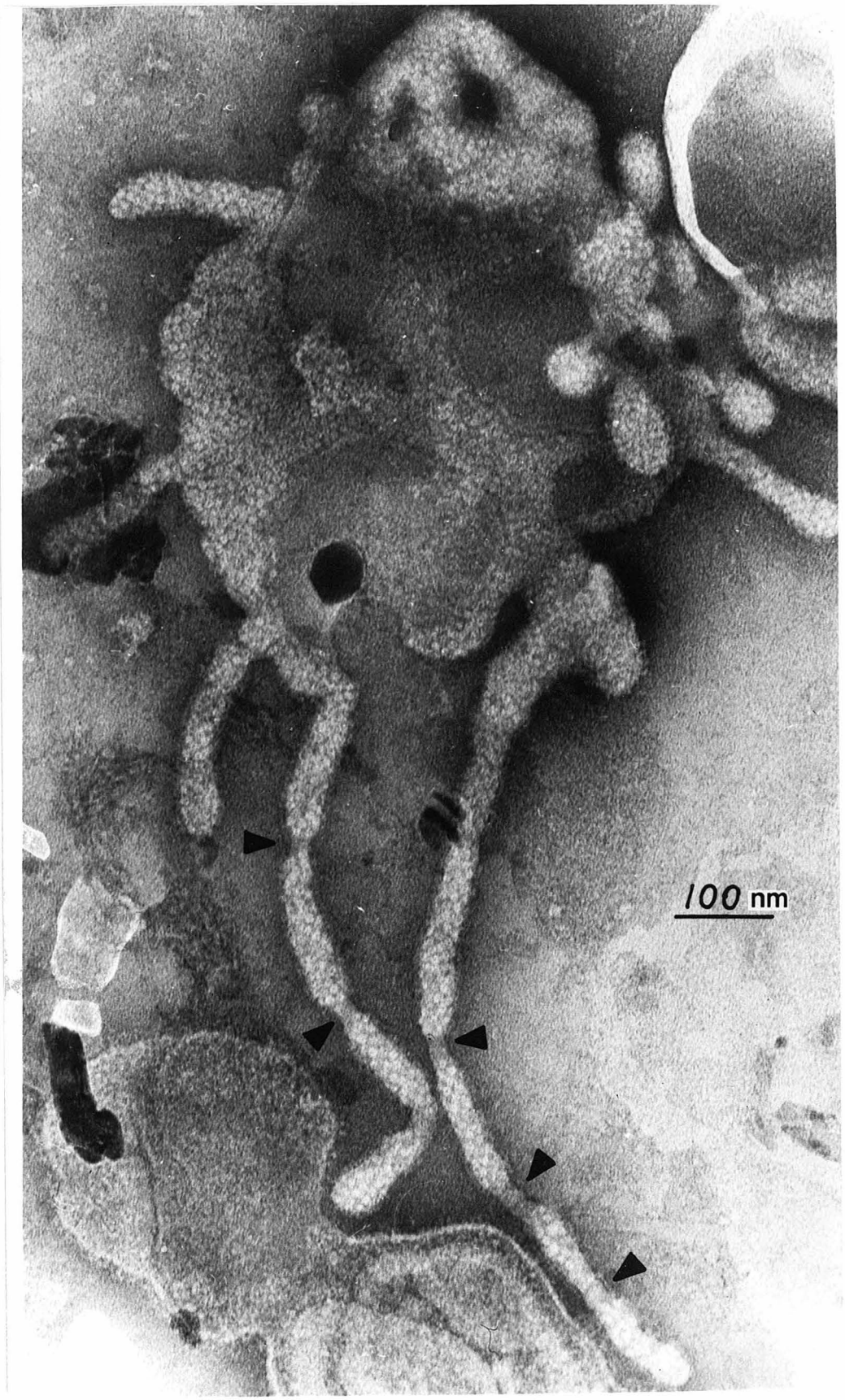


Figure 3

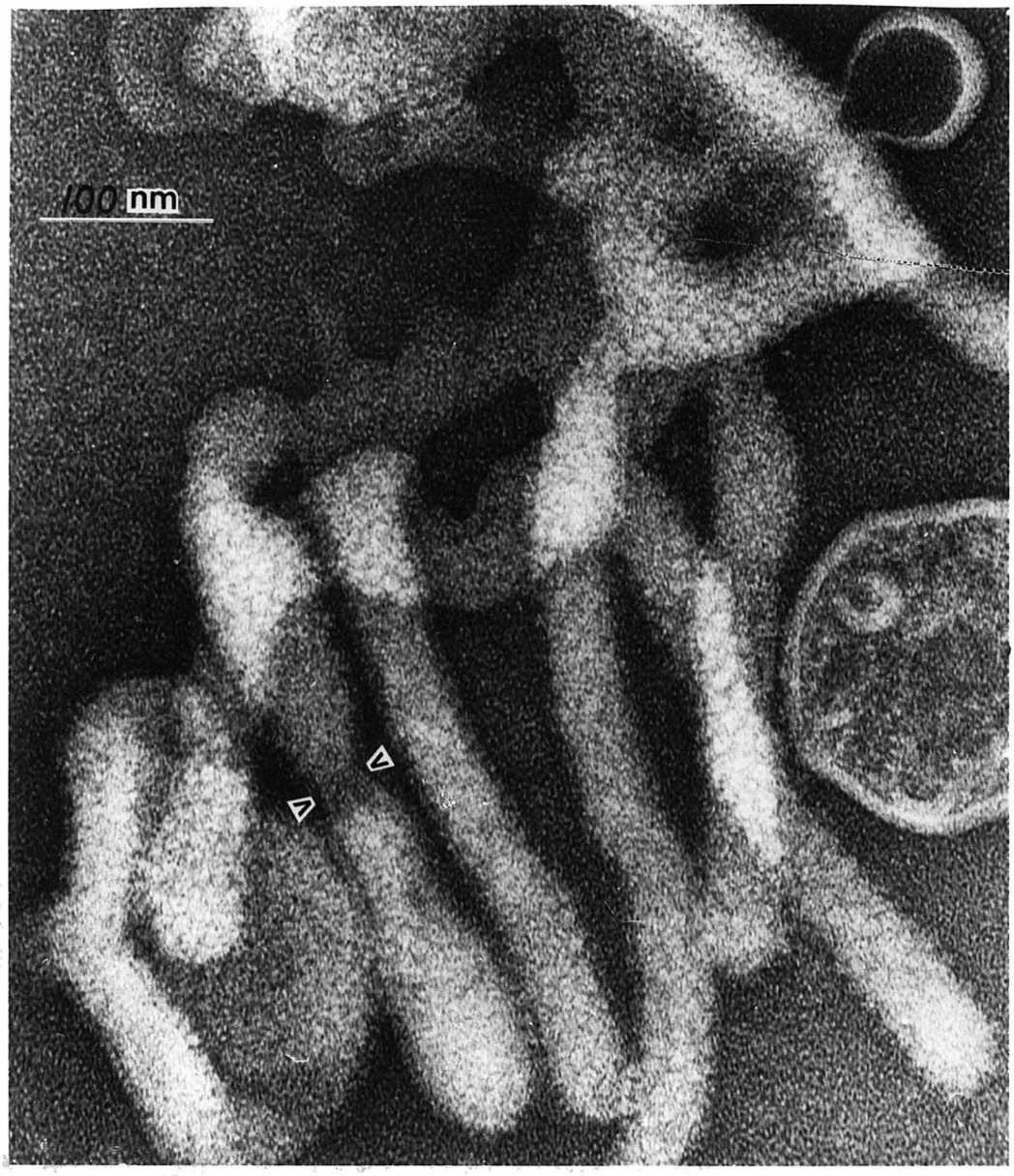


Figure 4

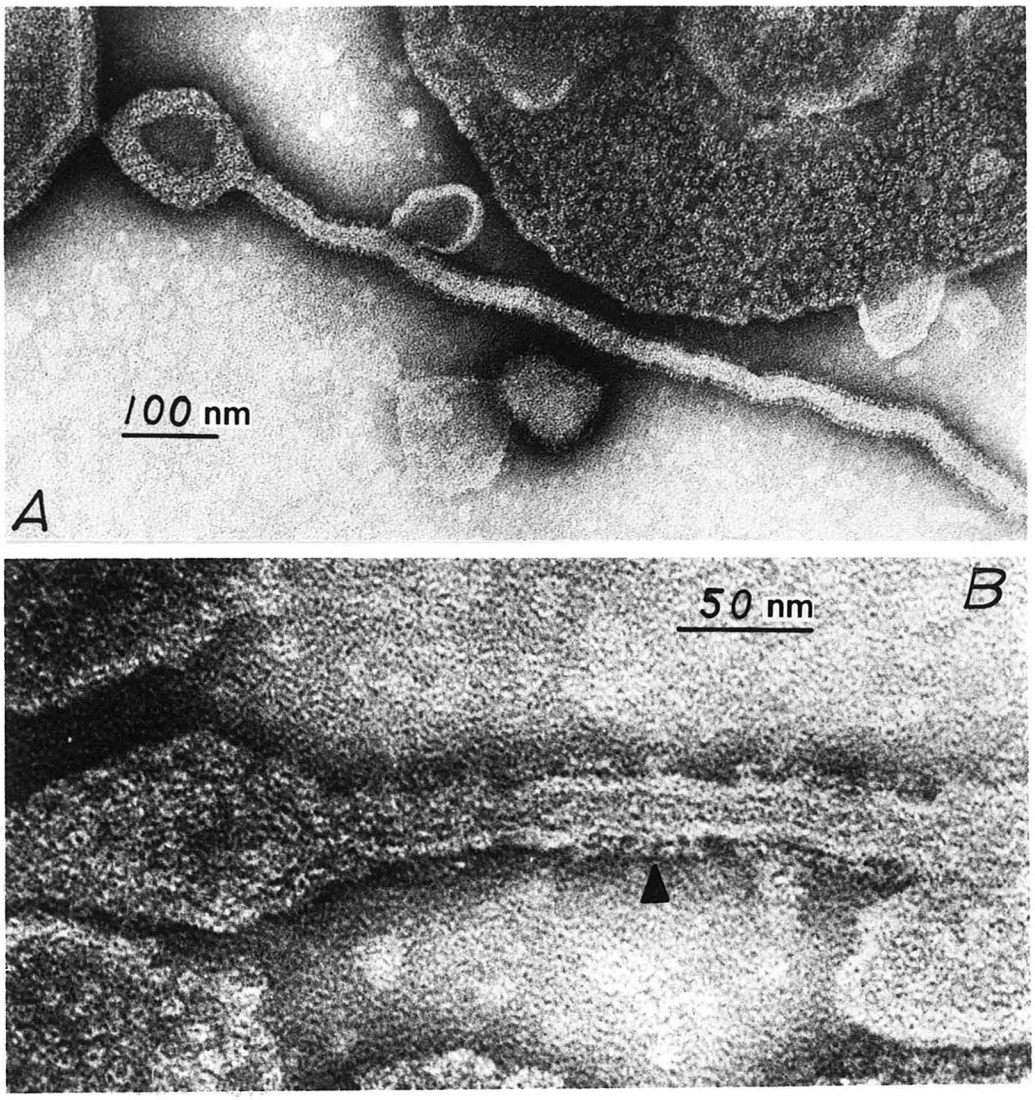


Figure 5

APPENDIX III - RECEPTOR MEMBRANE SHEETS FORMED UNDER NEGATIVE STAIN CONDITIONS

Receptor vesicles exist as spherical vesicles in solution and rapid-freeze, deep-etch, rotary-shadow electron microscopy preserves this solution structure (Chapter Four, Part 1). However, under standard negative stain conditions these vesicles are often broken into sheets (figures 1 & 2), sometimes into quite small regions and even single receptor molecules are seen (figure 1). In sheets that remain intact (figure 2) the sheets sometimes fold over each other thus exposing both intra and extra cellular surfaces (figure 2b). In the areas of sheet overlap image confusion is apparent (figure 2b). The presence of the projected head of the receptor at the sheet bend (figure 2b) indicates that the membrane may be in either of two geometries (figure 3), which cannot be distinguished due to the projected nature of electron microscopic images.

Considering the large differences in the amount of the receptor extending on the two sides of the membrane (Chapters Two, Three and Five) it was somewhat surprising that both sides in these folded sheets appeared quite similar, and indicates that the negative stain is located on both surfaces of the membrane sheet.

This similarity of receptor image, independent of the membrane's orientation conclusively demonstrates that the large crystalline sheets sometimes observed in receptor-rich membrane fractions are <u>not</u> made up of the acetylcholine receptor (Chapter Five), since in these cryst-

alline sheets the particles do not resemble the receptor in either phosphotungstate or methylamine tungstate, and have only a shallow central hole in uranyl stains, compared to the deep central hole of the receptor (Chapters Three and Five).

FIGURE LEGENDS:

Figure 1.

Under negative stain conditions some membrane vesicles fragment into small sheets and even single receptor molecules (within circles). Bar marks 100 nm in figures 1 & 2. All figures shown here are stained with phosphotungstate at pH 7.4.

Figure 2.

Membrane sheets are formed which are fairly intact (A) although some further fragmentation is apparent around the periphery. Folds (f) are also observed which reveal receptor heads (arrow) and assuming that the fold is above the rest of the sheet indicates that the entire sheet is extracellular head up (away from the carbon support film). More rarely the membrane folds over onto itself (B) so that both surfaces of the membrane are visualized. Both appear quite similar except for the image confusion which appears in the doubled sheeted region 'ds', when compared to the single sheet 'ss' region. The presence of the extracellular head (arrows) indicates the geometry of the fold (see figure 3).

figure 3.

Schematic indicates the two possible orientations of the membrane in figure 2b.

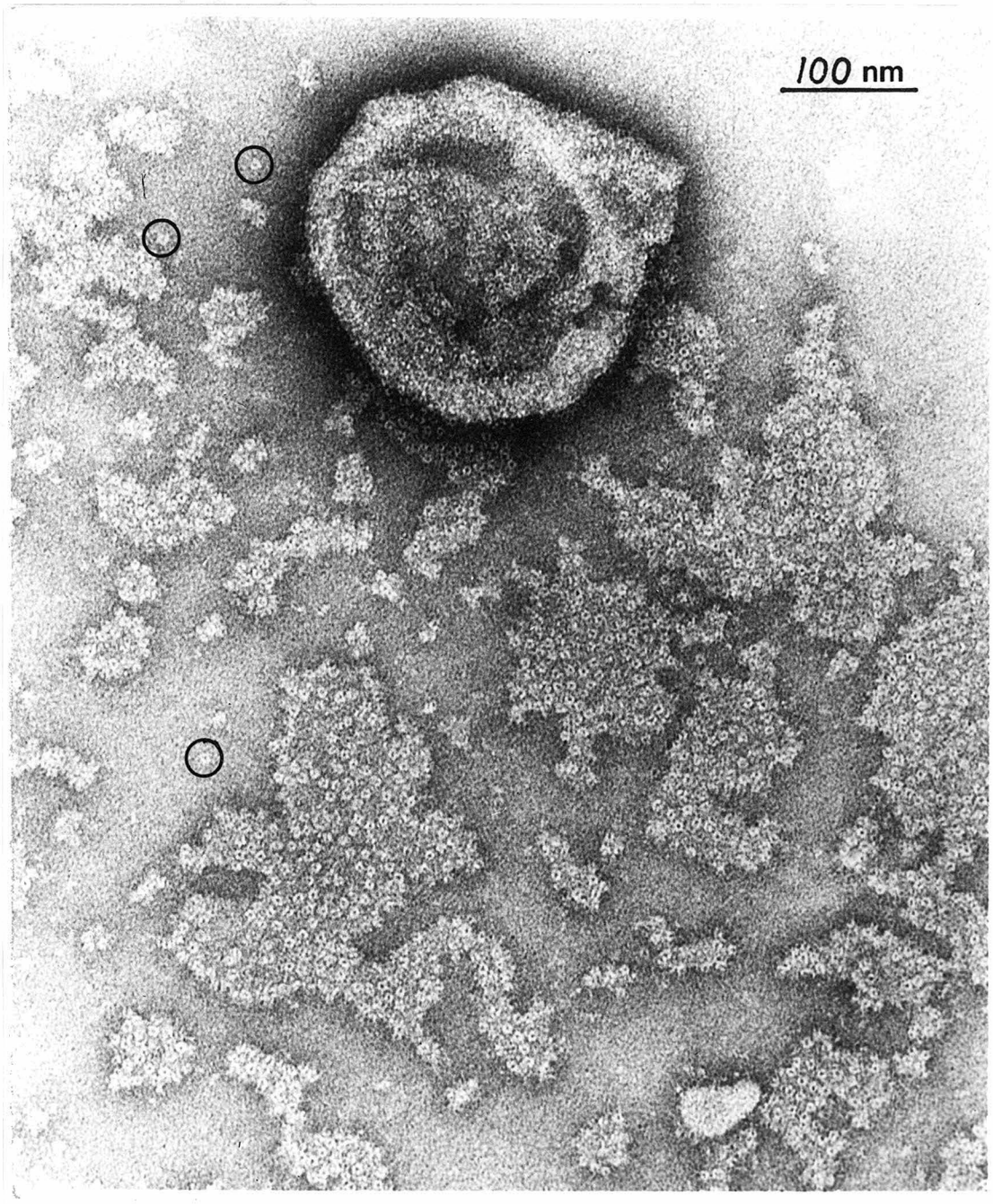


Figure 1

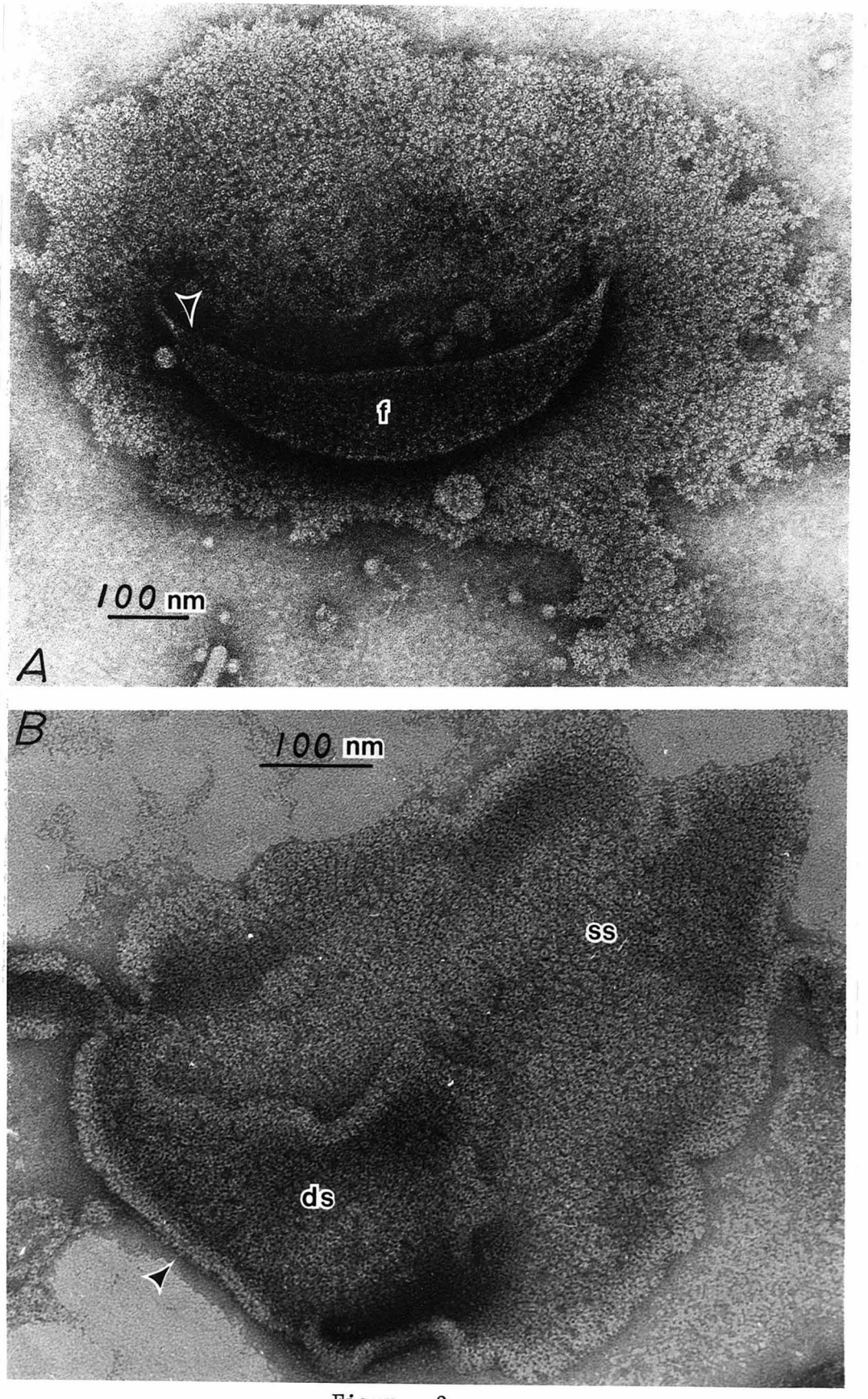


Figure 2

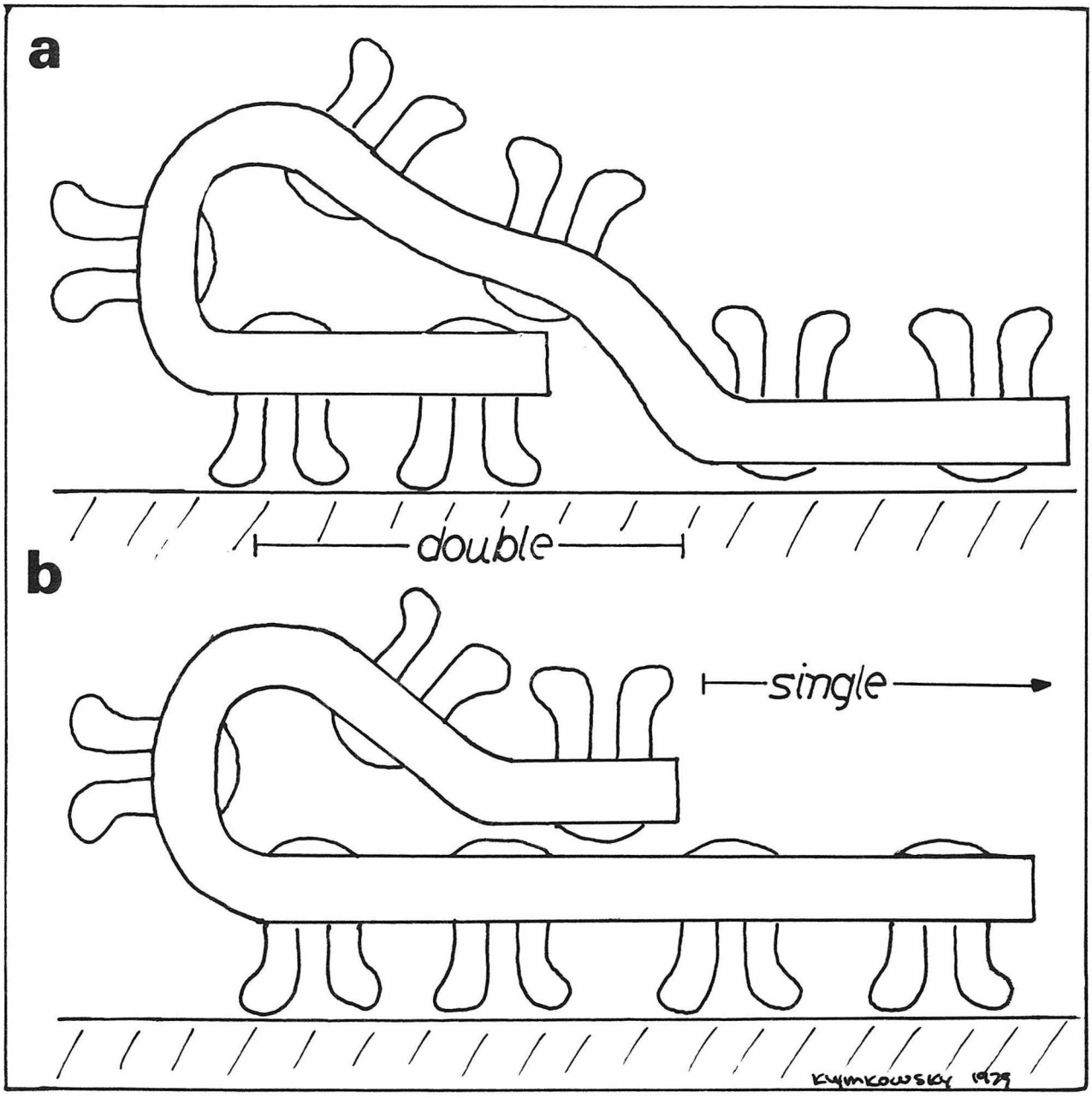


Figure 3

APPENDIX IV - RECEPTOR MEMBRANE SHEETS FORMED ON ULTRACLEAN WATER SURFACES

The osmotic activity of receptor vesicles can be demonstrated by light scattering, since scattering is inversely proportional to vesicle diameter (Bangham et al 1967)(figure 1). Since they are osmotically sealed they can be broken open into sheets and trapped by surface tension on ultraclean water surfaces (Korenbrot & Pramik, 1977). These sheets can then be compressed in a Langmuir trough and subsequently transferred onto either hydrophilic (i.e., polylysine coated glass or parlodion films) or hydrophobic (silanated glass) surfaces by moving the surface through the water/surface film/air interface. The surface can be moved either down into the aqueous phase or up from the aqueous phase into the air. The transfer of material onto the surface was monitored by the decreasing surface film area as the surface pessure was kept constanst (figure 2). Working with Dr. Juan Korenbrot (Department of Biochemistry, UCSF), I was able to show that receptor membranes could be formed into surface films (figure 2) containing significant proportions of sheets. These films are asymmetric in that hydrophilic surfaces showed different amounts of film transfer depending on which direction they were moved through the membrane surface film (figure 2). Hydrophilic surfaces would pick up membrane only when travelling from below the water interface to air. Hydrophobic surfaces would not transfer efficiently in either direction (figure 2).

Membrane films transferred onto surfaces were visualized either by platinum shadowing (angle 20° to 30°) with a carbon backing, or by negative stain electron microscopy. Negative staining was done by first adhering copper electron microscope grids to a piece of acid-cleaned glass coverslip by dropping a film of parlodion down onto them, in the same way as carbon support films are placed down by floating them onto water surface and then dropping the water level, and then baking the glass-grid-parlodion sandwich at 120°C for 10 to 15 minutes. This baking appeared essential to prevent the parlodion from pealing off when the glass/grid sandwich was placed in position under the water surface for membrane film transfer.

Resolution in the shadowed membranes was disappointing (figure 3a) and the 5 nm receptor heads could not be resolved, but the difference between sheets and vesicles (which can be trapped at the water surface) could be discerned (figure 3a). Negative stain (2% phosphotungstate pH 7.4) proved more useful and individual molecules were resolved and they displayed the characteristic donut morphology of negative stained receptor imaged under standard conditions (figure 3b).

This technique of forming receptor membrane films might be useful in 'crystallization' attempts in which ionic and temperature conditions were adjusted in the aqueous phase, especially since the nearly homogeneous alkali-stripped receptor membranes appear to have a much greater tendency to form ordered regions. The membrane film technique avoids much of the trauma of standard negative stain (Appendix III), since the sheets are preformed on the water surface and are not the result of

the tearing open of the vesicles. The sheet geometry seems much more hospitable to lattice formation, since most ordered areas observed in conventionally negative stained membranes occur in sheets.

The usefulness of surface films might be even greater if used with ethanol-treated,lipid depleted receptor membranes (Appendix I).

REFERENCES

Bangham, A.D., Dieger, J. & Grevell, G.D. (1967). Chem. Phys. Lipids 1, 225-246.

Korenbrot, J.I. & Pramik, M.J. (1977) J. Memb. Biol. 37, 235-250.

FIGURE LEGENDS

Figure 1.

The osmotic activity of receptor vesicles was assayed by means of light scattering. Absorbance was measured at 450 nm and membranes were diluted with 1/5 volume saturated NaCl solution at time 0, increasing absorbance indicates decreasing vesicle size. At time 15 minutes membranes were again diluted 1 to 5 with isotonic buffer, and in this case the simple dilution effect was observed.

Figure 2.

Membranes were loaded onto water suface at position marked START and the film was then compressed by a movable teflon barrier to the break in the curve. The increasing pressure with decreasing area indicated that a membrane film had been formed. Four film transfers were then attempted (I,II,III, & IV). The length of the lines next to the roman numerals indicates the extent of the surface transferred. The break in the main curve indicates the total area transferred in all four attempts while the surface pressure was being held constant by adjustment of the teflon barrier. Resumption of area compression leads first to a noticeable (and reproducible) shoulder (single arrow) in the curve and then the total collapse of the film (double arrow).

Figure 3.

Membrane sheets transferred to hydrophilic surfaces were visualized by either platinum shadowing (a) or negative stain (b). Bar marks 100 nm in both parts. In part (a) 'v' marks small vesicle and 's's mark two overlapping sheets.

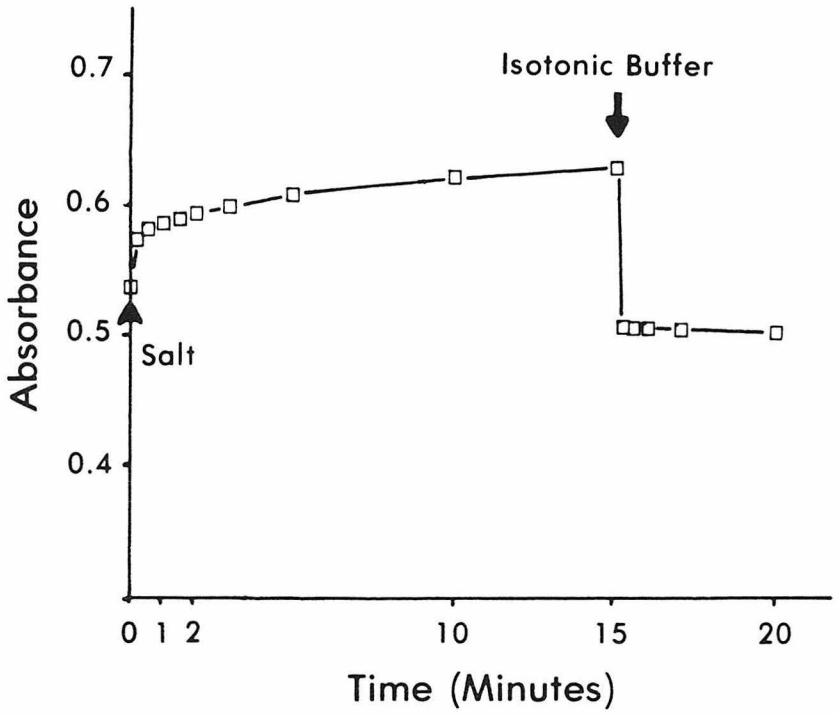

Isotonic Buffer
0.7
0.6
0.5
0.4
Absorbance
Salt
0 1 2
10
15
20
Time (Minutes)

FIGURE 1.

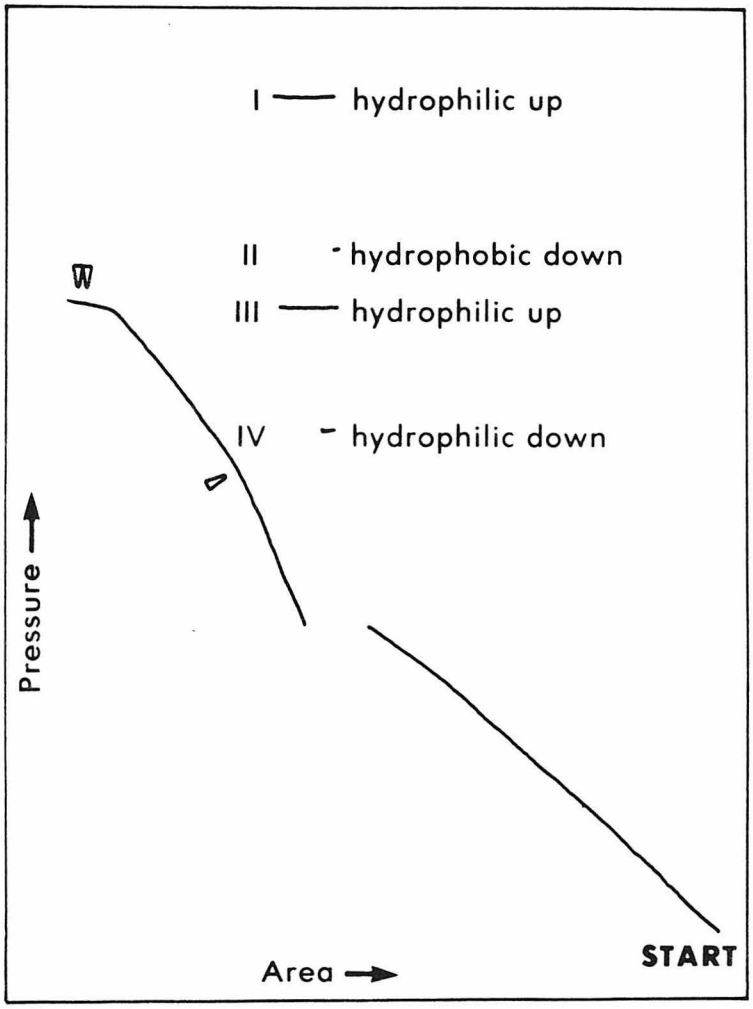

I — hydrophilic up
II - hydrophobic down
III — hydrophilic up
IV - hydrophilic down
W
Pressure
Area
START

FIGURE 2.

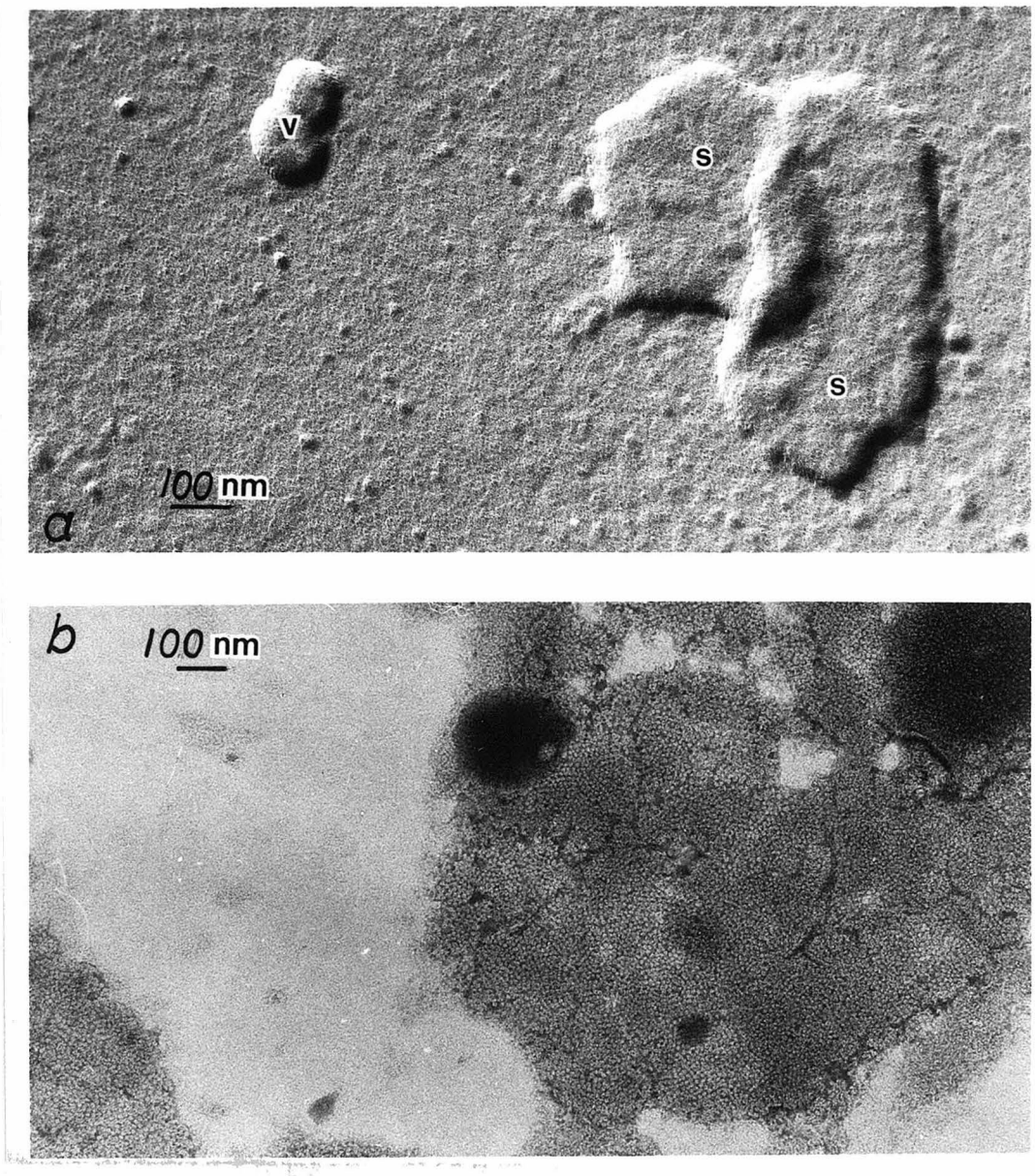


Figure 3